ELUCIDATING NATURAL AND ANTHROPOGENIC MARINE PROCESSES USING

MOLECULAR BIOMARKERS

by

LYDIA BABCOCK-ADAMS

(Under the Direction of Patricia M. Medeiros)

ABSTRACT

Molecular biomarkers were first used in fossil fuel geochemistry, marking the beginning

of the organic geochemistry field, but soon their utilization expanded to environmental research.

This thesis uses both nonpolar and polar biomarker analysis of environmental samples to track

inputs, transport, and transformations of organic carbon in the marine environment. In the

second chapter, the results showed a massive accumulation of petroleum-derived compounds in

Gulf of Mexico sediments after the Macondo well blowout that reached a maximum in the fall of

2010, followed by a strong decrease in concentration. In the third chapter, increased levels of

energy reserve compounds (e.g. sugars) and n-alkanols were determined to be an indicator of

seasonal thermal stress that corals located in the Florida Keys were subjected to in 2000, and

possibly in previous years, providing a chemical distinction between bleaching resistant and non-

resistant zooxanthellae (a symbiotic dinoflagellate species that lives in the coral tissue).

INDEX WORDS:

Biomarkers; Carbon isotopes; Oil; Gulf of Mexico; Coral bleaching;

Upper Florida Keys; Organic Geochemistry

ELUCIDATING NATURAL AND ANTHROPOGENIC MARINE PROCESSES USING MOLECULAR BIOMARKERS

by

LYDIA BABCOCK-ADAMS

A Thesis Submitted to the Graduate Faculty of The University of Georgia in Partial Fulfillment of the Requirements for the Degree

MASTER OF SCIENCE

ATHENS, GEORGIA

2016

© 2016

Lydia Babcock-Adams

All Rights Reserved

ELUCIDATING NATURAL AND ANTHROPOGENIC MARINE PROCESSES USING MOLECULAR BIOMARKERS

by

LYDIA BABCOCK-ADAMS

Major Professor: Committee: Patricia M. Medeiros Jonathan I. Amster Brian M. Hopkinson

Electronic Version Approved:

Suzanne Barbour Dean of the Graduate School The University of Georgia May 2016

DEDICATION

This work is dedicated to my incredible parents, Nigel and Lucia, for always supporting me and encouraging me to follow my dreams.

ACKNOWLEDGEMENTS

I would first like to thank my committee members, Jon Amster and Brian Hopkinson. Thank you both for your insightful comments and critiques as well as writing letters of recommendation for me. I would also like to thank my wonderful advisor, Patricia Medeiros, for her dedication to teaching and providing me with as many opportunities as possible. I am so happy that three years ago you agreed to take a sophomore on as your Master's student. I am eternally grateful for everything you've taught me in the lab and in life. I have grown tremendously as a scientist and a person through my time with you. I must also thank my fellow lab members, Michael (Micha) Seidel, Ding (Oliver) He, and Maria Letourneau for all of your help, advice, instruction, and laughter-labelling, filling, and cleaning 100+ TOC vials wouldn't have been the same without you! You are all incredible people and I feel privileged to have been able to work with you all.

I also want to thank the UGA Honors Program for sponsoring the Combined Degree Program that has allowed me to graduate with two Bachelor's degrees and a Master's degree in five years, as well as all of the business office staff in Marine Sciences for helping me figure out the logistics of being a hybrid undergraduate/graduate student. I especially want to thank Catherine Mills for being my go-to person whenever I had an administrative question. I would also like to thank my friends, both in Athens and those previously graduated. Finally, thank you to my amazing family. There is no way I could have made it to this point without your continual love and support!

TABLE OF CONTENTS

		Page
ACKNO	WLEDGEMENTS	v
LIST OF	TABLES	viii
LIST OF	FIGURES	ix
СНАРТЕ	ER	
1	INTRODUCTION AND LITERATURE REVIEW	1
	1. Biomarkers	1
	2. Thesis Overview	2
	References	5
2	HYDROCARBON COMPOSITION AND LEVELS IN THE GULF SEDIM	1ENTS
	WITHIN 3 YEARS FOLLOWING THE MACONDO WELL BLOWOUT .	7
	Abstract	8
	1. Introduction	8
	2. Experimental Methods	10
	3. Results and Discussion	13
	4. Conclusions	21
	Figures and Tables	23
	Acknowledgements	29
	References	30
	Supporting Information	34

3	ASSESSING CORAL RESPONSE TO BLEACHING EVENTS USING	
	MULTIMOLECULAR BIOMARKERS	47
	Abstract	48
	1. Introduction	49
	2. Experimental Methods	51
	3. Results and Discussion	53
	4. Conclusions	57
	Figures	59
	Acknowledgements	69
	References	70
4	CONCLUSIONS	73
	References	75
APPEND	DIX	
A	EXPORT OF TERRIGENOUS DISSOLVED ORGANIC MATTER IN A B	ROAD
	CONTINENTAL SHELF	76

LIST OF TABLES

Pag	e
Table 2.1: Total aliphatics and petroleum biomarkers and bulk measurements for surface and	
subsurface sediments	4
Table 2.S1a: Total aliphatics and petroleum biomarkers found in surface sediments samples	
collected from 2010	5
Table 2.S1b: Total aliphatics and petroleum biomarkers found in surface sediment samples	
collected from 2011-2013	8
Table 2.S2a: Total aliphatics and petroleum biomarkers found in sub-surface sediments samples	
collected from 20104	1
Table 2.S2b: Total aliphatics and petroleum biomarkers found in sub-surface sediment samples	
collected from 2011-20134-	4

LIST OF FIGURES

Page
Figure 2.1: Location of sediment samples collected in the Gulf of Mexico
Figure 3.1: Location of Little Grecian Reef and Admiral Reef
Figure 3.2: Zooxanthellae clade distribution at Little Grecian Reef for <i>O. annularis</i> 60
Figure 3.3: Concentrations of monosaccharides in <i>O. annularis</i> from Little Grecian Reef61
Figure 3.4: Concentrations of sugar alcohols in <i>O. annularis</i> from Little Grecian Reef62
Figure 3.5: Concentrations of fatty acids in <i>O. annularis</i> from Little Grecian Reef63
Figure 3.6: Concentrations of <i>n</i> -alkanols in <i>O. annularis</i> from Little Grecian Reef64
Figure 3.7: Concentrations of sterols in <i>O. annularis</i> fro Little Grecian Reef65
Figure 3.8: Monthly averaged sea surface temperature in 2000
Figure 3.9: Zooxanthellae clade distribution at Admiral Reef for <i>O. annularis</i> 67
Figure 3.10: Zooxanthellae clade distribution at Little Grecian Reef for <i>O. faveolata</i> 68
Figure A1: South Atlantic Bight study area95
Figure A2: Wind stress, Altamaha River discharge, and DOC flux96
Figure A3: Time evolution of components as a function of distance from the coast97
Figure A4: Vertical profiles of frequency of occurrence of t-Peaks and their contribution98
Figure A5: Time series of expected change in salinity anomaly of the plume99
Figure A6: Scatter plots of measured tDOM versus spectral slope coefficient and estimated
tDOM versus measured tDOM
Figure A7: Heat maps of surface salinity and estimated terrigenous DOM

Figure A.S1: Spatial distribution of t-Peak contribution to total peaks1	10
Figure A.S2: Scatter plots of first principal component of FT-ICR MS-derived DOM	
composition and $\delta^{13}\text{C}$ SPE-DOC and loadings of PC1 shown in van Krevelen space1	11
Figure A.S3: Time series of frequency of occurrence of t-Peaks and their contribution to all	
peaks during dark incubations and photo-irradiation experiments1	12

CHAPTER 1

INTRODUCTION AND LITERATURE REVIEW

1. Biomarkers

The analytical technique of using molecular biomarkers to uncover information about organic matter is one that has greatly expanded its applicability over eighty years of research. Molecular biomarkers have beginnings in fossil fuel geochemistry though the term was not coined until 1969 (Streibl and Herout). In 1936, Treibs found a diagenic link between chlorophyll-a from living organisms and porphyrins in petroleum. This link elucidated the organic origin of petroleum. From the 1950s through the 1970s, organic chemists used both low and high resolution mass spectrometry (MS) to determine structures of natural products, marking the beginning of the organic geochemistry field (Medeiros and Simoneit, 2007). The development of biomarkers experienced a major advancement when gas chromatography (GC) was coupled with the mass spectrometer, giving rise to the GC-MS. In this coupled instrument, the GC separates the compounds and the MS acts as the detector, providing information about the compound ions and fragment ions. At first this method was only applicable to nonpolar compounds, but later different instrumentation and derivatization (mainly silylation of the polar functional group) methods were introduced, which expanded the analytical window of the biomarker technique (Medeiros and Simoneit, 2007). The development of derivatization meant that polar compounds could be transformed into a GC-MS amenable fraction, opening an entirely new realm of study. Molecular biomarkers could now be used for investigations of both nonpolar and polar compounds, as well as studies on the fossil record (e.g. petroleum) and studies of modern organic samples (e.g. fresh material produced by an algae bloom or the terrestrial material transported from land to ocean).

Not only do molecular biomarkers provide the data to identify and quantify specific compounds in a sample, but biomarkers also allow for the analysis of the organic origin of a sample. This is due to the strong chemical signature left by flora, fauna, and microorganisms in the distribution and relative abundances of organic compounds in the environment. For example, a sample that shows a predominance of high molecular weight n-alkanes (C > 21) with an odd to even carbon number preference in the carbon chain $(C_{25}-C_{35})$ is likely influenced by major terrestrial inputs (Simoneit, 1977). Additionally, the hopane series (biomarkers derived from bacteria) provides an important tool used in environmental petroleum studies due to its resistance to degradation throughout the geological time (Simoneit, 1984; Jaffé, 2003). Thus, molecular biomarkers are not just useful for contamination studies, but are in fact applicable to numerous environmental investigations of organic matter fate in the atmosphere (e.g., Simonet and Mazurek, 1982; Rogge et al., 1993; Fine et al., 2001; Killin et al., 2004), soils (e.g., Rohmer et al., 1980; Zelles and Bai, 1993; Malosso et al., 2004), and sediments (e.g. Simoneit, 1977; Goñi and Hedges, 1990; Hedges et al., 1997; Jaffe et al., 2001). Furthermore, this technique is expanding to other disciplines such as the pharmaceutical industry (e.g., disease detection), food industry (e.g., fraudulent alterations), and forensic science (e.g., crime investigation; Medeiros and Simoneit, 2007).

2. Thesis Overview

All the work in this thesis is concerned with using organic compounds (i.e. molecular biomarkers) to track inputs, transport, and transformations of organic carbon in the marine environment. The progression of this thesis follows the development of biomarkers, thus chapter two begins at the origin of organic geochemistry - nonpolar biomarkers used for the analysis of petroleum-derived investigations. This chapter looks at the levels and distribution pattern of petroleum derived compounds in Gulf of Mexico sediments following the catastrophic Deepwater Horizon oil spill that occurred in April 2010. Sediment samples were collected to the northwest of the Macondo well from approximately 20 days after the accident in 2010 to the summer of 2013. The third chapter takes the thesis to the time after the development of derivatization methods and therefore uses the analysis of polar biomarkers to examine the suite of organic compounds found in coral tissue. The aim of this study is to characterize biomarker indicators of stress and/or recovering conditions following a major bleaching event in 1997-1998 during the strongest El Niño on record (McPhaden, 2015). Appendix A uses an extensive dataset to look at the South Atlantic Bight system in order to investigate the seasonal evolution and distribution of terrestrial dissolved organic matter (DOM) across the continental shelf and to assess the mechanisms controlling terrestrial DOM distribution and potential importance of degradation processes. Although this appendix does not use molecular biomarkers, it uses an advanced mass spectrometry technique, Fourier Transform Ion Cyclotron Resonance (FT-ICR) mass spectrometry, along with bulk carbon measurements such as total dissolved organic carbon (DOC), stable carbon isotope (δ^{13} C), and chromophoric dissolved organic matter (CDOM). This Appendix demonstrates the power of using different techniques with different analytical

windows in order to get a full picture of a system, a growing approach used in conjunction with biomarkers to better understand complex environmental processes.

References

- Fine, P. M., Cass, G. R. & Simoneit, B. R. T. Chemical characterization of fine particle emissions from fireplace combustion of woods grown in the northeastern United States. *Environ. Sci. Tech.* **35**, 2665-2675 (2001).
- Goñi, M. A. & Hedges, J. I. The diagenetic behavior of cutin acids in buried conifer needles and sediments from a coastal marine environment. *Geochim. Cosmochim. Acta.* **54**, 3083-3093 (1990).
- Hedges, J. I., Keil, R. G. & Benner, R. What happens to terrestrial organic matter in the ocean? *Org. Geochem.* **27**, 195-212 (1997).
- Jaffé, R., Mead, R., Hernandez, M. E., Peralba, M. C. & DiGuida, O. A. Origin and transport of sedimentary organic matter in two subtropical estuaries: A comparative biomarkers-based study. *Org. Geochem.* **32**, 507-526 (2001).
- Jaffé, R. *et al.* Organic compounds and trace metals of anthropogenic origin in sediments from Montego Bay, Jamaico: Assessment of sources and distribution pathways. *Environ. Pollut.* **123**, 291-299 (2003).
- Killin, R. K., Simonich, S. L., Jaffe, D. A., DeForest, C. L. & Wilson, G. R. Transpacific and regional atmospheric transport of anthropogenic semivolatile organic compounds to Cheeka Peak Observatory during the spring of 2002. *J. Geophys. Res. D Atmos.* **109**, 1-11(2004).
- Malosso, E. Use of 13C-labelled plant materials and ergosterol, PLFA and NLFA analyses to investigate organic matter decomposition in Antarctic soil. *Soil Biol. Biochem.* **36**, 165-175 (2004).
- McPhaden, M. J. Playing hide and seek with El Niño. *Nature Clim. Change.* 5, 791–795 (2015).
- Medeiros, P. M. & Simoneit, B. R. T. Gas chromatography coupled to mass spectrometry for analyses of organic compounds and biomarkers as tracers for geological, environmental, and forensic research. *J. Sep. Sci.* **30**, 1516-1536 (2007).
- Rogge, W. F., Hildemann, L. M., Mazurek, M. A., Cass, G. R. & Simoneit, B. R. T. Sources of fine organic aerisik. 2. Noncatalyst-equipped automobiles and heavy-duty diesel trucks. *Environ. Sci. Tech.* **27**, 636-651 (1993).
- Rohmer, M., Dastillung, M. & Ourisson, G. Hopanoids from C30 to C35 in recent muds. *Naturwissenschaften* **67**, 456-458 (1980).

- Simoneit, B. R. T. Diterpenoid compounds and other lipids in deep-sea sediments and their geochemical significance. *Geochim. Cosmochim. Acta.* **41,** 463-476 (1977).
- Simoneit, B. R. T. & Mazurek, M. A. Organic matter of the troposphere-III. Characterization and sources of petroleum and pyrogenic residues in aerosols over the western United States.
- Streibl, M. & Herout, V. in *Organic Geochemistry* (eds. Eglinton, G. & Murphy, M. T. J.) 401-424 (Springer Berlin Heidelberg, 1969).
- Treibs, A. Chlorophyll and hemin dericatives in organic materials. *Angew. Chemie.* **49**, 682-686 (1936).
- Zelles, L. & Bai, Q. Y. Fractionation of fatty acids derived from soil lipids by solid phase extraction and their quantitative analysis by GC-MS. *Soil Biol. Biochem.* **25**, 495-507 (1993).

CHAPTER 2

HYDROCARBON COMPOSITION AND LEVELS IN THE GULF SEDIMENTS WITHIN 3 ${\tt YEARS~FOLLOWING~THE~MACONDO~WELL~BLOWOUT}^1$

¹Babcock-Adams, L., Chanton, J. P., Joye, S. B. & Medeiros, P. M. To be submitted to *Environ*. *Sci. Technol*.

Abstract

In 2010, the Macondo well blowout in the northern Gulf of Mexico resulted in an unprecedented release of oil into the water column at a depth of approximately 1500 m. Surface and subsurface sediments were collected to the northwest of the well from 2010 to 2013 for molecular biomarker and carbon isotopic analyses. The time series of surface sediments showed a clear pattern: total concentrations of n-alkanes, unresolved complex mixture (UCM), and petroleum biomarkers (terpanes, hopanes, steranes) increased from May to September 2010, peaking in November 2010, and strongly decreased in the subsequent years. The hydrocarbon concentrations were corroborated by higher organic carbon contents, more depleted $\Delta^{14}C$ values and biomarker ratios similar to those of the initial MC252 crude oil reported in the literature. These results indicate that at least part of the submerged oil plume observed in the first stages after the accident sedimented on the seafloor in the subsequent months, resulting in an apparent accumulation of hydrocarbons by the end of 2010. In the following years, oil-derived biomarker concentrations strongly decreased and geochemical parameter signatures of oil input were not as clear as before. Sediment resuspension and transport in the deep sea may have contributed to the redistribution of sedimented oil-fallout after the Macondo well spill. In addition, overlying deposition of organic matter from multiple sources may further lead to the dilution of oil signatures in those sediments.

1. Introduction

The Gulf of Mexico (GoM) is a prolific hydrocarbon basin encompassing an area of 1.6 x 10^6 km². At least 22,000 natural seeps exist in the GoM (Joye et al., 2014), releasing in up to 604,150 liters of oil per year (MacDonald, 1998). These largely diffuse and variable oil inputs pale in comparison to the focused discharge generated through the 2010 Macondo blowout. The

catastrophic explosion and sinking of the Deepwater Horizon drilling rig at the MC252 Macondo well site in April 2010 released 650 million liters of oil (Bianchi et al., 2014) into the northern GoM during an 86-day period. The blowout resulted not only in a massive, but also an unprecedented release of oil into the water column at a depth of approximately 1500 m. This intense, localized input of oil was roughly 15 times the total input from natural seeps across the entire GoM ecosystem (Joye et al., 2014). Previous oil discharges into the deep sea were from sunken ships with finite cargos (NRC, 2002) or from well blowouts at depths within the oceanic mixing layer such as the Ixtoc I exploratory well in the Bay of Campeche, Gulf of Mexico, considered the largest oil spill in the history of oil exploration (Jernelöv and Lindén, 1981) until the Macondo accident.

Nearly 7 million liters of dispersants were applied to the oil in an effort to protect the Gulf's ecologically sensitive coastlines, with about 3 million of which applied directly to the wellhead at a depth of 1544 m (Hazen et al., 2010; Schmidt, 2010). A subsurface layer of oil between approximately 1000 m and 1400 m deep was first detected in May 2010, less than a month after the explosion (Schrope, 2010). Several teams of researchers confirmed the presence of a large and deep plume extending at least as far as 13 km to the west of the wellhead during later research cruises in the Gulf (Camilli et al., 2010; Schmidt, 2010; Valentine et al., 2010). To some degree, subsurface plumes may arise from intense physical pressures at the mile-deep wellhead, which breaks the oil into droplets that never reach the surface; however, underwater use of dispersants may also play a part by shaping the oil into smaller droplets (Schmidt, 2010; Schrope, 2010). While observations of the presence of subsurface oil have been made in conjunction with both natural (Harvey et al., 1979) and human-induced releases (e.g., Boehm and Fiest, 1982; Johansen et al., 2003), studies of subsurface distributions of oil and its chemical

components in deep waters remain limited, particularly for a release of the magnitude of the Deepwater Horizon event. Much of what happens to chemically dispersed oil at sea remains a mystery. The rate at which it binds to sediments, how quickly it breaks down in the ocean, how it is taken up by undersea organisms, and what sorts of by-products are created when microbes degrade it are mostly unknown (NRC, 2005). However, after the spill, studies on the interactions between dispersed oil and microbes have started revealing important findings on the biodegradation of oil versus dispersed oil (e.g., Kleindienst et al, 2015; Seidel et al., 2015). More recently, it has been suggested that the oil initially suspended in deep waters settled to the underlying seafloor (Valentine et al., 2014; Chanton et al., 2015).

Here, we present time series data from the three years following the Macondo oil spill (2010-2013) that tracks the composition and levels of oil-derived hydrocarbons in deep sediments collected in the Gulf of Mexico. We used a multi-tracer approach encompassing oil-derived molecular biomarkers and carbon isotopic analyses in order to elucidate the temporal and spatial oil distribution and depositional characteristics to the northwest of the Macondo well.

2. Experimental Methods

2.1. Sample Location and Collection

Sediment samples were collected mostly to the northwest of the Macondo well (**Figure 2.1**) using multi-cores during multiple research cruises to the Gulf of Mexico: May, September, and late November 2010, July 2011, 2012, and 2013. The sampling site located to the southeast of the well was our control site. Immediately after collection, sediments were sliced in 3 cm layers, placed in pre-cleaned glass jars with Teflon lids, and stored frozen at -20°C until lab analyses. Here, we present the results of surface (0-3 cm) and sub-surface (3-6 cm) sediments.

2.2. Extraction and Analyses

2.2.1. Oil-Derived Hydrocarbons

The analytical procedure summarized below is based on UNEP (1991) and Medeiros and Bícego (2004). Hydrocarbons were extracted from dried and ground sediment samples (~ 10 g) with a mixture of hexane:dichloromethane (1:1, v/v) using accelerated solvent extraction (ASE 350, Dionex) at 100°C and 1000 psi (3 static cycles). The extracts were concentrated in a RapidVap (solvent evaporation system) to about 3 mL, then fractionated into aliphatic and aromatic hydrocarbons using a column of alumina and silica-gel, and gradient solvents as eluent: *n*-hexane and 3:1 dichloromethane:hexane for aliphatic and aromatic fractions, respectively. Fractionated extracts were concentrated again to ~ 5 mL, and then further to 1 mL using a stream of ultra-high purity nitrogen. Here, we report results for the aliphatic fraction containing nalkanes, isoprenoids, petroleum biomarkers (hopanes, terpanes, and steranes), and UCM (unresolved complex mixture); analyses of aromatic hydrocarbons are underway and will be reported elsewhere. Sediment extracts were analyzed by GC-MS with an Agilent 6890 gas chromatograph interfaced with an Agilent 5973 mass selective detector (MSD). The injector and ion source temperatures were set to 280 °C and 230 °C, respectively. A DB5-MS capillary column (30 m x 0.25 mm i.d. and film thickness of 0.25 µm, Agilent) was used with helium as the carrier gas. The GC operating program consisted of injection (splitless) at 50 °C, hold for 1 min, temperature increase of 5 °C min⁻¹ to 300 °C, followed by an isothermal hold at 300 °C for 10 min. The MSD was operated in the electron impact mode with an ionization energy of 70 eV and scan range from 50 to 650 Da. In addition to the full scan mode, selected samples were analyzed for petroleum biomarkers using selected ion mode (SIM) for specific mass to charge ratios (m/z) of 191.

Data were acquired and processed with the HP-Chemstation software. Individual compounds were identified by comparison of mass spectra with literature and library data, comparison of mass spectra and GC retention times with those of authentic standards and/or interpretation of mass spectrometric fragmentation patterns. Compounds were quantified using the total ion current (TIC) peak area, and converted to compound mass using calibration curves of external standards: *n*-eicosene (Sigma-Aldrich) for *n*-alkanes, isoprenoids, and UCM; 17β, 21β-hopane (Chiron Laboratories) for petroleum biomarkers (terpanes, hopanes, steranes). A procedural blank was run in sequence to sediment samples, which presented no significant background interferences.

2.2.2. Bulk Organic Carbon Contents and Isotopic Compositions

Prior to analysis, key sediment samples were treated with 10% HCl to remove carbonates, rinsed, freeze-dried, and ground. Samples were then analyzed for percent organic carbon (%OC), and δ^{13} C and Δ^{14} C signatures. The first two analyses were performed on a Carlo Erba elemental analyzer coupled to a Delta XP Thermo Finnigan isotope ratio mass spectrometer. Results are presented relative to VPDB (δ^{13} C = (Rsam/Rstd – 1) × 1000, where R = 13 C/ 12 C) and the standard is known relative to NBS-19 (Chanton at al., 2015). The analytical precision is $\pm 0.1\%$ or better. Sediments for 14 C analysis were combusted and purified CO₂ samples (water vapor and noncondensable gases were removed by cryogenic separation on a vacuum line) were prepared as graphite targets and analyzed by accelerator mass spectrometry at the National Ocean Sciences Accelerator Mass Spectrometry Facility (NOSAMS). Values are reported according to the Δ notation. The Δ notation normalizes the radiocarbon content of a sample to nominal δ^{13} C value (–25‰) and the collection time point. The scale is linear and starts

at -1000% when a sample has undetectable levels of 14 C, which represents petroleum residue (Chanton et al., 2015). The 14 C blanks were generally between 1.2 and 5 μ g of C, producing a negligible effect on samples which were over 1200 μ g of C. The analysis of 17 replicate sediment samples yields an average analytical reproducibility of $\pm 6.5\%$.

3. Results and Discussion

Table 2.1 gives the total concentrations of *n*-alkanes (ranging from C_{10} to C_{38}), isoprenoids (pristane and phytane), petroleum hydrocarbons (terpanes, hopanes and steranes) and unresolved complex mixture (UCM) for surface and sub-surface sediment samples collected from 2010 to 2013, as well as their bulk total organic carbon contents (%OC) and isotopic values (δ^{13} C and Δ^{14} C). Concentrations of all individual compounds found in this study are shown in **Supporting Tables 2.S1 and 2.S2**.

3.1. Total Organic Carbon and Hydrocarbon Biomarkers

Total organic carbon percentages for all sediments ranged from 0.9 to 2.2%, with higher contents found in the surface samples collected in September and November 2010 (1.7% OC on average; **Table 2.1**). These sediments presented ~20% more OC than those collected in May 2010 (1.4%) and subsequent years (1.3%). Interestingly, while all other subsurface sediments had on average 1.3% OC, subsurface sediments collected in September and November 2010 had higher OC contents, ranging from 1.2 to 1.8% OC (1.5% on average), indicating an additional source input of OC to these sediments during these months that was detected not only on the top (0-3 cm), but also down core (3-6 cm).

3.1.1. Aliphatic Hydrocarbons

Resolved aliphatic hydrocarbons consisted mainly of C₁₅-C₃₆ n-alkanes with total nalkane concentrations ranging from 534 to 6159 ng g⁻¹ for surface and from 325 to 1415 ng g⁻¹ for subsurface sediments (Tables 2.1 and 2.S1). The time series of surface sediments showed a clear pattern: total *n*-alkane concentrations progressively increased from May to September, peaking in November 2010, and strongly decreased in the subsequent years (Figure 2.2A; Table **2.1**). In general, the short-chain *n*-alkane ($C \le 21$) distributions had no significant odd/even carbon number preferences ($CPI_{10-21} \sim 1.0$) for most sediments in both the surface and subsurface, suggesting fossil fuel inputs as an important source for these locales (Mazurek and Simoneit, 1984). The long-chain ($C \ge 23$) *n*-alkane profiles prevailed and accounted for > 50%of the total *n*-alkanes in most samples. The dominant peaks (C_{max}) occurred mainly at C_{29} or C_{31} with an elevated odd to even carbon number preference, as reflected in the high CPI₂₃₋₃₈ values (mostly > 2.5), especially for the subsurface samples (**Table 2.1**). This pattern is characteristic of higher plant waxes (Eglinton and Hamilton, 1967) and, thus reveals the occurrence of prominent terrestrial inputs to these sediments. These sampling sites are located to the NW of the Macondo well (see **Figure 2.1**), and therefore, the terrigenous signature in these sediments may be due to the influence of the Mississippi and Atchafalaya Rivers. However, relatively lower CPI₂₃₋₃₈ values (average 1.8) were detected in surface sediments collected in September and especially those collected in November 2010, which is indicative of oil derived hydrocarbons, mixing with the terrigenous OC, thus lowering the CPI values.

Total *n*-alkanes found in the samples represented only a minor amount of the total aliphatic hydrocarbons. The majority of the compounds present in the aliphatic fraction are molecules that cannot be resolved by capillary GC columns and termed UCM (Unresolved Complex Mixture).

The UCM was present in all sediment samples encompassing > 80% of the total aliphatic hydrocarbon concentrations. Lowest UCM values were present in the control and most subsurface sediments, as well as in May 2010 top sediments (**Table 2.1**). The May collection occurred 20 days after the explosion of the Macondo rig, when research vessels could not approach the area surrounding the well. The UCM concentrations followed a similar pattern observed for the *n*-alkanes with a more prominent increase from May to September, and a huge peak in November 2010, and a progressive decrease afterwards (**Figure 2.2B**).

3.1.2. Petroleum Biomarkers

The terpane, hopane and sterane series were determined in the GC-MS data by monitoring m/z 191 and 217 + 218, respectively. Petroleum-related hopanes are resistant to environmental alteration and, therefore, can be used to detect oil input in recent sediments even after fairly extensive degradation has occurred, and/or in the presence of an overwhelming abundance of biogenic compounds (Bouloubassi et al., 2001). Their composition is usually characteristic for sources of petroleum allowing for their use as a source identifier of petroleum inputs (Peters and Moldowan, 1993). Hopanes were the most abundant petroleum biomarker series analyzed ranging from C_{27} to C_{35} (**Table 2.S1**). The major identified compounds had the thermodynamically stable $17\alpha(H)$,21 $\beta(H)$ configuration, maximizing at the C30 homologue, supporting the petrogenic origin of the hydrocarbons of those sites (Philp, 1985; Peters and Moldowan, 1993). Extended hopanes ($C \ge 31$) were also present as pairs of the C-22 diastereoisomers (22R, 22S), which also typifies petrogenic material (Aboul-Kassim and Simoneit, 1996). The total hopane concentrations ranged between 36 and 1572 ng g⁻¹ (**Table 2.1**). The presence of the tricyclic terpanes (ranging from C_{21} to C_{29}), an important geochemical

tracer occurring in most crude oils, and tetracyclic terpanes (from C_{24} to C_{29}), derivatives of hopanes (Aquino Neto et al., 1983), is a further indication for an input of oil derived hydrocarbons at these sites. Steranes and diasteranes are also useful biomarker indicators for petroleum input in urban coastal areas (e.g., Grimalt et al., 1990; Aboul-Kassim and Simoneit, 1996) and were detected in all samples analyzed. While diasteranes had 13β , 17α configuration, steranes were had mainly the 5α , 14β , 17β and minor 5α , 14α , 17α configurations, both occurring as 20S and 20R epimers. The total sterane concentrations in the study area ranged between 10 and 1128 ng g^{-1} (**Table 2.1**).

Identically to *n*-alkanes and UCM, higher concentrations for all petroleum biomarkers were observed in surface samples, especially for September and November 2010 collections particularly at stations close to the well (**Figure 2.2C**). Station #1 in November presented approximately 20 times more total petroleum biomarkers than subsurface sediments collected at this locale.

3.2. Organic Geochemical Ratios

In order to better understand the source, distribution and extent of biodegradation of the oil-derived compounds identified and quantified in the sediment samples collected from 2010 to 2013, we used specific biomarker ratios and carbon isotopic compositions. Geochemical ratios have been applied successfully to characterize and elucidate molecular changes in oil compounds subjected to various environmental processes (e.g., Aboul-Kassim and Simoneit, 1996; Natter et al., 2012).

3.2.1. Biomarker Ratios

Pristane (2,6,10,14-tetramethylpentadecane) and phytane (2,6,10,14-tetramethylhexadecane) are products of geologic alteration of phytol and other isoprenoidyl natural products, and are not primary constituents of most terrestrial biota (Peters and Moldowan, 1993). In uncontaminated sediments, the ratio pristane/phytane (Pr/Ph) is higher than 1, typically between 3 and 5 (Steinhauer and Boehm, 1992). Sediments had Pr/Ph ratios ranging from 0.94 to 2.2, with values lower than or close to 1 observed for samples collected in September and November 2010 (**Figure 2.3A**), indicating mainly an oil source.

The extent of biodegradation was determined using the individual concentrations of pristane/C₁₇ and phytane/C₁₈ since bacteria generally attack n-alkanes before the isoprenoids pristane and phytane (Peters et al., 2005). It was clear that the oil that reached our sediment samples in September 2010 had been subjected to biodegradation to some extent reflected in the high ratios of both pristane/ C_{17} (**Figure 2.3B**) and phytane/ C_{18} (**Figure 2.3C**). In November 2010, though, when the highest concentrations were observed for all petroleum biomarkers, both ratios strongly decreased to values similar to those found in the subsequent collections. This result indicates that further degraded oil was collected by the end of 2010 with the posterior biodegradation of pristane and phytane following the n-alkanes. Since isoprenoids are subject to removal as degradation advances, we used specific petroleum biomarkers as parameters for identifying source correlations of oil compounds as cyclic biomarkers resist biodegradation (Peters et al., 2005). Biomarker ratios of selected parameters (e.g., Ts/Tm, 24Tri/23Tri, C29/C30) have been used to correlate solvent extracts of oiled samples with BP crude oil (Rosenbauer et al., 2010; Natter et al., 2012). Unfortunately, we did not have access to initial BP crude oil, therefore we used parameter ratios of selected biomarkers associated with initial BP

crude oil available in the literature. The ratios of selected parameters of m/z 191 terpane and hopane biomarkers agreed well with those found in Natter et al. (2012) for both BP crude oil and sediment samples. Ts/Tm (Ts/Tm = 18α -22,29,30-trisnorneohopane/ 17α -22,29,30-trisnorhopane) ratios of our samples varied from 0.687 to 1.086 for surface, and from 0.466 to 1.543 for subsurface sediments (see individual compound concentrations in **Tables 2.S1** and **2.S2**). The closest values to initial BP crude oil ratio (1.070; Natter et al., 2012) were found in surface samples collected in September and November 2010 (Ts/Tm = 1.024 on average, **Figure 2.4A**). Lower ratios compared to BP crude oil were observed for other time collections similar to sediments analyzed by Natter et al. (2012). Similar results were obtained for 24Tri/23Tri (24Tri/23Tri = C24 tricyclic terpane/C23 tricyclic terpane), $C29/C30 \text{ (C}29/C30 = 17\alpha,21\beta(\text{H})-12\alpha,21$ 30-norhopane/ 17α ,21 β (H)-hopane) and 35S/34S (35S/34S = 17α ,21 β (H)-pentakishomohopane $(22S)/17\alpha$, 21β (H)-tetrakishomohopane (22S)) ratios presenting values more similar to BP crude oil in the fall of 2010 (Figures 2.4B,C,D, respectively). These biomarker ratios indicate BP crude oil as a likely source for the apparent input of oil-derived compounds to our sediments observed in September and November 2010.

3.2.2. Carbon Isotopic Composition

Stable (δ^{13} C) and radiocarbon (Δ^{14} C) isotopic measurements were conducted in sediments in order to better elucidate source inputs to these samples. Before the spill, the likely sources of organic matter to the seafloor included recent photosynthetic production at the surface, sediments and POC from Mississippi and Atchafalaya Rivers, organic materials from natural seeps, and material from upslope that was advected downward (Chanton et al., 2015). After the Macondo blowout, this natural background sediment organic matter was superimposed

by an overlying layer of sediment containing fossil petrocarbon. BP MC252 oil has a δ^{13} C value of $-27 \pm 0.2\%$ (Natter et al., 2012), comparable to other reported values (-26.6 to -33.0%) of crude oils from different reservoir rocks in the Gulf of Mexico (Stahl, 1977; Macko et al., 1981), as well as with the values observed in sediments sampled at GC600, a natural seep (-26.5 \pm 0.8%), measured in this study. Sediment isotopic values varied from $\delta^{13}C = -20.3$ to -23.1% and Δ^{14} C = -144.2 to -484.5‰ in the 0-3 cm interval (**Table 2.1**). The mean value for surface samples is $\delta^{13}C = -21.3\%$ which is identical to the mean value reported for Gulf sediments by Chanton et al. (2015), but slightly enriched relative to the values found in station #1 in September and November 2010 (δ^{13} C = -23.1%). As mentioned previously, these samples presented higher concentrations of petroleum biomarkers (Figure 2.2), which could explain the relatively more depleted δ^{13} C values. However, this is difficult to affirm due to other OC sources potentially influencing the isotopic composition of these samples. For example, POC associated with the outflow from the Mississippi River has been reported to range from $\delta^{13}C = -23.3$ to -26.0% (Roseinheim et al., 2016), masking the oil signatures. ¹⁴C is a more powerful tool to trace oil input to the sediments than stable isotope composition because of the greater range in ¹⁴C composition between oil and potentially more modern natural sources of carbon to the sediments. In fact, the most depleted Δ^{14} C values were observed in September and November 2010 surface samples at stations closer to the well (#1 and #2, **Table 2.1**). Whereas the mean value for Δ^{14} C previous and after the fall 2010 collections is -220.9\%, surface sediments collected in September and November 2010 at those stations had Δ^{14} C ranging from -210.1 to -484.5% (-281.6% on average). These values are more depleted than those reported for the Mississippi River POC $(\Delta^{14}\text{C} - 86 \text{ to } -223\%)$, Roseinheim et al., 2016) as well as for the subsurface sediments (mean Δ^{14} C -269‰) (**Table 2.1**). These results indicate the deposition of radiocarbon depleted

petrocarbon within the 0-3 cm interval in the fall 2010 especially at stations closer to the well, corroborating the hydrocarbon data.

3.3. Temporal Changes in Hydrocarbon Distribution and Levels in the Gulf Sediments

Our data showed that there was a prominent input of oil-derived compounds to the sediments located to the northwest of the Macondo well in 2010. Our collections captured a progressive increase in concentrations of *n*-alkanes, UCM and the petroleum biomarkers (terpanes, hopanes and steranes) from May to September 2010, peaking in November 2010 at stations closer to the well. Interestingly, hydrocarbon levels in May 2010 (sediments sampled approximately 20 days after the accident) were comparable to those observed for collections conducted in 2011 to 2013. This may be due to the fact that we could not approach the well at that time for seafloor sediment collection. The biomarker results were corroborated by more depleted $\Delta^{14}C$ values indicating petrocarbon inputs to the same surface samples and biomarker ratios similar to those of the initial MC252 crude oil reported in the literature. Since a deep subsurface layer of oil was first reported in May to the northwest of the well (Camilli et al., 2010; Schrope, 2010), our results indicate that at least part of this oil plume sedimented on the seafloor in the subsequent months being reflected in our results in September (when a ~5-cm fresh flocculated layer was visible on the top of our cores collected in the NW of the well, probably a result of sinking oil-particle aggregates; Ziervogel et al., 2014), and in November, reflecting the accumulation of an apparent oil deposition by the end of 2010. In the following collection conducted in July 2011, oil-derived biomarker concentrations strongly decreased and geochemical parameter signatures of oil inputs were not as clear as before. Not even a more pronounced UCM was observed as would be expected in the subsequent years as biodegradation advances with time. Bottom nepheloid layers (BNLs) in the deep sea transport and remobilize considerable amounts of particulate matter (Ziervogel et al., 2015). Such resuspension had been proposed as a possible mechanism for the redistribution of sedimented oil-fallout after the Deepwater Horizon spill (Ziervogel et al., 2015), thus diluting its signature. In addition, overlying deposition of OC from multiple sources (e.g., Mississippi River, algal blooms, etc.) makes the understanding on the fate of Macondo oil on surface sediments even more challenging.

4. Conclusions

Collectively, our results showed increasing concentrations of oil-derived compounds in surface samples collected in the NW of the Macondo well approximately 5 months after the blowout. The subsurface oil plume observed in the first stages of the spill seemed to start sedimenting on the seafloor by September 2010 increasing the concentrations of n-alkanes, petroleum biomarkers, UCM, and total organic carbon contents with the concomitant depletion of Δ^{14} C values. These parameters peaked by late November indicating that oil-particle aggregates continued to settle in the fall 2010. However, a different scenario was observed for the subsequent collections in July 2011-2013 with a strong dilution of petrocarbon signatures in the surface sediments including oil-derived biomarker concentrations and isotopic data, presenting values much closer to those observed in May 2010 and subsurface sediments. Strong resuspension and lateral transport in the deep sea may be the primary cause for the redistribution of sedimented oil fallout from the Macondo spill.

Figures and Tables

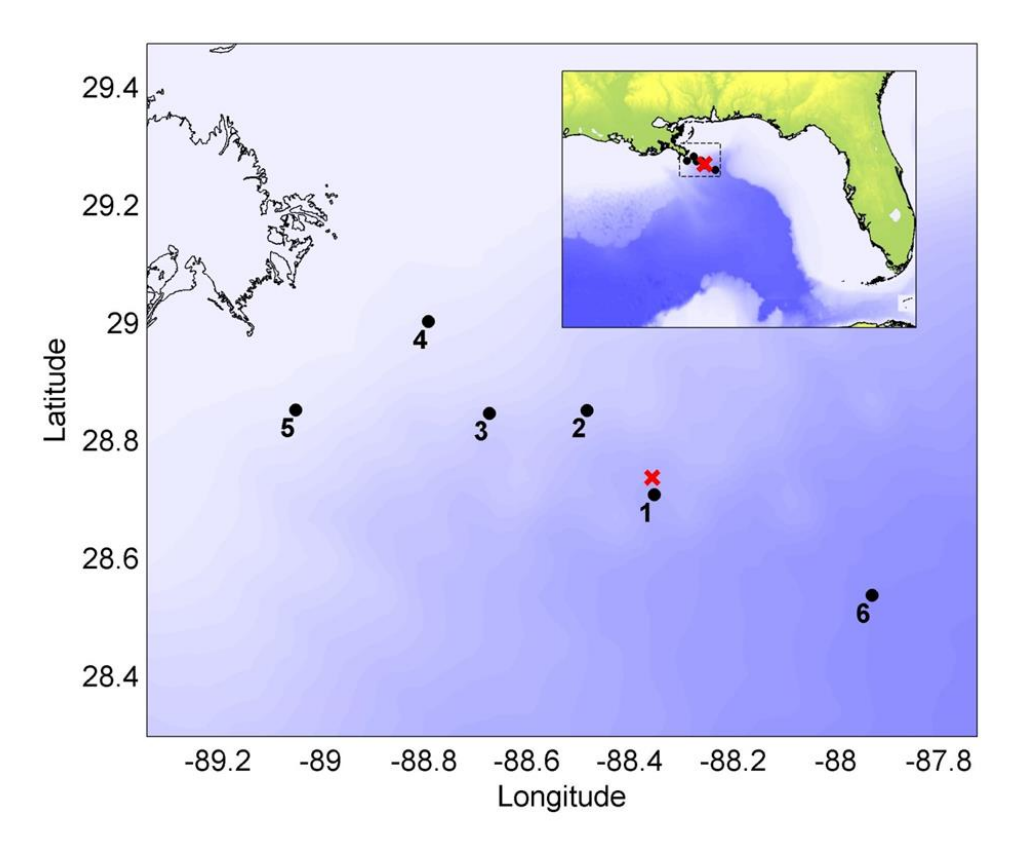


Figure 2.1. Location of sediment samples collected during multiple cruises in the northern Gulf of Mexico: May, September, and late November 2010, July 2011, 2012, and 2013. Red cross shows location of Macondo well blowout.

Table 2.1. Total aliphatics and petroleum biomarkers, and bulk measurements for surface and subsurface sediments collected in the Gulf of Mexico from 2010 to 2013.

	Aliphatics				Petro	Petroleum Biomarkers			Bulk measurements		
Month/Year-Station	<i>n</i> -Alkanes	CPI ^a	$C_{\text{max}}^{}b}$	UCM^{c}	Terpanes	Hopanes	Steranes	OC	$\delta^{13}C$	Δ^{14} C	
Surface sediments	$(ng g^{-1})$			$(\mu g g^{-1})$	$(ng g^{-1})$	$(ng g^{-1})$	$(ng g^{-1})$	(%)	(‰)	(‰)	
May/2010 - #2	1765.2	2.7	C_{31}	32161	27.2	277.0	84.1	1.9	-20.8	-179.4	
May/2010 - #3	864.7	2.5	C_{31}	18541	5.3	86.9	19.4	1.0	-20.4	-207.7	
May/2010 - #4	1604.4	2.5	C_{31}	26417	29.6	258.2	75.1	1.5	-20.8	-192.8	
May/2010 - #5	1155.6	2.7	C_{31}	16134	11.9	148.8	38.4	1.2	-20.5	-221.5	
September/2010 - #1	2440.3	1.8	C_{31}	84679	61.2	399.1	168.3	1.4	-23.1	-290.4	
September/2010 - #2	1825.3	1.3	C_{31}	54341	39.4	262.6	136.0	1.6	-21.3	-311.4	
September/2010 - #3	1230.6	2.0	C_{31}	93175	37.0	266.7	143.0	2.2	-21.2	-267.5	
September/2010 - #4	1538.3	2.4	C_{31}	63259	46.5	349.0	118.6	1.9	-22.1	-216.4	
September/2010 - #5	1731.4	2.5	C_{31}	66972	49.9	374.7	149.1	1.8	-22.3	-225.6	
September/2010 - #6	489.5	1.9	C_{31}	5452	5.0	46.0	9.6	1.2	-20.8	-246.5	
November/2010 - #1	6158.9	1.1	C_{33}	461241	338.0	1572.2	1128.1	1.8	-23.1	-484.5	
November/2010 - #2	3456.8	1.8	C_{31}	217990	146.2	793.0	444.8	1.8	-21.1	-210.1	
November/2010 - #3	3156.3	1.8	C_{31}	105779	81.2	694.3	273.3	1.5	-21.7	na^d	
November/2010 - #4	2501.8	1.4	C_{31}	65441	47.2	347.8	201.0	1.6	-21.1	na	
July/2011 - #1	2006.3	1.4	C_{31}	89931	70.4	291.4	184.0	1.1	-21.3	-276.4	
July/2011 - #2	865.8	3.0	C_{31}	170599	64.3	199.9	100.2	2.0	-21.5	-219.5	
July/2011 - #6	534.4	4.1	C_{29}	10894	12.6	62.3	17.7	1.2	-21.1	na	
July/2012 - #1	2765.0	2.8	C_{29}	118567	92.8	316.9	92.4	1.0	-20.7	-273.8	
July/2012 - #2	1622.3	2.0	C_{31}	80302	51.5	251.6	98.9	1.1	-20.3	-187.6	
July/2012 - #3	1334.6	2.8	C_{29}	34461	29.2	122.8	37.6	1.0	-20.4	na	
July/2013 - #1	3063.6	1.5	C_{31}	132544	85.2	424.7	225.7	2.1	-21.0	-209.8	
July/2013 - #2	1372.1	5.0	C_{29}	102854	50.6	387.1	162.1	1.2	-21.6	-185.1	
July/2013 - #3	1216.0	3.4	C_{31}	26247	31.2	242.8	132.4	1.3	-21.8	-196.8	

July/2013 - #6	639.3	3.9	C_{29}	19764	18.2	92.8	42.1	1.1	-21.1	-144.2
Subsurface sediments										
May/2010 - #2	1415.6	3.2	C_{31}	8877	5.1	77.6	25.1	1.3	-21.0	na
May/2010 - #3	940.8	3.9	C_{31}	4879	4.2	44.4	17.7	1.1	-20.4	na
May/2010 - #4	1320.3	3.1	C_{31}	9649	8.3	78.7	24.3	1.2	-20.8	na
May/2010 - #5	1249.5	3.0	C_{31}	8877	5.1	78.4	25.1	1.1	-20.5	na
September/2010 - #1	608.8	2.1	C_{31}	53387	34.4	273.4	96.4	1.6	-20.6	-265.8
September/2010 - #2	689.8	3.4	C_{31}	46328	16.6	188.9	57.2	1.5	-21.2	na
September/2010 - #3	1414.7	3.4	C_{31}	33936	23.9	144.1	66.7	1.8	-21.0	na
September/2010 - #4	957.0	3.4	C_{31}	16501	16.7	76.4	26.7	1.5	-21.4	na
September/2010 - #5	1217.6	4.3	C_{31}	18703	11.5	87.1	34.0	1.7	-22.3	na
September/2010 - #6	942.8	2.5	C_{31}	5327	1.9	35.5	10.3	1.2	-20.2	na
November/2010 - #1	1004.8	2.5	C_{31}	49841	37.2	158.6	66.0	1.6	-21.1	-271.3
November/2010 - #2	639.9	3.5	C_{31}	25637	20.7	102.1	27.7	1.4	-20.9	na
July/2011 - #1	480.1	3.0	C_{29}	26131	21.8	90.7	73.5	1.1	-20.5	na
July/2011 - #2	394.0	4.5	C_{27}	5963	15.9	39.3	53.1	1.2	-21.3	na
July/2011 - #6	432.4	5.3	C_{29}	10894	12.0	46.7	41.2	0.9	-20.6	na
July/2012 - #1	476.8	2.4	C_{29}	7241	8.7	46.4	42.5	1.0	-20.7	na
July/2012 - #2	324.7	4.3	C_{29}	5985	16.2	53.6	38.4	1.1	-20.2	na
July/2012 - #3	425.2	2.7	C_{29}	4657	10.3	43.6	41.2	1.2	-20.6	na
July/2013 - #1	1070.9	3.4	C_{29}	53438	33.3	226.2	119.4	1.6	-20.7	na
July/2013 - #2	667.1	3.9	C_{29}	29764	21.5	163.5	51.0	1.5	-21.7	na
July/2013 - #6	399.1	4.7	C_{29}	9750	15.9	67.3	49.6	0.9	-20.7	na

 $^{^{}a}Carbon\ Preference\ Index\ -\ CPI_{23-38;}\ ^{b}C_{max}=dominant\ peak;\ ^{c}UCM=Unresolved\ Complex\ Mixture.$

 $^{^{}d}$ na = not analyzed.

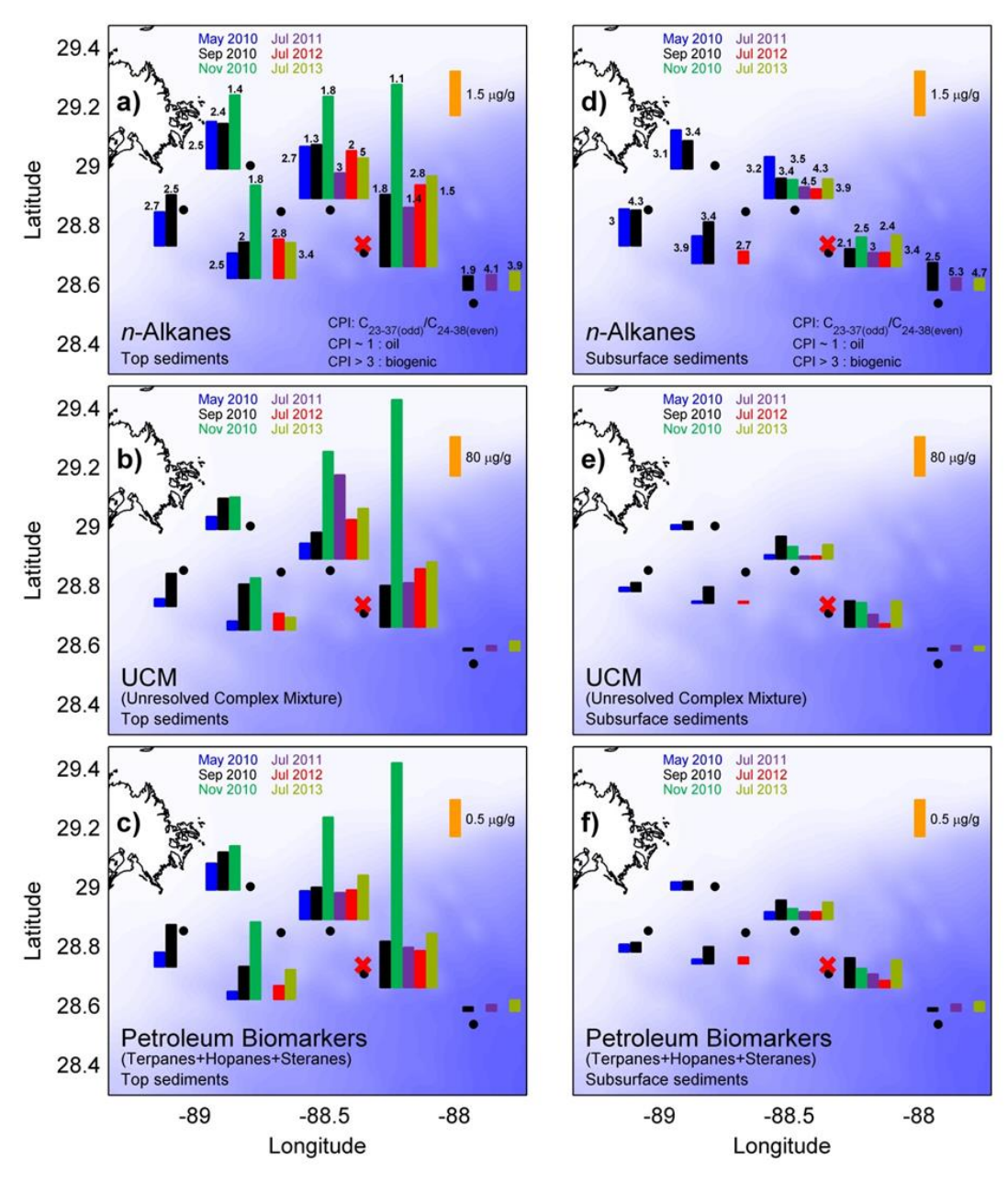


Figure 2.2. Total concentrations of *n*-alkanes, UCM, and petroleum biomarkers in surface and subsurface sediments in the Gulf of Mexico. Bars are color coded according with timing of sampling. Scale is shown on the top right corner of each panel in orange. Numbers on top panels are CPIs, which are defined on the bottom right corner of the top panels. Red cross shows location of Macondo well blowout.

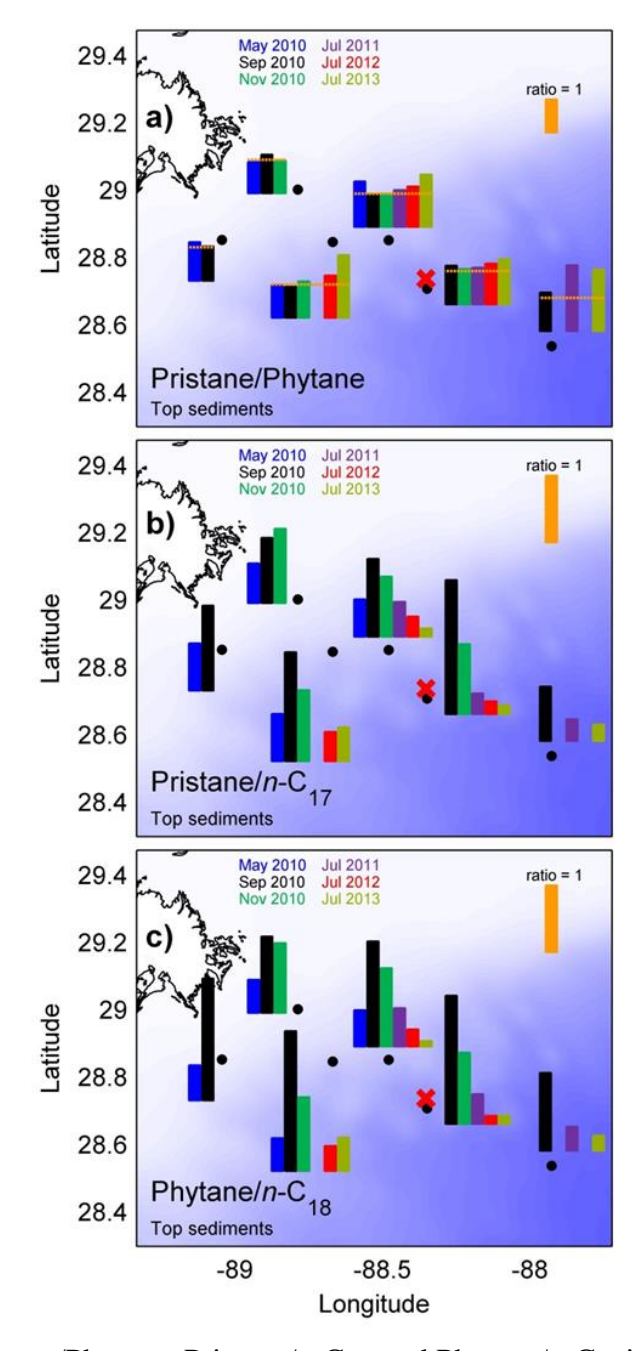


Figure 2.3. Ratios Pristane/Phytane, Pristane/n- C_{17} , and Phytane/n- C_{18} in top sediments in the Gulf of Mexico. Bars are color coded according with timing of sampling. Scale is shown on the top right corner of each panel in orange. Horizontal line on top panel indicates a ratio = 1. Red cross shows location of Macondo well blowout.

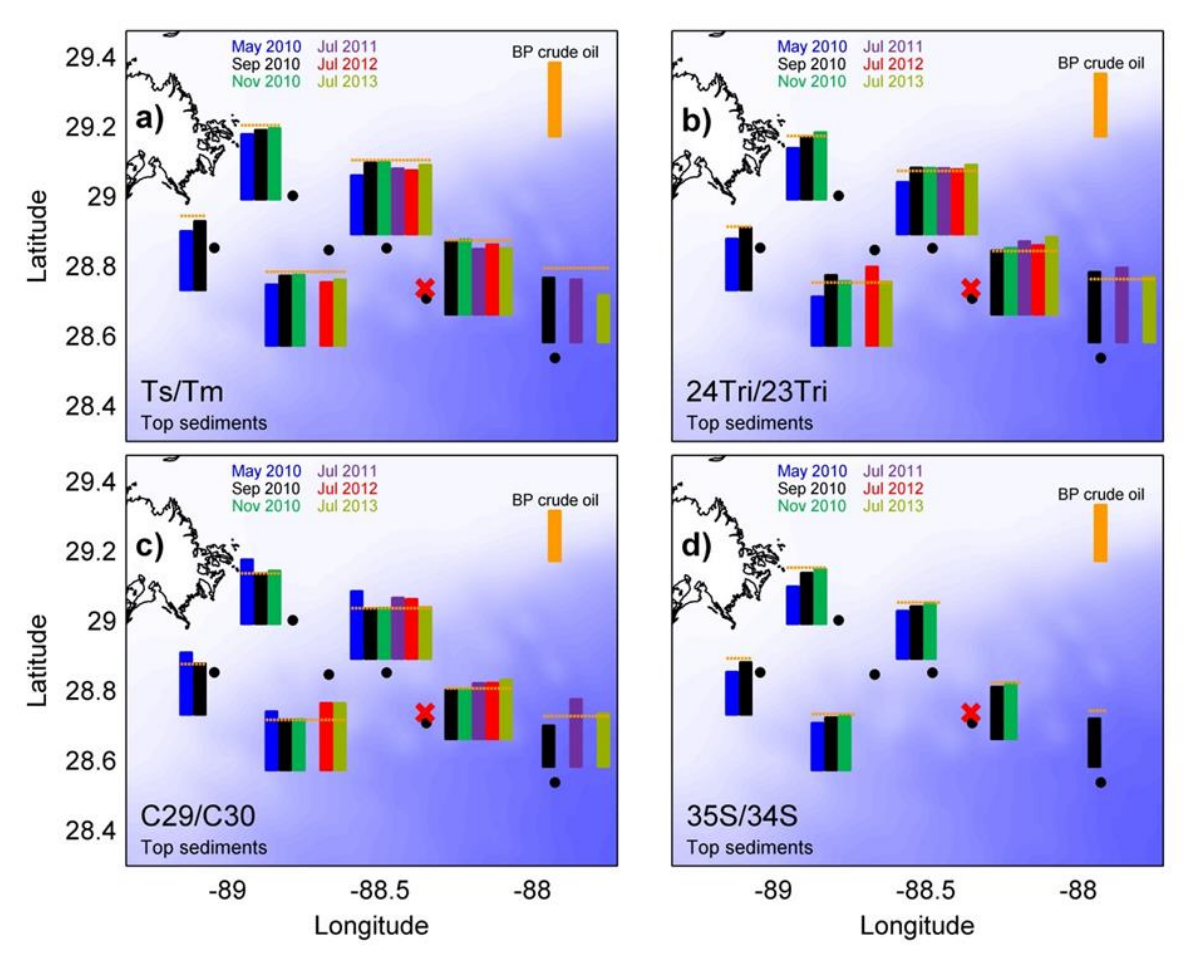


Figure 2.4. Ratios Ts/Tm (18α(H)-22,29,30-trisnorneohopane/17α-22,29,30-trisnorhopane), 24Tri/23Tri (C24 tricyclic terpane/C23 tricyclic terpane), C29/C30 (17α,21β(H)-norhopane/17α,21β(H)-hopane) and 35S/34S (17α,21β(H)-pentakishomohopane (22S)/17α,21β(H)-tetrakishomohopane (22S)) in top sediments in the Gulf of Mexico. Bars are color coded according with timing of sampling. Scale shown on the top right corner of each panel in orange indicates characteristic value of BP crude oil (Natter et al., 2012). Horizontal orange line in each panel also indicates the characteristic value of BP crude oil for reference. Red cross shows location of Macondo well blowout.

Acknowledgements

We thank the captain and the crew of the *R/V* Pelican, Oceanus, Atlantis, and Endeavor as well as J. Montoya for their valuable help during the sampling campaigns. S. Bosman is acknowledged for assisting with the isotopic measurements. This research was supported by the Gulf of Mexico Research Initiative by funding provided to the consortium 'Ecosystem Impacts of Oil and Gas Inputs to the Gulf' (ECOGIG) and the National Science Foundation (OCE-1057683).

References

- Aboul-Kassim, T.A.T., Simoneit, B.R.T. Lipid geochemistry of superficial sediments from the coastal environment of Egypt: I. Aliphatic hydrocarbons characterization and sources. *Mar. Chem.* **1996**, 54, 135–158.
- Aquino Neto, F.R., Trendel, J.M., Restle, A., Connan, J., Albrecht, P. Occurrence and formation of tricyclic and tetracyclic terpanes in sediments and petroleum. In: Bjorøy, M. et al. (Eds.), Advances in Organic Geochemistry 1981. Wiley, Chichester, **1983**, p. 676–695.
- Bianchi, T.S., Osburn, C., Shields, M.R., Yvon-Lewis, S., Young, J., Guo, L., Zhou, Z. Deepwater Horizon oil in the Gulf of Mexico waters after 2 years: Transformation into the dissolved organic matter pool. *Environ. Sci. Technol.* **2014**, 48, 9288-9297.
- Boehm, P.D., Fiest, D.L. Subsurface distributions of petroleum from an offshore well blowout: The Ixtoc I blowout, Bay of Campeche. *Environ. Sci. Technol.* **1982**, 16, 67-74.
- Bouloubassi, I., Fillaux, J., Saliot, A. Hydrocarbons in surface sediments from the Changjiang (Yangtze River) Estuary, East China Sea. *Mar. Pollut. Bull.* **2001**, 42, 1335–1346.
- Camilli, R., Reddy, C.M., Yoerger, D.R., Van Mooy, B.A.S., Jakuba, M.V., Kinsey, J.C., McIntyre, C.P., Sylva, S.P., Maloney, J.V. Tracking hydrocarbon plume transport and biodegradation at Deepwater Horizon. *Science* **2010**, 330, 201-204.
- Chanton, J., Zhao, T., Resenheim, B.E., Joye, S., Bosman, S., Brunner, C., Yeager, K.M., Diercks, A.R., Hollande, D. Using natural abundance radiocarbon to trace the flux of petrocarbon to the seafloor following the Deepwater Horizon oil spill. *Environ. Sci. Technol.* **2015**, 49, 847-854.
- Eglinton, G., Hamilton, R.J. Leaf epicuticular waxes. Science 1967,156, 1322–1335.
- Grimalt, J., Olive, I., Gbmez-Behnchon, J.I. Assessment of organic source contributions in coastal waters by principal component and factor analysis of the dissolved and particulate hydrocarbon and fatty acid contents. *Int. J. Environ. Anal. Chem.* **1990**, 28, 305-320.
- Hedges, J.I. and Prahl, F.G., 1993. Early diagenesis: consequences
- Harvey, G.R., Requejo, A.G., McGillivary, P.A., Tokar, J.M. Observation of a subsurface oilrich layer in the open ocean. *Science* **1979**, 205, 999-1001.

- Hazen, T.C., Dubinsky, E.A., DeSantis, T.Z., Andersen, G.L., Piceno, Y.M., Singh, N., plus 26 co-authors. Deep-sea oil plume enriches indigenous oil-degrading bacteria. *Science* **2010**, 330, 204-208.
- Jernelöv, A., Lindén, O. Ixtoc I: A case study of the world's largest oil spill. *Ambio* **1981**, 10, 299-306.
- Johansen, O., Rye, H., Cooper, C. DeepSpill-field study of a simulated oil and gas blowout in deep water. *Spill Sci. Technol. Bull.* **2003**, 8, 433-443.
- Joye, S.B., Teske, A.P., Kotska, J.E. Microbial dynamics following the Macondo oil well blowout across Gulf of Mexico environments. *BioScience* **2014**, 64, 766-777.
- Kleindienst, S., Seidel, M., Ziervogel, K., Grim, S.L., Loftis, K.M., Perkins, M.J., Field, J.A., Sogin, M., Dittmar, T., Passow, U., Medeiros, P.M., Joye, S.B. Chemical dispersants suppress the activity of natural oil-degrading microorganisms. *Proceed. Nat. Acad. Sci.* **2015**, 112, 14900-14905.
- MacDonald, I.R. Natural oil spills. Sci. Amer. 1998, 279, 51-66.
- Macko, S., Parker, P., Botello, A. Persistence of spilled oil in a Texas salt marsh. *Environ. Pollut.* **1981**, 2, 119–128.
- Mazurek, M., Simoneit, B.R.T. Characterization of biogenic and petroleum derived organic matter in aerosols over remote, rural and urban areas. In: Keith LH, editor. *Identification and analysis of organic pollutants in air*. Woburn, MA, Ann Arbor Science/Butterworth, **1984**. p. 353–370.
- Medeiros, P.M., Bícego, M.C., Castelao, R.M., Del Rosso, C., Filmann, G., Zamboni, A.J. Natural and anthropogenic hydrocarbon inputs to sediments of Patos Lagoon Estuary, Brazil. *Environ. Internat.* **2005**, 31, 77-87.
- Natter, M., Keevan, J., Wang, Y., Keimowitz, A.R., Okeke, B.C., Son, A., Lee, M-K. Level and degradation of Deepwater Horizon spilled oil in coastal marsh sediments and pore-water. *Environ. Sci. Technol.* **2012**, 46, 5744-5755.
- NRC (National Research Council). *Oil in the Sea III: Inputs, Fates, and Effects*. Washington, D.C., National Academies Press, **2002**.
- NRC (National Research Council). *Oil Spill Dispersants: Efficacy and Effects*. Washington, D.C., National Academies Press, **2005**.
- Peters, K.E., Moldowan, J.M. *The biomarker guide. Interpreting molecular fossils in petroleum and ancient sediments.* Englewood Cliffs (NJ), Prentice Hall, **1993**. 363 p.

- Peters, K.E., Walters, C.C., Moldowan, J.M. Biomarkers in the environment. *In: The Biomarker Guide. Biomarkers and Isotopes in the Environment and Human History*. Volume 1. 2nd Ed., Cambridge University Press, **2005**, p. 274-321.
- Philp, R.P. Fossil fuel biomarkers. Methods in Geochemistry and Geophysics, vol. 23. New York, Elsevier, **1985**, 292 p.
- Rosenheim, B. E., Pendergraft, M. A., Flowers, G. C., Carney, R., Sericano, J., Amer, R. M., Chanton, J., Dincer, Z., Wade, T. Employing extant stable carbon isotope data in Gulf of Mexico sedimentary organic matter for oil spill studies. *Deep-Sea Res. II* **2016**, in press.
- Rosenbauer, R.J., Campbell, P.L., Lam, A., Lorenson, T.D., Hostettler, F.D., Thomas, B., Wong, F.L. Reconnaissance of Macondo-1 well oil sediment and tarballs from the northern Gulf of Mexico shoreline, Texas to Florida. USGS A preliminary report to the U.S. Coast Guard. **2010**, 1-22.
- Schmidt, C.W. Between the devil and the deep blue sea. Dispersants in the Gulf of Mexico. *Environ. Health Perspec.* **2010**, 118, A338-A344.
- Schrope, M. Oil cruise finds deep-sea plume. *Nature* **2010**, 465, 274-275.
- Seidel, M., Kleindienst, S., Dittmar, T., Joye, S.B., Medeiros, P.M. Influence of dispersants on the biodegradation of crude oil in deep sea water from the Gulf of Mexico: Insights from ultrahigh resolution mass spectrometry. *Deep Sea Res. II* **2016**, in press.
- Stahl, W. Carbon and nitrogen isotopes in hydrocarbon research and exploration. *Chem. Geol.* **1977**, 20, 121–149.
- Steinhauer, M.S., Boehm, P.D. The composition and distribution of saturated and aromatic hydrocarbons in nearshore sediments, river sediments, and coastal peat of Alaskan Beaufort Sea: implications for detecting anthropogenic hydrocarbon inputs. *Mar. Environ. Res.* **1992**, 33, 223–253.
- UNEP (United Nations Environment Programme). *Determinations of petroleum hydrocarbons in sediments*. Reference Methods for Marine Pollution Studies **1991**, 20, 97 p.
- Valentine, D.L., Kessler, J.D., Redmond, M.C., Mendes, S.D., Heintz, M.B., Farwell, C., Hu, L., Kinnaman, F.S., Yvon-Lewis, S., Du, M., Chan, E.W., Tigreros, F.G., Villanueva, C.J. Propane respiration jump-starts microbial response to a deep oil spill. *Science* **2010**, 330, 208-211.
- Ziervogel, K., Joye, S.B., Arnosti, C. Microbial enzymatic activity and secondary production in sediments affected by the sedimentation pulse following the Deepwater Horizon oil spill. *Deep Sea Res. II* **2014**, in press.

Ziervogel, K., Dike, C., Asper, V., Montoya, J., Battles, J., D'souza, N., Passow, U., Diercks, A., Esch, M., Joye, S., Dewald, C., Arnosti, C. Enhanced particle fluxes and heterotrophic bacterial activities in Gulf of Mexico bottom waters following storm-induced sediment resuspension. *Deep Sea Res. II* 2015, in press.

SUPPORTING INFORMATION

HYDROCARBON COMPOSITION AND LEVELS IN THE GULF SEDIMENTS WITHIN 3 ${\bf YEARS~FOLLOWING~THE~MACONDO~WELL~BLOWOUT}^1$

¹Babcock-Adams, L., Chanton, J. P., Joye, S. B. & Medeiros, P. M. To be submitted to *Environ*. *Sci. Technol*.

Table 2.S1a. Concentration (ng g⁻¹) of aliphatic and petroleum biomarkers found in surface sediments collected in the Gulf of Mexico in 2010.

		May	2010				Sep	otember 2	010			Noveml	ber 2010	
Class	#2	#3	#4	#5	#1	#2	#3	#4	#5	#6	#1	#2	#3	#4
Individual compound														
n-Alkanes														
n-Decane	10.7	16.2	16.1	12.3	14.5	16.1	17.8	12.4	18.4	5.4	-	-	-	-
n-Heneidecane	17.4	17.5	21.9	28.1	16.4	17.7	11.6	7.9	12.7	5.5	-	-	-	-
n-Dodecane	18.3	16.6	25.9	29.2	16.5	18.1	11.4	11.9	12.2	5.2	9.4	-	-	-
n-Tridecane	16.9	13.7	18.5	19.4	14.3	17.1	10.0	11.4	10.5	4.1	15.4	10.0	25.4	28.2
n-Tetradecane	28.0	28.1	39.1	39.7	27.1	24.6	21.2	18.7	18.6	8.5	20.9	19.3	38.2	35.7
n-Pentadecane	24.5	19.8	35.7	28.0	44.7	27.2	26.1	21.1	30.4	8.0	41.0	35.3	55.8	28.3
n-Hexadecane	14.0	13.3	26.6	18.9	21.1	22.6	18.0	13.0	13.4	4.1	68.3	74.5	32.2	33.7
n-Heptadecane	16.8	14.6	26.5	16.8	30.3	22.1	20.7	12.9	20.3	3.6	148.4	101.9	67.4	33.2
Pristane	9.5	10.4	15.8	11.9	60.5	25.7	33.7	12.7	25.8	2.9	155.4	91.9	71.6	36.8
n-Octadecane	11.8	10.1	18.2	12.9	23.2	16.8	17.2	9.5	13.7	2.1	136.7	80.0	59.3	35.9
Phytane	6.5	5.0	9.1	6.8	44.4	26.3	35.8	10.9	24.9	2.5	146.0	93.7	65.5	37.4
n -Nonadecane	14.0	11.1	16.9	13.2	28.8	31.0	12.1	16.8	16.1	3.6	106.7	55.9	39.9	41.9
n -Eicosane	23.2	13.8	38.9	19.8	34.8	44.0	18.8	18.6	14.4	9.4	91.7	57.4	45.9	55.1
n-Heneicosane	22.8	14.2	19.7	22.9	37.1	41.6	19.7	27.8	31.9	6.7	76.4	78.1	48.2	52.7
n-Docosane	27.4	17.0	20.8	19.7	46.4	54.6	23.5	34.5	34.1	15.9	57.2	75.2	57.5	65.7
n-Tricosane	41.3	20.2	28.6	26.1	48.0	62.2	24.4	42.8	41.1	10.5	80.8	83.0	59.1	73.3
n-Tetracosane	33.8	14.4	23.2	18.5	43.4	58.0	19.6	56.3	39.1	8.4	74.2	76.0	54.5	68.9
n-Pentacosane	63.4	28.6	48.5	38.3	71.5	60.9	41.4	56.5	72.3	12.9	108.6	120.8	82.6	72.0
n-Hexacosane	39.7	18.6	28.7	24.8	67.4	65.9	27.8	26.7	32.1	12.7	121.8	92.5	78.5	76.8
n-Heptacosane	113.2	55.7	94.6	75.3	127.6	77.8	74.5	118.4	134.2	29.8	157.0	267.1	238.7	88.9
n -Octacosane	70.8	28.7	51.7	40.2	94.0	78.0	40.0	80.5	68.8	20.4	133.6	157.5	105.4	88.8
n -Nonacosane	303.0	117.1	225.1	168.0	317.9	174.7	158.2	247.0	275.0	69.2	245.8	394.1	428.9	285.7
n -Triacontane	72.6	31.2	60.6	43.1	191.0	120.1	53.4	95.9	95.7	23.5	425.7	167.4	292.0	231.1
n -Hentriacontane	335.8	136.2	269.0	184.8	413.6	187.4	192.0	293.4	326.8	86.1	861.9	422.9	524.6	298.4
n -Dotriacontane	67.6	28.5	60.9	33.2	126.3	113.1	61.8	71.1	108.2	29.0	903.9	287.9	247.3	224.1
n-Tritriacontane	119.7	56.2	132.5	65.9	176.9	120.2	79.7	112.7	129.8	28.4	916.3	391.9	287.9	231.2
n-Tetratriacontane	39.4	21.5	43.8	24.8	111.0	94.5	53.7	25.4	27.8	15.0	658.0	226.9	111.0	104.7
n -Pentatriacontane	72.2	29.1	59.0	41.7	95.9	86.5	57.2	40.4	51.1	15.4	444.3	181.3	101.0	97.6
n -Hexatriacontane	41.8	22.4	43.9	25.8	64.1	71.1	42.3	16.1	27.1	12.0	254.7	-	75.2	82.2
n -Heptatriacontane	60.2	28.4	56.8	36.2	81.1	56.7	38.8	20.5	33.5	12.7	-	-	-	67.8
n -Octatriacontane	44.8	21.7	52.8	28.0	55.6	44.6	37.8	18.0	21.7	21.1	-	-	-	-
Total n-Alkanes	1765.2	864.7	1604.4	1155.6	2440.3	1825.3	1230.6	1538.3	1731.4	489.5	6158.9	3456.8	3156.3	2501.8
CPI ₍₂₃₋₃₈₎	2.7	2.5	2.5	2.7	1.8	1.3	2.0	2.4	2.5	1.9	1.1	1.8	1.8	1.4
(0)														

Tricyclic terpanes														
C ₂₁ -tricyclic	1.6	0.3	1.2	1.0	3.4	4.0	3.1	2.9	4.6	_	53.6	15.2	4.4	5.0
C ₂₃ -tricyclic	4.0	0.5	3.5	2.0	7.3	5.2	4.9	8.4	7.9	0.4	73.5	26.7	8.3	6.2
C ₂₄ -tricyclic	3.0	0.4	2.6	1.5	6.8	5.0	5.0	7.6	7.1	0.4	71.1	25.6	7.8	6.0
C ₂₅ -tricyclic	3.2	0.5	2.7	1.1	7.2	3.4	4.8	6.8	5.9	3.5	62.8	24.5	8.2	4.4
C ₂₆ -tricyclic (S)	3.5	0.4	4.4	1.0	8.4	3.5	2.9	3.4	5.3	-	41.5	18.0	9.4	5.5
C ₂₆ -tricyclic (R)	2.6	0.4	3.6	0.9	12.5	3.4	4.2	4.3	4.7	_	17.7	7.7	22.5	4.4
C ₂₈ -tricyclic (K)	1.1	0.4	0.9	0.5	1.3	1.1	2.0	2.1	1.8	_	-	-	2.3	2.1
C ₂₉ -tricyclic	1.1	0.2	1.7	1.0	1.2	1.7	2.3	0.9	2.5	0.2	-	_	2.2	2.1
Tetracyclic terpanes	1.9	0.4	1.7	1.0	1.2	1.7	2.3	0.9	2.3	0.2	-	-	2.2	-
-	3.2	1.3	5.5	1.4	9.4	7.9	3.1	6.9	7.0		12.5	28.5	10.4	8.9
C ₂₄ -tetracyclic										- 0.4				
C ₂₈ -tetracyclic	2.1	0.7	2.8	1.0	2.6	3.7	2.8	2.8	2.0	0.4	5.3	-	3.6	4.7
C ₂₉ -tetracyclic	1.0	0.2	0.7	0.5	1.1	0.5	2.1	0.5	1.1	0.2	-	-	2.1	-
Total Tri + Tetracyclic terpanes	27.2	5.3	29.6	11.9	61.2	39.4	37.0	46.5	49.9	5.0	338.0	146.2	81.2	47.2
Pentacyclic triterpanes or Hopanes														
18α(H)-22,29,30-Trisnorneohopane (Ts)	6.5	1.5	7.5	3.4	12.8	7.3	3.0	14.1	14.1	0.7	75.8	53.6	23.9	8.4
17α(H)-22,29,30-Trisnorhopane (Tm)	7.6	1.7	7.9	4.0	12.2	7.0	2.9	14.0	14.1	0.7	69.8	51.2	23.3	8.1
17α,21β(H)-Norhopane	54.5	10.8	49.5	26.6	57.5	49.9	40.1	54.3	66.3	5.6	273.8	138.7	118.6	59.8
17β,21α(H)-Norhopane	8.8	1.4	9.0	3.7	15.1	3.8	7.8	16.5	14.0	-	-	-	26.2	4.9
17α,21β(H)-Hopane	69.6	15.8	66.3	36.9	100.1	85.9	67.9	92.6	111.7	11.7	473.5	235.2	200.1	97.0
$17\alpha,21\beta(H)$ -Homohopane (22S)	32.6	7.6	29.0	16.2	45.9	24.2	30.7	37.1	38.5	5.2	165.1	72.3	56.8	35.2
$17\alpha,21\beta(H)$ -Homohopane (22R)	21.4	6.1	19.3	11.5	34.2	16.8	27.2	29.9	29.4	3.9	123.4	53.1	45.3	27.9
$17\alpha,21\beta(H)$ -Bishomohopane (22S)	18.0	6.1	18.5	11.1	26.8	15.7	24.6	26.3	24.7	3.3	105.3	43.6	37.9	26.8
$17\alpha,21\beta(H)$ -Bishomohopane (22R)	15.0	4.1	14.7	7.6	19.8	11.5	13.6	14.4	11.3	2.5	73.4	31.3	29.9	22.6
$17\alpha,21\beta(H)$ -Trishomohopane (22S)	14.2	8.6	13.2	10.2	19.7	14.3	13.3	12.6	13.6	2.8	69.6	27.2	29.8	25.4
$17\alpha,21\beta(H)$ -Trishomohopane (22R)	7.5	3.5	7.1	4.5	13.7	7.4	10.3	8.0	9.3	1.9	43.3	18.0	24.8	8.5
17α,21β(H)-Tetrakishomohopane (22S)	7.4	7.8	6.4	4.6	14.3	7.2	9.7	10.3	9.2	2.6	34.9	24.5	27.4	8.3
17α,21β(H)-Tetrakishomohopane (22R)	5.6	4.9	4.0	3.7	11.8	4.1	5.7	8.4	7.4	2.3	24.7	16.9	22.9	5.2
17α,21β(H)-Pentakishomohopane (22S)	5.2	5.4	3.5	2.9	10.8	5.5	7.5	7.7	7.0	1.8	28.5	19.8	21.9	6.6
17α,21β(H)-Pentakishomohopane (22R)	3.3	1.6	2.2	1.9	4.5	2.0	2.3	2.7	4.1	0.9	11.2	7.7	5.6	3.1
Total Pentacyclic triterpanes	277.0	86.9	258.2	148.8	399.1	262.6	266.7	349.0	374.7	46.0	1572.2	793.0	694.3	347.8
Steranes + Diasteranes														
13β,17α(H)-Diacholestane (20S)	6.2	1.0	5.2	2.4	13.8	7.1	7.5	8.7	13.7	_	49.6	20.1	24.9	8.2
$13\beta,17\alpha(H)$ -Diacholestane (20R)	3.3	0.6	3.0	1.3	9.2	4.6	3.2	5.5	7.2	_	28.4	13.2	10.3	5.7
$5\alpha,14\alpha,17\alpha(H)$ -Cholestane (20S)	7.6	1.9	5.2	3.0	13.7	7.3	9.3	8.1	8.5	_	47.1	16.4	24.8	8.4
13β,17α(H)-Ethyldiacholestane (20S)	12.1	2.1	9.2	4.9	26.3	20.9	21.9	17.9	23.5	1.4	207.4	94.7	37.4	31.8
$5\alpha,14\alpha,17\alpha(H)$ -Cholestane (20R)	1.6	0.7	4.9	1.1	3.9	3.1	3.5	2.4	4.7	-	57.3	10.0	4.8	4.2
- , , , (, ()														

$13\beta,17\alpha(H)$ -Ethyldiacholestane (20R)	8.9	1.8	7.8	3.6	15.1	17.7	20.1	11.8	15.1	1.4	177.6	75.0	26.2	28.8
$5\alpha,14\alpha,17\alpha(H)$ -Methylcholestane (20S)	4.9	0.9	3.0	2.3	8.4	6.3	5.1	8.7	8.1	0.7	19.5	11.0	9.5	7.4
$5\alpha,14\beta,17\beta(H)$ -Methylcholestane (20R)	3.5	0.8	3.0	1.7	8.1	8.5	6.8	5.1	6.6	0.5	69.7	22.5	9.2	9.6
$5\alpha,14\beta,17\beta(H)$ -Methylcholestane (20S)	6.2	0.9	4.5	3.0	11.2	8.0	7.5	8.7	9.7	0.7	61.2	24.0	22.3	9.1
$5\alpha,14\alpha,17\alpha(H)$ -Methylcholestane (20R)	1.9	0.9	2.0	1.4	4.3	5.4	4.9	2.9	5.1	0.4	40.5	14.5	5.4	6.5
$5\alpha,14\alpha,17\alpha(H)$ -Ethylcholestane (20S)	9.6	2.6	8.7	4.9	18.6	14.0	20.1	13.3	15.6	1.8	105.4	46.6	29.7	24.9
$5\alpha,14\beta,17\beta(H)$ -Ethylcholestane (20R)	7.7	2.1	8.1	3.9	14.0	11.7	12.6	12.1	12.2	1.2	105.1	40.6	24.9	22.8
$5\alpha,14\beta,17\beta(H)$ -Ethylcholestane (20S)	5.4	1.2	5.7	2.2	10.3	9.7	9.6	7.8	9.8	0.6	74.2	26.6	21.4	10.8
$5\alpha,14\alpha,17\alpha(H)$ -Ethylcholestane (20R)	5.0	2.1	4.9	2.6	11.4	11.8	11.1	5.9	9.4	0.9	85.0	29.7	22.5	22.9
Total Steranes + Diasteranes	84.1	19.4	75.1	38.4	168.3	136.0	143.0	118.6	149.1	9.6	1128.1	444.8	273.3	201.0
Total Petroleum Biomarkers	388.3	111.6	362.9	199.1	628.5	438.0	446.7	514.1	573.6	60.6	3038.3	1384.0	1048.7	596.0
UCM (Unresolved Complex Mixture, µg g ⁻¹)	32161	18541	26417	16134	84679	54341	93175	63259	66972	5452	461241	217990	105779	65441

Table 2.S1b. Concentration (ng g⁻¹) of aliphatic and petroleum biomarkers found in surface sediments collected in the Gulf of Mexico from 2011 to 2013.

		July 2011	<u> </u>		July 2012	,		July	2013	
Class	#1	#2	#6	#1	#2	#3	#1	#2	#3	#6
Individual compound										
n-Alkanes										
<i>n</i> -Tetradecane	-	-	-	-	-	-	94.5	-	-	-
<i>n</i> -Pentadecane	-	-	-	47.2	-	-	126.0	37.5	15.7	2.7
<i>n</i> -Hexadecane	22.3	20.6	6.6	136.1	28.7	20.2	128.9	86.2	18.9	14.6
<i>n</i> -Heptadecane	30.5	35.4	10.7	101.4	54.0	60.7	108.1	83.2	21.7	29.5
Pristane	9.6	18.6	3.6	19.9	16.5	27.0	14.9	10.8	11.1	7.4
<i>n</i> -Octadecane	19.3	29.0	4.9	128.2	51.7	55.7	84.0	78.4	11.6	17.2
Phytane	8.7	16.8	1.8	16.3	13.6	21.2	11.0	6.9	5.9	4.0
<i>n</i> -Nonadecane	16.2	18.2	10.8	131.0	46.0	64.3	57.2	44.0	29.2	29.1
<i>n</i> -Eicosane	23.6	17.6	18.5	140.3	52.1	71.7	122.0	63.9	28.6	61.9
n-Heneicosane	29.0	25.9	15.1	151.3	45.1	53.0	51.8	42.5	36.9	30.2
<i>n</i> -Docosane	32.2	21.6	12.2	119.7	53.4	52.2	40.9	31.3	32.6	23.4
<i>n</i> -Tricosane	38.4	24.5	20.0	101.9	41.1	48.2	45.4	45.3	35.5	30.9
<i>n</i> -Tetracosane	23.1	18.0	12.0	91.3	29.2	38.3	40.0	25.7	29.0	21.5
<i>n</i> -Pentacosane	40.8	34.4	29.4	150.6	45.8	66.1	101.2	73.5	45.4	35.1
<i>n</i> -Hexacosane	28.1	21.7	14.1	94.0	33.3	43.6	64.5	34.7	32.7	24.2
<i>n</i> -Heptacosane	88.9	84.8	61.9	264.2	94.7	115.8	168.4	142.6	95.8	65.2
<i>n</i> -Octacosane	46.4	29.6	23.9	99.7	45.2	50.3	113.8	35.6	38.6	15.9
<i>n</i> -Nonacosane	184.1	135.1	118.6	384.8	176.8	186.0	257.9	251.2	246.1	112.3
<i>n</i> -Triacontane	158.3	39.4	17.0	65.3	100.2	53.0	192.9	31.0	48.4	16.0
<i>n</i> -Hentriacontane	332.8	137.9	98.8	269.8	257.3	178.4	369.8	164.1	248.9	79.9
<i>n</i> -Dotriacontane	252.1	38.2	14.7	83.0	140.6	40.2	284.9	29.2	49.2	10.6
<i>n</i> -Tritriacontane	269.2	80.9	37.6	148.7	171.9	85.6	363.7	109.6	91.9	21.9
<i>n</i> -Tetratriacontane	174.0	27.3	7.5	53.5	89.0	27.3	209.2	-	38.3	-
<i>n</i> -Pentatriacontane	127.0	25.8	-	50.4	66.1	24.0	159.4	-	36.8	-

n -Hexatriacontane	70.1	-	-	-	-	-	99.5	-	-	-
Total n-Alkanes	2006.3	865.8	534.4	2765.0	1622.3	1334.6	3063.6	1372.1	1216.0	639.3
CPI ₍₂₃₋₃₆₎	1.4	3.0	4.1	2.8	2.0	2.8	1.5	5.0	3.4	3.9
Tricyclic terpanes										
C ₂₁ -tricyclic	7.6	5.9	-	12.6	5.9	5.1	8.5	-	6.1	3.3
C ₂₃ -tricyclic	13.4	11.4	1.6	10.2	7.7	4.4	11.6	8.1	5.4	3.1
C ₂₄ -tricyclic	14.2	11.0	1.7	10.2	7.3	5.0	13.0	8.2	5.0	2.9
C ₂₅ -tricyclic	12.7	12.8	-	-	8.2	-	11.4	6.8	-	-
C ₂₆ -tricyclic (S)	7.4	8.5	0.9	6.4	6.2	2.3	9.3	4.0	3.3	-
C ₂₆ -tricyclic (R)	3.8	3.2	0.5	-	2.1	0.6	3.2	2.0	1.6	-
Tetracyclic terpanes										
C ₂₄ -tetracyclic	11.4	11.5	7.9	53.5	14.1	11.8	28.3	21.5	9.8	9.0
Total Tri + Tetracyclic terpanes	70.4	64.3	12.6	92.8	51.5	29.2	85.2	50.6	31.2	18.2
Pentacyclic triterpanes or Hopanes										
18α(H)-22,29,30-Trisnorneohopane (Ts)	13.7	7.9	9.3	15.9	11.6	4.0	14.4	40.9	9.0	2.3
17α(H)-22,29,30-Trisnorhopane (Tm)	14.4	8.2	10.2	15.7	12.5	4.3	15.0	40.6	9.3	3.3
$17\alpha,21\beta(H)$ -Norhopane	58.1	51.0	10.4	64.9	52.2	21.8	87.7	51.0	61.0	20.7
$17\alpha,21\beta(H)$ -Hopane	89.8	72.1	13.2	99.4	75.2	28.0	127.6	84.8	78.1	33.2
$17\alpha,21\beta(H)$ -Homohopane (22S)	29.9	17.5	7.6	36.2	25.6	15.5	50.7	35.9	28.6	18.2
$17\alpha,21\beta(H)$ -Homohopane (22R)	19.8	16.8	4.9	28.9	18.8	15.3	40.9	34.7	16.8	15.2
$17\alpha,21\beta(H)$ -Bishomohopane (22S)	19.2	10.8	3.7	12.5	15.0	13.6	19.0	79.1	21.9	-
$17\alpha,21\beta(H)$ -Bishomohopane (22R)	14.2	9.4	3.0	20.6	10.9	7.9	29.4	9.6	10.6	-
17α,21β(H)-Trishomohopane (22S)	12.3	6.2	-	22.7	10.6	12.3	28.9	9.9	7.5	-
17α,21β(H)-Trishomohopane (22R)	9.4	-	-	-	6.6	-	10.2	0.6	-	-
17α,21β(H)-Tetrakishomohopane (22S)	5.3	-	-	-	6.2	-	0.5	-	-	-
17α,21β(H)-Tetrakishomohopane (22R)	5.2	-	-	-	6.3	-	0.4	-	-	-
Total Pentacyclic triterpanes	291.4	199.9	62.3	316.9	251.6	122.8	424.7	387.1	242.8	92.8

Steranes + Diasteranes										
$13\beta,17\alpha(H)$ -Diacholestane (20S)	4.2	7.5	0.5	6.6	3.2	1.8	12.1	13.2	8.0	3.2
$13\beta,17\alpha(H)$ -Diacholestane (20R)	2.4	3.9	0.3	3.6	2.5	2.3	4.9	11.7	5.3	1.7
$5\alpha,14\alpha,17\alpha(H)$ -Cholestane (20S)	8.9	5.6	-	4.7	4.9	4.6	6.9	11.2	10.0	1.2
$13\beta,17\alpha(H)$ -Ethyldiacholestane (20S)	41.9	21.9	3.0	16.2	24.0	5.8	46.2	16.8	24.8	6.8
$5\alpha,14\alpha,17\alpha(H)$ -Cholestane (20R)	3.6	2.7	-	5.0	2.8	-	6.1	11.2	8.6	1.2
$13\beta,17\alpha(H)$ -Ethyldiacholestane (20R)	26.5	11.7	1.7	9.0	12.1	3.1	44.9	14.5	15.4	4.5
$5\alpha,14\alpha,17\alpha(H)$ -Methylcholestane (20S)	5.1	1.1	1.2	2.0	3.2	2.5	9.9	13.6	5.8	3.6
$5\alpha,14\beta,17\beta(H)$ -Methylcholestane (20R)	9.5	5.0	0.6	3.9	4.8	1.8	7.4	13.0	7.7	3.0
$5\alpha,14\beta,17\beta(H)$ -Methylcholestane (20S)	9.7	4.1	2.6	4.9	4.6	1.7	14.1	-	9.0	-
$5\alpha,14\alpha,17\alpha(H)$ -Methylcholestane (20R)	7.5	1.5	-	2.1	4.3	-	8.0	-	5.3	-
$5\alpha,14\alpha,17\alpha(H)$ -Ethylcholestane (20S)	20.1	17.4	2.3	11.0	12.3	4.7	21.5	15.9	9.1	5.9
$5\alpha,14\beta,17\beta(H)$ -Ethylcholestane (20R)	17.9	7.2	2.1	9.5	8.0	3.8	16.3	15.4	10.0	5.4
$5\alpha,14\beta,17\beta(H)$ -Ethylcholestane (20S)	12.2	5.2	1.9	7.8	4.8	2.2	11.7	13.3	6.8	3.3
$5\alpha,14\alpha,17\alpha(H)$ -Ethylcholestane (20R)	14.5	5.6	1.5	6.1	7.3	3.2	15.7	12.3	6.5	2.3
Total Steranes + Diasteranes	184.0	100.2	17.7	92.4	98.9	37.6	225.7	162.1	132.4	42.1
Total Petroleum Biomarkers	545.9	364.4	92.6	502.1	401.9	189.5	735.6	599.8	406.4	153.1
UCM (Unresolved Complex Mixture, µg g ⁻¹)	89931	170599	10894	118567	80302	34461	132544	102854	26247	19764

Table 2.S2a. Concentration (ng g⁻¹) of aliphatic and petroleum biomarkers found in sub-surface sediments collected in the Gulf of Mexico in 2010.

		May	2010				Septemb	er 2010			Novemb	er 2010
Class	#2	#3	#4	#5	#1	#2	#3	#4	#5	#6	#1	#2
Individual compound												
n-Alkanes												
n-Decane	51.5	45.2	195.3	226.4	25.0	26.5	36.4	41.1	0.0	27.6	-	-
n-Heneidecane	21.7	9.4	23.3	30.1	8.2	10.7	14.4	8.0	13.7	15.8	-	-
n-Dodecane	21.4	11.6	21.4	28.0	8.0	9.9	12.7	9.5	11.1	12.4	9.1	6.4
<i>n</i> -Tridecane	17.1	11.8	16.0	19.3	6.1	8.0	10.4	8.2	10.1	9.3	7.4	7.1
<i>n</i> -Tetradecane	29.5	26.7	27.9	42.5	12.5	13.0	17.6	14.3	13.7	16.6	6.9	8.9
<i>n</i> -Pentadecane	19.1	21.4	21.8	30.0	10.5	16.1	22.3	16.4	22.3	16.6	5.5	5.6
<i>n</i> -Hexadecane	12.7	15.8	14.4	22.3	6.7	9.4	12.2	9.5	9.7	8.0	19.1	6.8
<i>n</i> -Heptadecane	12.5	17.2	14.3	19.2	6.4	10.2	10.9	10.0	12.4	9.1	9.5	9.2
Pristane	6.9	12.2	7.4	12.2	9.0	8.5	9.3	10.4	15.9	4.5	7.5	6.8
n-Octadecane	9.0	12.8	10.5	16.8	7.6	5.6	7.2	6.3	7.6	7.8	8.3	4.6
Phytane	3.8	6.5	4.5	8.1	8.2	4.8	6.1	6.3	8.3	3.5	6.1	5.8
<i>n</i> -Nonadecane	11.0	13.5	10.5	13.4	6.0	9.2	15.4	11.2	11.8	9.8	18.1	11.1
<i>n</i> -Eicosane	12.3	14.2	10.6	13.0	17.1	14.4	19.9	16.5	5.6	17.3	22.2	12.0
<i>n</i> -Heneicosane	17.1	20.2	15.4	17.1	13.0	10.5	19.7	30.9	20.4	17.6	31.7	13.1
<i>n</i> -Docosane	17.2	17.3	14.8	17.2	26.0	11.0	19.0	42.8	19.8	29.1	24.5	10.7
<i>n</i> -Tricosane	35.4	24.9	23.7	27.0	12.7	19.2	32.4	18.3	25.1	31.1	31.3	14.5
<i>n</i> -Tetracosane	22.5	17.0	16.1	19.0	10.8	12.1	24.5	14.3	17.6	24.5	22.1	10.4
<i>n</i> -Pentacosane	61.0	37.1	40.6	40.9	16.9	26.8	52.3	26.5	42.1	38.5	43.8	23.5
<i>n</i> -Hexacosane	34.5	22.8	23.3	24.9	10.3	16.8	30.2	15.6	21.3	28.8	24.1	13.2
n-Heptacosane	129.2	71.4	83.7	77.2	34.5	54.7	103.9	60.4	89.2	67.3	97.1	58.9
<i>n</i> -Octacosane	50.6	34.6	41.3	34.1	18.7	26.7	56.0	27.2	44.0	39.0	40.8	22.1
n-Nonacosane	222.1	154.6	196.3	147.0	73.3	118.5	263.8	151.8	263.2	134.1	126.4	110.1
<i>n</i> -Triacontane	62.1	32.1	38.8	31.2	26.7	25.2	58.5	29.1	44.6	39.2	55.1	25.4
<i>n</i> -Hentriacontane	240.4	165.2	213.0	163.9	90.5	128.8	287.1	172.6	294.1	149.7	139.2	114.5
<i>n</i> -Dotriacontane	38.3	20.5	36.1	24.3	31.8	17.3	39.4	27.9	37.5	27.2	53.1	20.6
<i>n</i> -Tritriacontane	108.8	51.2	75.6	55.6	37.4	38.5	90.6	75.3	91.3	54.7	85.7	57.3
<i>n</i> -Tetratriacontane	20.5	0.0	16.6	16.7	19.7	8.4	22.6	18.9	13.8	20.5	40.2	12.4
<i>n</i> -Pentatriacontane	40.0	22.5	31.0	27.6	22.2	15.2	49.9	29.7	33.0	24.9	28.4	16.2
<i>n</i> -Hexatriacontane	25.5	12.6	17.4	16.9	16.7	7.3	20.6	23.2	11.2	21.2	22.4	13.8
<i>n</i> -Heptatriacontane	44.7	28.2	32.1	22.7	16.7	10.2	38.5	23.7	16.3	24.3	18.9	15.9

n-Octatriacontane	27.8	9.1	38.5	25.3	16.9	9.7	26.2	17.5	15.2	20.7	13.8	12.7
Total n-Alkanes	1415.6	940.8	1320.3	1249.5	608.8	689.8	1414.7	957.0	1217.6	942.8	1004.8	636.9
CPI ₍₂₃₋₃₈₎	3.2	3.9	3.1	3.0	2.1	3.4	3.4	3.4	4.3	2.5	2.5	3.5
Tricyclic terpanes												
C ₂₁ -tricyclic	_	0.3	0.5	0.7	1.7	0.9	2.2	0.5	0.9	_	2.9	2.3
C ₂₃ -tricyclic	0.5	0.5	1.0	0.9	6.1	2.2	3.3	4.2	1.4	0.5	5.2	3.2
C ₂₄ -tricyclic	0.5	0.5	1.0	0.8	5.9	2.3	3.3	3.9	1.5	0.6	4.9	3.2
C ₂₅ -tricyclic	0.3	0.3	0.7	0.4	3.1	1.7	3.4	1.4	0.9	0.3	5.3	3.4
	0.3	0.5	0.7	0.4	2.8	1.7	1.4	0.7	1.0		3.8	2.8
C ₂₆ -tricyclic (S)										-		
C ₂₆ -tricyclic (R)	0.3	0.4	0.5	0.3	3.6	1.8	3.0	0.8	0.9	-	2.2	0.7
C ₂₈ -tricyclic	0.5	0.2	0.4	0.4	1.3	0.4	-	0.6	0.0	-	-	-
C ₂₉ -tricyclic	-	0.3	0.7	0.3	0.9	1.1	-	-	0.5	-	-	-
Tetracyclic terpanes												
C ₂₄ -tetracyclic	2.0	0.7	1.2	0.6	5.6	2.3	6.3	3.8	2.5	0.2	12.8	5.0
C ₂₈ -tetracyclic	0.3	0.3	1.1	0.4	2.7	1.6	1.0	0.8	0.7	0.3	-	-
C ₂₉ -tetracyclic	-	0.1	0.3	-	0.5	0.6	-	-	1.2	-	-	-
Total Tri + Tetracyclic terpanes	5.1	4.2	8.3	5.1	34.4	16.6	23.9	16.7	11.5	1.9	37.2	20.7
Pentacyclic triterpanes or Hopanes												
18α(H)-22,29,30-Trisnorneohopane (Ts)	3.5	1.1	1.9	3.3	9.3	5.9	4.7	1.4	2.0	0.8	6.1	4.2
17α(H)-22,29,30-Trisnorhopane (Tm)	7.1	1.8	3.9	7.1	14.6	10.8	8.6	2.1	3.8	1.7	7.0	5.3
17α,21β(H)-Norhopane	10.5	6.5	13.3	10.5	37.3	28.5	21.1	11.1	10.9	7.4	25.3	14.8
17β,21α(H)-Norhopane	5.4	2.2	2.5	5.4	12.0	12.2	7.9	-	6.1	-	-	-
$17\alpha,21\beta(H)$ -Hopane	16.6	10.2	22.5	17.6	65.3	50.6	37.1	20.1	21.3	9.8	37.9	21.4
17α,21β(H)-Homohopane (22S)	9.1	4.0	7.5	9.1	31.1	24.6	18.3	7.9	11.2	4.1	15.9	8.4
$17\alpha,21\beta(H)$ -Homohopane (22R)	5.8	3.3	5.8	5.8	22.1	17.9	14.0	9.4	7.2	2.8	17.5	9.2
$17\alpha,21\beta(H)$ -Bishomohopane (22S)	5.2	2.3	5.1	5.2	21.0	9.9	12.0	3.8	5.8	2.5	11.1	5.5
$17\alpha,21\beta(H)$ -Bishomohopane (22R)	3.2	1.8	3.3	3.2	13.8	8.4	7.2	4.0	4.7	2.1	8.1	4.7
17α,21β(H)-Trishomohopane (22S)	3.0	2.3	3.0	3.0	14.0	6.8	5.2	6.4	3.7	2.2	6.5	5.5
17α,21β(H)-Trishomohopane (22R)	2.5	1.6	2.6	2.5	8.5	3.9	2.5	3.1	2.7	1.0	4.2	6.3
17α,21β(H)-Tetrakishomohopane (22S)	2.1	3.5	2.3	2.1	8.9	3.5	1.9	3.9	3.1	0.8	8.6	7.2
17α,21β(H)-Tetrakishomohopane (22R)	1.5	0.6	1.9	1.5	5.7	1.9	1.3	3.3	1.8	0.3	3.5	4.2
17α,21β(H)-Pentakishomohopane (22S)	1.3	2.5	1.6	1.3	6.6	2.8	1.1	-	2.4	-	6.9	5.5
17α,21β(H)-Pentakishomohopane (22R)	0.8	0.8	1.5	0.8	3.1	1.3	1.3	-	0.5	-	-	-
Total Pentacyclic triterpanes	77.6	44.4	78.7	78.4	273.4	188.9	144.1	76.4	87.1	35.5	158.6	102.1

Steranes + Diasteranes												
13β,17α(H)-Diacholestane (20S)	1.0	0.8	1.4	1.0	8.9	3.8	5.3	1.3	-	-	3.6	1.7
13β,17α(H)-Diacholestane (20R)	0.8	0.6	0.7	0.8	5.5	2.3	3.1	0.8	-	-	1.9	1.3
$5\alpha,14\alpha,17\alpha(H)$ -Cholestane (20S)	1.7	0.9	1.4	1.7	4.8	4.6	3.9	2.1	-	-	3.2	1.8
$13\beta,17\alpha(H)$ -Ethyldiacholestane (20S)	2.0	1.7	2.8	2.0	16.3	7.4	9.6	3.9	5.1	1.5	11.8	4.4
$5\alpha,14\alpha,17\alpha(H)$ -Cholestane (20R)	1.4	1.0	1.2	1.4	2.2	1.4	2.0	0.6	2.3	-	3.1	2.1
13β,17α(H)-Ethyldiacholestane (20R)	1.3	1.4	2.0	1.3	10.5	5.7	6.6	2.6	4.7	1.0	8.5	3.3
$5\alpha,14\alpha,17\alpha(H)$ -Methylcholestane (20S)	3.4	1.4	1.8	3.4	5.2	4.3	4.4	1.3	1.2	0.8	1.4	0.6
$5\alpha,14\beta,17\beta(H)$ -Methylcholestane (20R)	1.1	0.8	1.4	1.1	4.1	2.1	3.5	1.5	2.1	0.6	3.8	1.1
$5\alpha,14\beta,17\beta(H)$ -Methylcholestane (20S)	3.0	1.3	2.5	3.0	6.4	4.2	4.1	1.6	1.9	0.7	4.3	1.9
$5\alpha,14\alpha,17\alpha(H)$ -Methylcholestane (20R)	1.9	1.0	1.2	1.9	2.5	1.9	2.6	1.2	1.2	0.6	2.5	0.5
$5\alpha,14\alpha,17\alpha(H)$ -Ethylcholestane (20S)	1.8	2.1	2.3	1.8	10.0	6.7	7.2	3.0	7.5	1.5	7.6	3.2
$5\alpha,14\beta,17\beta(H)$ -Ethylcholestane (20R)	2.2	1.7	2.4	2.2	8.3	5.5	5.8	2.5	3.2	1.4	6.1	2.4
$5\alpha,14\beta,17\beta(H)$ -Ethylcholestane (20S)	0.9	1.0	1.1	0.9	5.9	3.0	4.0	2.0	2.3	0.9	3.8	1.7
$5\alpha,14\alpha,17\alpha(H)$ -Ethylcholestane (20R)	2.6	2.1	2.3	2.6	5.7	4.3	4.5	2.3	2.5	1.3	4.6	1.7
Total Steranes + Diasteranes	25.1	17.7	24.3	25.1	96.4	57.2	66.7	26.7	34.0	10.3	66.0	27.7
Total Petroleum Biomarkers	107.8	66.2	111.3	108.6	404.2	262.7	234.8	119.8	132.7	47.7	261.8	150.5
UCM (Unresolved Complex Mixture, µg g ⁻¹)	8877	4879	9649	8877	53387	46328	33936	16501	18703	5327	49841	25637

Table 2.S2b. Concentration (ng g⁻¹) of aliphatic and petroleum biomarkers found in sub-surface sediments collected in the Gulf of Mexico from 2011 to 2013.

		July 2011	1		July 2012	2		July 2013	3
Class	#1	#2	#6	#1	#2	#3	#1	#2	#6
Individual compound									
n-Alkanes									
<i>n</i> -Tetradecane	-	2.8	-	-	-	-	-	-	-
<i>n</i> -Pentadecane	13.3	9.3	-	6.1	7.4	7.3	18.1	2.7	-
<i>n</i> -Hexadecane	3.7	3.0	5.5	9.9	1.3	6.9	43.5	14.6	4.1
<i>n</i> -Heptadecane	33.4	15.5	9.6	17.9	16.4	18.9	70.5	29.5	18.2
Pristane	45.9	24.7	19.7	35.7	29.7	49.1	48.6	45.3	44.8
<i>n</i> -Octadecane	28.5	11.9	7.7	15.5	13.1	15.7	45.8	42.2	21.9
Phytane	40.0	18.5	11.5	22.1	19.4	22.1	35.8	38.7	30.5
<i>n</i> -Nonadecane	24.7	13.8	9.7	16.2	10.2	12.8	35.3	29.1	15.5
<i>n</i> -Eicosane	26.6	13.6	13.5	20.4	9.7	17.0	32.9	61.9	16.6
<i>n</i> -Heneicosane	26.8	15.3	10.1	22.4	13.2	19.0	45.9	30.2	18.4
<i>n</i> -Docosane	23.7	10.5	7.2	18.7	9.2	15.3	31.5	23.4	15.7
<i>n</i> -Tricosane	30.4	21.0	15.0	10.4	17.0	7.0	49.5	30.9	24.4
<i>n</i> -Tetracosane	19.1	12.7	9.0	20.9	12.5	17.5	27.2	21.5	15.7
<i>n</i> -Pentacosane	40.1	40.0	25.4	46.4	35.4	43.0	75.9	35.1	32.2
<i>n</i> -Hexacosane	18.5	13.7	9.1	23.3	10.6	19.9	33.5	24.2	14.0
<i>n</i> -Heptacosane	60.7	76.7	52.9	74.0	60.9	70.6	115.6	65.2	52.3
<i>n</i> -Octacosane	19.1	14.3	18.9	22.6	9.6	19.2	34.0	15.9	12.7
<i>n</i> -Nonacosane	64.5	72.6	108.6	74.8	61.9	71.4	155.9	112.3	75.3
<i>n</i> -Triacontane	13.1	7.6	12.0	17.4	7.2	14.0	54.5	16.0	7.4
<i>n</i> -Hentriacontane	21.7	23.9	85.8	30.8	19.9	27.4	132.4	79.9	46.0
<i>n</i> -Dotriacontane	5.7	6.3	9.7	17.3	5.8	13.9	21.5	10.6	0.8
<i>n</i> -Tritriacontane	6.5	9.4	22.6	11.6	3.4	8.2	47.4	21.9	7.7
Total n-Alkanes	480.1	394.0	432.4	476.8	324.7	425.2	1070.9	667.1	399.1
CPI ₍₂₃₋₃₃₎	3.0	4.5	5.3	2.4	4.3	2.7	3.4	3.9	4.7

Tricyclic terpanes									
C ₂₁ -tricyclic	2.7	2.1	1.9	1.2	2.3	1.1	7.5	3.3	2.2
C ₂₃ -tricyclic	3.4	3.2	1.6	1.1	3.5	1.1	5.0	3.1	2.8
C ₂₄ -tricyclic	3.5	3.7	1.7	1.2	3.6	1.3	4.9	3.1	3.0
C ₂₅ -tricyclic	2.9	1.8	2.1	1.1	1.8	1.3	3.9	2.5	1.8
C ₂₆ -tricyclic (S)	2.8	2.1	0.9	1.5	2.1	2.1	3.3	2.7	2.1
C ₂₆ -tricyclic (R)	0.9	1.4	0.5	0.8	1.3	1.6	3.1	1.8	1.7
Tetracyclic terpanes									
C ₂₄ -tetracyclic	5.5	1.6	3.3	1.7	1.6	1.8	5.6	5.1	2.3
Total Tri + Tetracyclic terpanes	21.8	15.9	12.0	8.7	16.2	10.3	33.3	21.5	15.9
Pentacyclic triterpanes or Hopanes									
18α(H)-22,29,30-Trisnorneohopane (Ts)	4.1	4.9	6.4	4.2	5.1	3.3	24.7	6.5	4.5
17α(H)-22,29,30-Trisnorhopane (Tm)	4.3	5.1	7.2	4.9	6.3	3.5	24.5	6.8	5.1
$17\alpha,21\beta(H)$ -Norhopane	16.4	5.8	7.4	8.5	8.2	5.4	25.9	30.7	9.1
$17\alpha,21\beta(H)$ -Hopane	24.2	8.0	9.2	13.3	10.3	7.6	37.3	43.2	11.9
$17\alpha,21\beta(H)$ -Homohopane (22S)	8.1	4.4	4.6	4.2	5.8	5.3	27.3	18.2	8.3
$17\alpha,21\beta(H)$ -Homohopane (22R)	6.3	3.4	3.9	3.1	4.8	4.8	24.4	15.2	7.2
$17\alpha,21\beta(H)$ -Bishomohopane (22S)	6.4	2.0	2.7	2.6	4.3	4.5	15.6	13.7	6.8
$17\alpha,21\beta(H)$ -Bishomohopane (22R)	4.8	1.5	2.0	2.5	3.2	3.2	11.3	11.7	5.4
$17\alpha,21\beta(H)$ -Trishomohopane (22S)	5.2	1.8	1.9	1.8	3.1	3.6	10.8	9.5	4.9
$17\alpha,21\beta(H)$ -Trishomohopane (22R)	4.3	1.2	1.4	1.3	2.6	2.4	9.3	8.0	4.1
17α,21β(H)-Tetrakishomohopane (22S)	3.9	1.3	-	-	-	-	8.6	-	-
17α,21β(H)-Tetrakishomohopane (22R)	2.8	-	-	-	-	-	6.5	-	-
Total Pentacyclic triterpanes	90.7	39.3	46.7	46.4	53.6	43.6	226.2	163.5	67.3
Steranes + Diasteranes									
$13\beta,17\alpha(H)$ -Diacholestane (20S)	3.9	4.3	2.5	2.5	2.5	3.1	8.0	4.4	5.1
$13\beta,17\alpha(H)$ -Diacholestane (20R)	2.9	3.3	3.3	2.7	2.1	2.2	5.3	3.3	2.7
$5\alpha,14\alpha,17\alpha(H)$ -Cholestane (20S)	6.5	5.3	6.6	3.4	4.3	2.8	10.0	3.9	2.6

$13\beta,17\alpha(H)$ -Ethyldiacholestane (20S)	10.1	8.7	7.1	6.7	5.4	6.7	14.8	7.9	8.7
$5\alpha,14\alpha,17\alpha(H)$ -Cholestane (20R)	5.4	4.8	5.1	3.2	3.7	3.3	8.6	4.4	4.6
$13\beta,17\alpha(H)$ -Ethyldiacholestane (20R)	9.6	6.7	6.7	5.8	4.9	4.1	11.4	6.2	5.0
$5\alpha,14\alpha,17\alpha(H)$ -Methylcholestane (20S)	7.9	5.1	1.2	4.1	3.7	2.7	5.8	4.9	3.5
$5\alpha,14\beta,17\beta(H)$ -Methylcholestane (20R)	8.0	4.6	0.6	3.5	2.8	0.6	7.7	2.4	4.1
$5\alpha,14\beta,17\beta(H)$ -Methylcholestane (20S)	6.4	3.8	2.6	3.3	3.1	2.5	9.0	3.5	2.2
$5\alpha,14\alpha,17\alpha(H)$ -Methylcholestane (20R)	4.7	2.7	1.3	2.8	2.4	1.6	5.3	1.6	2.3
$5\alpha,14\alpha,17\alpha(H)$ -Ethylcholestane (20S)	3.2	2.6	2.3	2.1	2.3	4.4	9.1	2.4	5.0
$5\alpha,14\beta,17\beta(H)$ -Ethylcholestane (20R)	1.6	-	-	1.3	-	3.9	11.0	2.0	3.7
$5\alpha,14\beta,17\beta(H)$ -Ethylcholestane (20S)	1.9	1.2	1.9	1.1	1.2	3.2	6.8	2.2	-
$5\alpha,14\alpha,17\alpha(H)$ -Ethylcholestane (20R)	1.4	-	-	-	-	-	6.5	1.8	-
Total Steranes + Diasteranes	73.5	53.1	41.2	42.5	38.4	41.2	119.4	51.0	49.6
Total Petroleum Biomarkers	186.0	108.2	99.9	97.6	108.2	95.1	378.9	236.0	132.8
UCM (Unresolved Complex Mixture, µg g ⁻¹)	26131	5963	10894	7241	5985	4657	53438	29764	9750

CHAPTER 3

ASSESSING CORAL RESPONSE TO BLEACHING EVENTS USING MULTIMOLECULAR ${\tt BIOMARKERS}^1$

¹Babcock-Adams, L., Miñarro, S., Fitt, W. K. & Medeiros, P. M. To be submitted to *Coral Reefs*.

Abstract

In the past, coral studies focused on the investigation of coral response to various environmental stressors using analyses of bulk lipid fractions. However, a compound specific analysis (such as biomarkers) can provide information about more subtle changes in composition that occur within a chemical class. In this study, coral tissue samples with various zooxanthellae clade associations (resistant, non-resistant, and a mixture of the two) from two reefs in the Upper Florida Keys (Little Grecian Reef and Admiral Reef) were collected in March, May, August, and November of 2000 – two years following the mass bleaching event caused by the 1997-1998 El Niño. These tissue samples were analyzed using a coupled gas chromatography-mass spectrometry (GC-MS) system to identify and quantify molecular biomarkers. The aim of this study was to characterize specific biomarkers indicative of stress and/or recovery. Two trends were seen in the biomarker data – a seasonal trend due to sea surface temperature and a longterm recovery trend from the 1997-1998 El Niño event. Due to the time period sampled, the seasonal trend was more easily detected in the dataset. A seasonal thermal stress event in August (sea surface temperature of just under 30°C) was reflected in the corals by changing concentrations of monosaccharides, sugar alcohols, n-alkanols, fatty acids, and sterols. In fact, corals associated with resistant zooxanthellae exhibited higher levels of monosaccharides and sugar alcohols, i.e. energy reserve components, whereas corals associated with non-resistant zooxanthellae presented higher levels of *n*-alkanols, especially hexadecanol (a biomarker for zooplankton). These findings indicate that while corals with resistant zooxanthellae seem to

store energy compounds to overcome the thermal stress, those associated with non-resistant zooxanthellae seem to increase consumption of zooplankton.

1. Introduction

Coral bleaching events can be caused by increased or decreased seawater temperatures, solar radiation, salinity, sedimentation, pollution, and/or ocean acidification (Brown, 1997; Hughes, 2003). One or a combination of these physical stressors can result in an expulsion of the endosymbiotic zooxanthellae found in the coral tissue, giving the coral a white or "bleached" appearance. While any of the aforementioned physical conditions could induce coral bleaching, elevated sea surface temperature (SST) is the dominant cause of mass bleaching events, and since corals live at the high end of the tolerated temperature range a relatively small increase in SST can exceed the temperature threshold of the zooxanthellae (Porter et al., 1989; Stat and Gates, 2011). The mutualistic symbiotic relationship between the coral host and the zooxanthellae (dinoflagellate in the genus Symbiodinium) operates in such a way that the coral receives photosynthetically fixed organic carbon from the zooxanthellae and the zooxanthellae receive inorganic compounds and a protected living environment inside the coral tissue (Muscatine, 1967). When healthy, the zooxanthellae can provide the coral with up to 100% of its daily metabolic energy requirements (Grottoli et al., 2006), and excess fixed carbon can be stored within the coral tissue as lipids (Harland et al., 1993). This symbiotic relationship is broken when the zooxanthellae are expelled due to a bleaching event leaving the coral without its energy source, and if the duration of the bleaching event is too long the coral is likely to die. However, it has been found that clade D Symbiodinium is resistant to thermal bleaching (Rowan, 2004) and thus has been called a "nugget of hope" for coral reefs (Berkelmans and Van Oppen, 2006). This clade D Symbiodinium is opportunistic and will repopulate the coral following the

expulsion of non-resistant symbionts (Kinzie III et al., 2001). Furthermore, it has been shown in the field that clade D increases in abundance following a bleaching event (Jones et al., 2008), aiding the recovery of the coral (Buddemeier and Fautin, 1993). While clade D *Symbiodinium* is resistant to bleaching, corals with this symbiont have been found to grow more slowly than when associated with a non-resistant clade (Little et al., 2004; Jones and Berkelmans, 2010). Thus, over a period of 2-3 years after the bleaching event, the coral will typically revert back to the original symbiont composition (Thornhill, 2006). This makes the clade D a useful biological marker of a stressed coral due to abiotic conditions (Stat and Gates, 2011).

Molecular biomarkers have been used previously to study coral response to stressors such as increased temperature and light (Downs et al., 2000; Rodrigues et al, 2008) and to investigate the coral food supply (Dodds, et al., 2009). However, previous studies have separated the coral extract into various lipid fractions (e.g. hydrocarbons, waxy esters) and analyzed them as bulk fractions (e.g. Rodrigues et al. 2007), and thus little is known about the specific organic compound composition of coral tissues under stress conditions and/or recovery from a bleaching event. In this context, the purpose of this study is to identify and quantify biomarker compounds in the tissue samples in order to determine if the biomarker composition and/or levels differ among the zooxanthellae clades (1) seasonally, (2) spatially, and (3) between species *O. annularis* and *O. faveolata*. Our primary goal is to characterize a suite of biomarker indicators of stress and/or recovering conditions after the bleaching event.

2. Experimental Methods

2.1 Sample Collection & Clade Identification

Twenty-six coral tissue samples (Orbicella annularis and Orbicella faveolata) were collected at Little Grecian Reef in the Florida Keys in March, May, August, and November of 2000. Additionally, eight coral tissue samples (Orbicella annularis) were collected at Admiral Reef also in the Florida Keys in March and May of 2000, for a total of thirty-four tissue samples (**Figure 3.1**). Both these sites were heavily impacted by the coral bleaching event caused by the 1997-98 El Niño, resulting in an extreme loss of zooxanthellae (Thornhill, 2006) and providing conditions for the opportunistic clade D Symbiodinium to populate the coral hosts. The Orbicella genus resides in the order Scleractinia, thus the corals belonging to this genus are hard corals that build calcium carbonate skeletons. O. annularis and O. faveolata are slow-growing corals (Hernández-Pacheco et al., 2011) that obtain the zooxanthellae horizontally (i.e. from the surrounding environment; Stat and Gates, 2011). Additionally, these two species of coral commonly have symbiont compositions that are made up of more than one clade of Symbiodinium (Rowan et al., 1997). Little Grecian Reef is an offshore reef habitat with corals at approximately 3 m depth while Admiral Reef is an inshore patch reef with corals at shallower depths of 1-2 m.

Coral tissue samples were collected following the procedure described previously by Thornhill (2006). Briefly, samples were collected via SCUBA and corals were tagged so that the same coral was sampled at each time point. A sample with a 5 cm diameter was obtained using a hammer and chisel from the top of the coral colony (i.e. the unshaded location) and immediately taken to the laboratory for zooxanthellae analysis. Coral tissue was then removed from the coral skeleton using 0.45 µm filtered seawater, the *Symbiodinium* cells were dispersed and isolated for

subsequent DNA extraction and identification of *Symbiodinium* clade following LaJeunesse (2001, 2002). The tissue samples were then freeze-dried and kept frozen (-20 °C) until chemical analyses.

2.2 Biomarker Extraction

Freeze-dried coral tissue samples were first weighed and then biomarkers were extracted with a dichloromethane:methanol (2:1, v/v) mixture using a Fisher Scientific FS30 sonicator. The extracts were concentrated in a RapidVap evaporator to approximately 2-mL, then further to 1-mL using a stream of high purity nitrogen gas. Aliquots of the total extracts were converted to their trimethylsilyl derivatives using N,O-bis(trimethlsilyl-trifluoroacetamide (BSTFA) containing 1% trimethylchlorosilane (TMCS) and pyridine (Pierce). The samples were derivatized for three hours at 70 °C. Aliquots of 1 µL of silvlated total extracts were analyzed within 24 hours using an Agilent 6890 gas chromatograph interfaced with an Agilent 5975 mass selective detector (GC-MS). A DB5-MS capillary column (30 m x 0.25 mm I.D. and film thickness of 0.25 µm) was used with helium as the carrier gas at a constant flow rate of 1.3 mL min⁻¹. The injector and MS source temperatures were maintained at 280°C and 230°C, respectively. The column temperature program consisted of injection at 65°C and hold for 2 min, temperature increase of 6°C min⁻¹ to 300°C, followed by an isothermal hold at 300°C for 15 min. The MS was operated in the electron impact mode with an ionization energy of 70 eV. The scan range was set from 50 to 650 Da and the samples were analyzed in splitless mode.

Data were acquired and processed with the Agilent-Chemstation software. Individual compounds were identified by comparison of mass spectra with literature and library data, comparison of mass spectra and GC retention times with those of authentic standards and/or

interpretation of mass spectrometric fragmentation patterns. Compounds were quantified using the total ion current (TIC) peak area and converted to compound mass using calibration curves of external standards: hexadecanoic acid for *n*-alkanoic and *n*-alkenoic acids, hexacosanol for *n*-alkanols, sitosterol for sterols, sorbitol for sugar alcohols, glucose for monosaccharides, and sucrose for disaccharides. A procedural blank was run in sequence presenting no significant background interferences. Recoveries for the organic compound classes analyzed ranged from 70 to 100% (Mazurek et al., 1987; Medeiros and Simoneit, 2007).

3. Results and Discussion

3.1. Seasonal Variation

3.1.1. Little Grecian Reef, Orbicella annularis

Zooxanthellae clade distribution at Little Grecian Reef (**Figure 3.2**) shows a continual decrease of the bleaching resistant zooxanthellae (blue bar) and an increase of the non-resistant zooxanthellae (green bar). Additionally, there is a maximum of corals associated with both resistant and non-resistant clades in May and August (red bar). This distribution seems to reflect the recovery from the 1997-1998 El Niño, the event that caused a mass bleaching in the Florida Keys due to increased water temperatures (Thornhill, 2006). In March 2000, *O. annularis* is still harboring the resistant zooxanthellae clade that populated the coral after the expulsion of the non-resistant symbiont in 1997-1998. However, throughout the year 2000 the corals are shifting their zooxanthellae associations back to the original composition of non-resistant symbionts. This observed pattern agrees with the premise that the coral will revert back to its original zooxanthellae composition two to three years following a bleaching event (Berkelmans et al., 2004; Elvidges et al., 2004; van Oppen et al., 2005; Thornhill, 2006).

In the biomarker data for Little Grecian Reef there seem to be two separate trends occurring during the year of sample collection- an apparent seasonal trend and a possible longterm recovery trend from the El Niño event. The seasonal trend is observed in the levels of monosaccharides (Figure 3.3), sugar alcohols (Figure 3.4), fatty acids (Figure 3.5), *n*-alkanols (**Figure 3.6**), and sterols (**Figure 3.7**). In August, monosaccharides, sugar alcohols, and *n*alkanols strongly increased in concentration, whereas fatty acids and sterols presented decreased levels at this time. The change in concentration is especially pronounced for the resistant clade of zooxanthellae (blue bar) in all compound classes, with the except of fatty acids that presented similar levels between the resistant clade and those of the non-resistant clade and mixture of resistant and non-resistant clades (Figure 3.5). This seasonal trend seems to be driven by the sea surface temperature of the Upper Florida Keys (Figure 3.8). In 2000, the SST in August was just under 30 °C, near the bleaching threshold for the Upper Florida Keys (Glynn and D'Croz, 1990). The increased temperature seen in August was short-lived, decreasing approximately 5 °C by the end of the year. This seasonal signal allows for a comparison of how the resistant and non-resistant clades react to a stress event. As compared to the non-resistant clade and the mixture of clades, the coral tissue associated with the resistant zooxanthellae showed higher levels of monosaccharides (primarily glucose followed by mannose) and sugar alcohols (inositols and mannitol), which are both important coral energy reserves (Schoepf et al., 2013). Furthermore, the corals associated with the resistant symbiont showed lower levels of sterols, a lipid class that is a component of eukaryotic membranes (Treignier et al., 2009). The reduction in sterol concentrations was due to the decrease of brassicasterol and fucosterol, i.e., sterols commonly found in algae (Volkman et al., 1998), indicating lower photosynthetic activity. This difference of compound concentrations indicates that the corals associated with the resistant

zooxanthellae have a stronger accumulation of monosaccharides and sugar alcohols and a stronger reduction of algal-derived sterols in response to the seasonal stress.

Corals associated with resistant, non-resistant, and a mixture of the two all exhibit lowered fatty acid and raised *n*-alkanol concentrations in August as a response to the thermal stress. Similar to sterols, fatty acids also contribute to the coral energy reserve and are a component of eukaryotic membranes. The *n*-alkanol that constituted the majority of the concentration was hexadecanol, a zooplankton biomarker (Wakeham et al., 2009; Burns and Brinkman, 2011). This indicates that the coral may have switched to heterotrophy during the period of thermal stress. It has been found that Scleractinian corals rely on heterotrophic feeding to survive bleaching events (Houlbrèque and Ferrier-Pagès, 2009), in which the corals will consume zooplankton. In August, the *n*-alkanols showed increased concentrations indicating increased consumption of zooplankton. Interestingly, the coral associated with the bleaching resistant zooxanthellae presented lower hexadecanol concentrations compared to the non-resistant and mixture associated corals, indicating that the coral did not participate in as much heterotrophy. This is likely because those corals have higher energy stores, as observed in the monosaccharide and sugar alcohol levels, to overcome the thermal stress.

The recovery trend from the El Niño event can be seen in the coral samples that were associated with the resistant zooxanthellae. This recovery is reflected in the concentrations of monosaccharides (**Figure 3.3**) and sugar alcohols (**Figure 3.4**). These compound classes exhibit concentrations in March that is similar to the concentrations seen in August, a time of thermal stress when the coral was perhaps increasing its energy stores in preparation for a bleaching event (though one did not occur). Hypothetically, the corals associated with the resistant zooxanthellae would have increased their monosaccharide and sugar alcohol concentrations prior

to the mass bleaching event in order to survive the 1997-1998 El Niño. Presumably, because the thermal stress due to this El Niño was more intense, the concentrations would have been higher than what was seen in the period of thermal stress in August 2000. Then these energy stores would have been consumed during bleaching in order to survive and the levels seen in March 2000 are perhaps still elevated from this event. However, in order to probe this hypothesis additional coral tissue samples collected at Little Grecian Reef in 2014 and 2015, (a period of strong bleaching due to thermal stress) will be analyzed and compared to results of the samples collected in March of 2000.

3.1.2. Admiral Reef, Orbicella annularis

The zooxanthellae clade distribution at Admiral Reef (**Figure 3.9**) shows a decrease of corals associated with a mixture of resistant and non-resistant zooxanthellae from March to May and an increase of corals associated with the non-resistant zooxanthellae from March to May. This pattern indicates that the corals have reverted to their original zooxanthellae compositions by May 2000. Due to the low number of coral tissue samples with comparable zooxanthellae clades, there was no observable pattern in the biomarker data.

3.2. Spatial Variation

As previously mentioned, the zooxanthellae distribution patterns at Little Grecian Reef and Admiral Reef (locations shown in **Figure 3.1**) show the repopulation of the original zooxanthellae composition during the year 2000. However, the zooxanthellae distribution at Admiral Reef from March to May follows the change as that at Little Grecian Reef from August to November. This indicates that Admiral Reef either has recovered more rapidly from the El

Niño event or that it was less heavily impacted. However, it is more likely that Admiral Reef experienced a faster recovery because both regions were reported to have undergone extensive bleaching during the 1997-1998 El Niño (Fitt et al., 2000). The specific zooxanthellae clades present in March and May at Little Grecian Reef and Admiral Reef were different, and therefore the biomarker data between the two did not show any definitive differences.

3.3. Variation Between Species O. annularis and O. faveolata at Little Grecian Reef

In March of 2000, coral tissue samples were taken from two species of coral at Little Grecian Reef. The *O. annularis* species collected was solely associated with the resistant zooxanthellae while the *O. faveolata* species was associated with non-resistant zooxanthellae clades as well as a mixture of both resistant and non-resistant clades (**Figures 3.2** and **3.10** respectively). This seems to indicate that *O. faveolata* has recovered more quickly from the 1997-1998 mass bleaching, similar to what was observed at Admiral Reef. Due to the differing zooxanthellae clades found in the two coral species at Little Grecian Reef, the cause of biomarker compound differences found could not be distinguished.

4. Conclusions

Zooxanthellae clade distributions for both Little Grecian and Admiral Reefs, and for both *O. annularis* and *O. faveolata*, showed that the corals were repopulated with their original zooxanthellae clade distribution during the year of 2000. Admiral Reef coral *O. annularis* and Little Grecian Reef coral *O. faveolata* seemed to recover their typical symbiont more rapidly than Little Grecian Reef coral *O. annularis*. Seasonality was evident in the biomarker data for *O. annularis* at Little Grecian Reef with a brief thermal stress event in August. The overall

response to this stress was increased energy reserves (monosaccharides and sugar alcohols) and *n*-alkanols, and decreased sterols and fatty acids (membrane components). The increase in monosaccharides and sugar alcohols was especially pronounced in the corals associated with the resistant zooxanthellae as was the decrease in sterols, indicating a chemically different response to thermal stress. Furthermore, the increase in *n*-alkanols (primarily hexadecanol, a marker for zooplankton) was less pronounced for the corals associated with the resistant zooxanthellae, indicating that the coral overcame the thermal stress (causing less photosynthetic activity) by storing energy compounds instead of increasing consumption of zooplankton.

An underlying long-term trend was observed in the Little Grecian Reef *O. annularis* dataset, which is thought to be continued recovery from the 1997-1998 El Niño. This trend is observed in the increased levels of monosaccharides and sugar alcohols in March, which are similar to the levels seen in August. These compounds contribute to the energy reserves, and thus could be at elevated levels from the zooxanthellae stress response that aided the coral survival during El Niño. Samples from during the bleaching event and the year after would need to be analyzed in order to investigate this further.

<u>Figures</u>

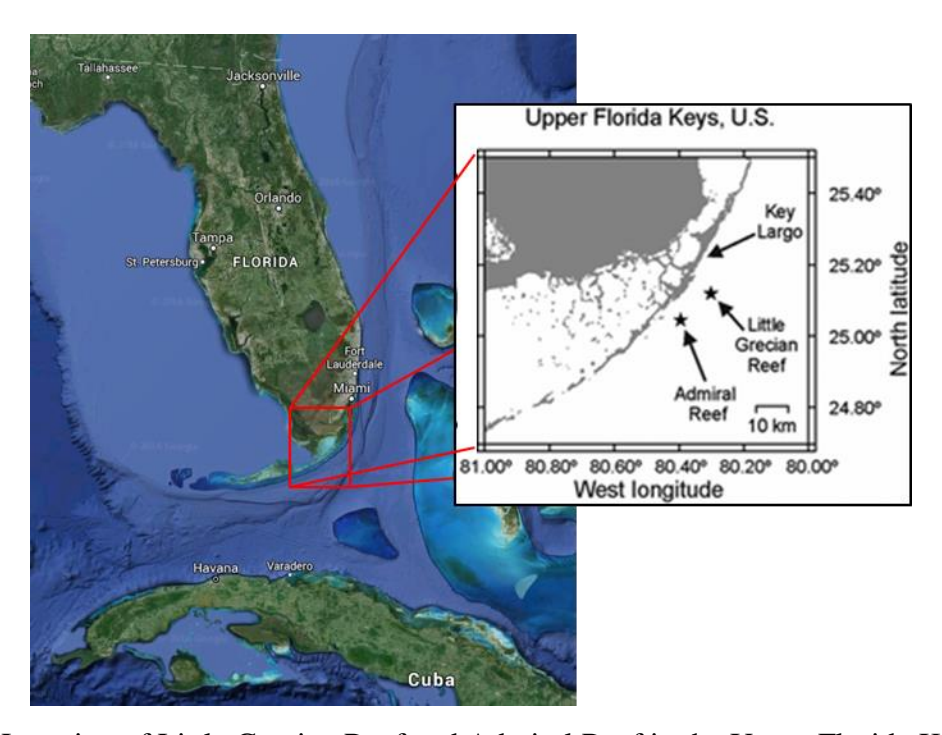
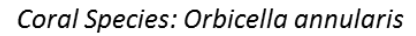


Figure 3.1. Location of Little Grecian Reef and Admiral Reef in the Upper Florida Keys, modified from Kemp et al. (2011).

Zooxanthellae Clade Distribution



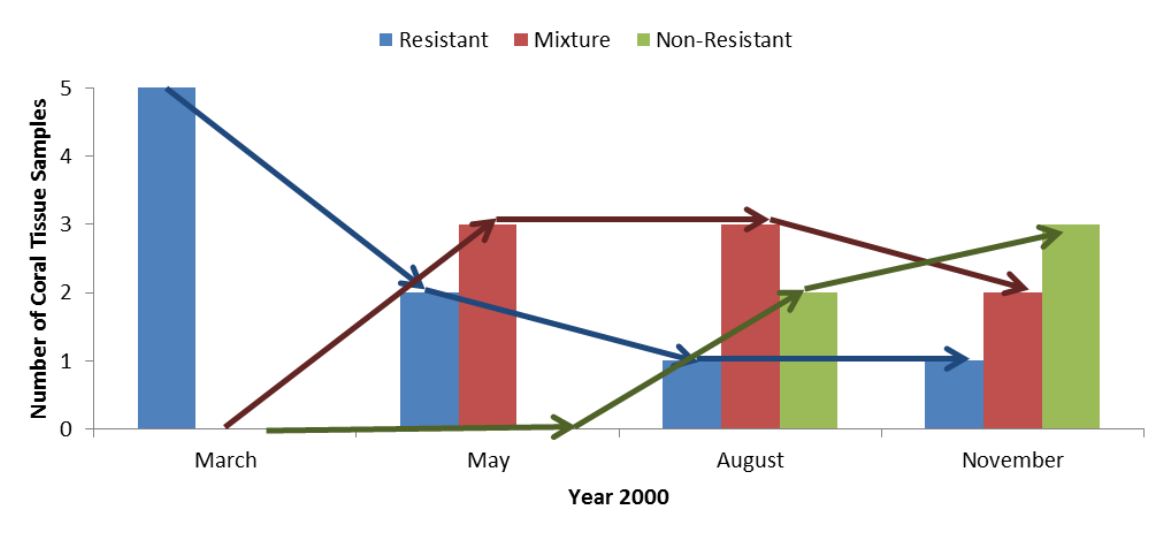


Figure 3.2. Zooxanthellae clade distribution at Little Grecian Reef for coral species *O. annularis*. The resistant zooxanthellae clade (blue bar) is clade D1, zooxanthellae clade mixture (red bar) is a combination of resistant and non-resistant clades, and non-resistant zooxanthellae clades (green bar) are clades B1 and B10.

Monosaccharides Resistant (D1) Mixture (B10, D1) Non-Resistant (B10) ×SST 2000.00 32.00 1800.00 31.00 30.00 29.00 28.00 27.00 25.00 25.00 24.00 23.00 1600.00 30.00 Concentration (mg/g) 1400.00 1200.00 1000.00 800.00 600.00 400.00 200.00 0.00 22.00 March May November August Year 2000

Figure 3.3. Concentration of monosaccharides in *O. annularis* coral tissue samples from Little Grecian Reef and monthly averaged sea surface temperature (black line) taken from NOAA buoy at Molasses Reef. The resistant zooxanthellae clade (blue bar) is clade D1, zooxanthellae clade mixture (red bar) is a combination of resistant and non-resistant clades, and non-resistant zooxanthellae clades (green bar) are clades B1 and B10.

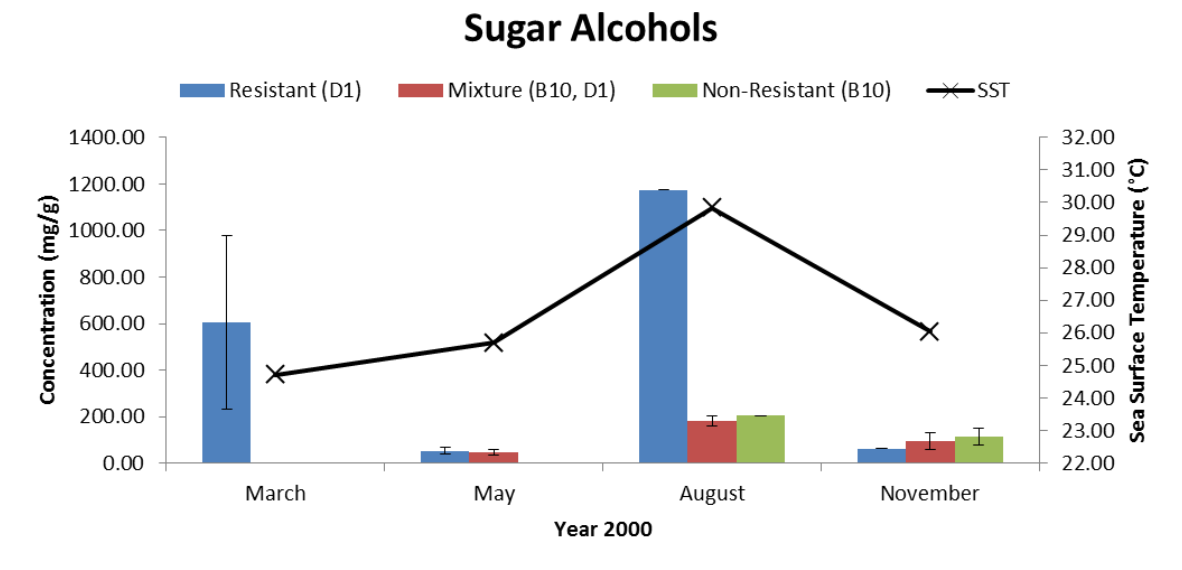


Figure 3.4. Concentration of sugar alcohols in *O. annularis* coral tissue samples from Little Grecian Reef and monthly averaged sea surface temperature (black line) taken from NOAA buoy at Molasses Reef. The resistant zooxanthellae clade (blue bar) is clade D1, zooxanthellae clade mixture (red bar) is a combination of resistant and non-resistant clades, and non-resistant zooxanthellae clades (green bar) are clades B1 and B10.

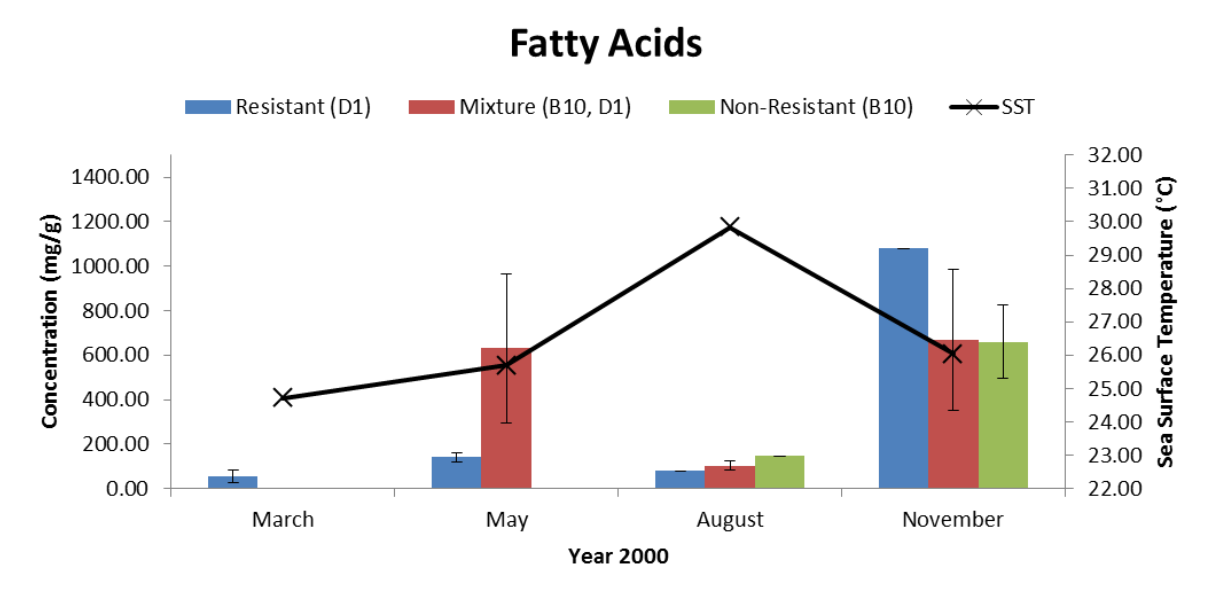


Figure 3.5. Concentration of fatty acids in *O. annularis* coral tissue samples from Little Grecian Reef and monthly averaged sea surface temperature (black line) taken from NOAA buoy at Molasses Reef. The resistant zooxanthellae clade (blue bar) is clade D1, zooxanthellae clade mixture (red bar) is a combination of resistant and non-resistant clades, and non-resistant zooxanthellae clades (green bar) are clades B1 and B10.

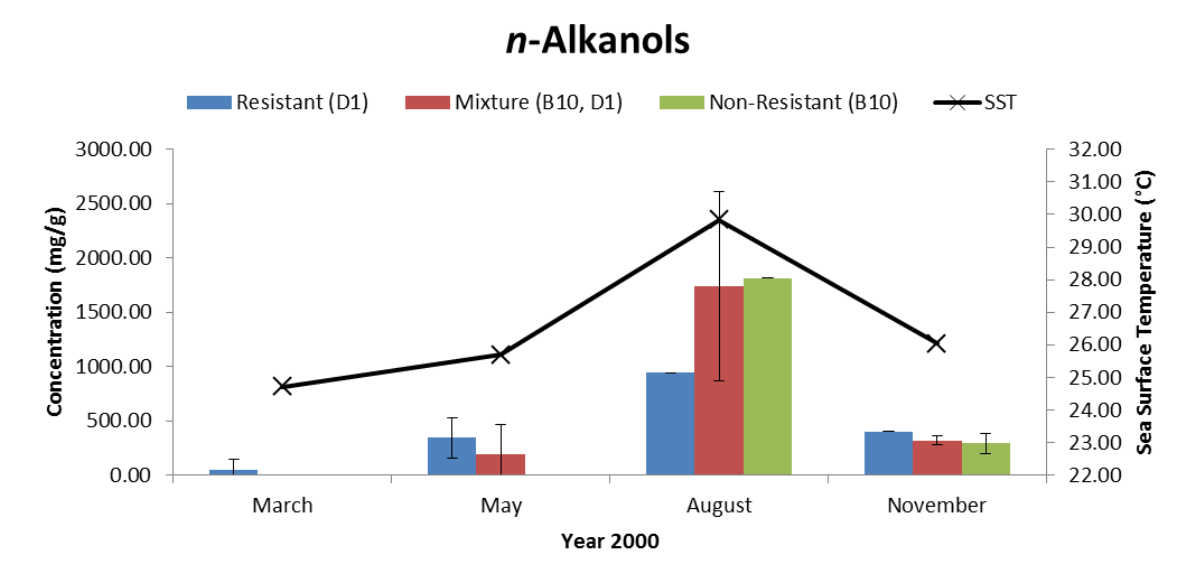


Figure 3.6. Concentration of n-alkanols in *O. annularis* coral tissue samples from Little Grecian Reef and monthly averaged sea surface temperature (black line) taken from NOAA buoy at Molasses Reef. The resistant zooxanthellae clade (blue bar) is clade D1, zooxanthellae clade mixture (red bar) is a combination of resistant and non-resistant clades, and non-resistant zooxanthellae clades (green bar) are clades B1 and B10.

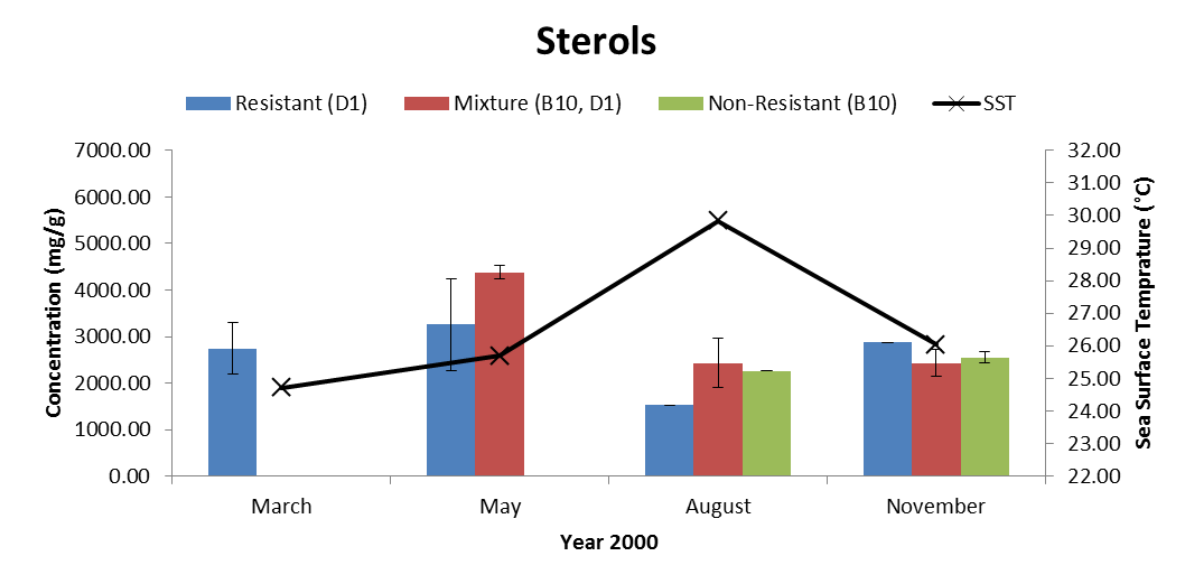


Figure 3.7. Concentration of sterols in *O. annularis* coral tissue samples from Little Grecian Reef and monthly averaged sea surface temperature (black line) taken from NOAA buoy at Molasses Reef. The resistant zooxanthellae clade (blue bar) is clade D1, zooxanthellae clade mixture (red bar) is a combination of resistant and non-resistant clades, and non-resistant zooxanthellae clades (green bar) are clades B1 and B10.

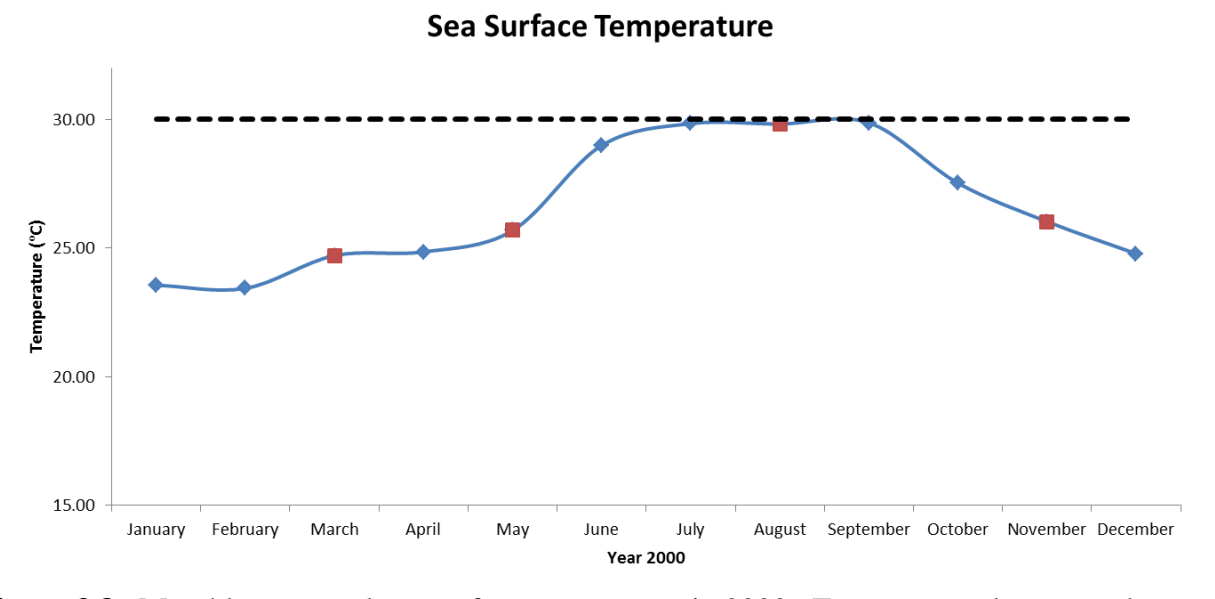


Figure 3.8. Monthly averaged sea surface temperature in 2000. Temperature data was taken from NOAA buoy at Molasses Reef (MLRF1), located in between Little Grecian Reef and Admiral Reef. Monthly temperatures are shown by the blue line and sample collections are shown by the red squares. The black dashed line shows the coral bleaching threshold (value taken from NOAA Coral Reef Watch).

Admiral Reef

Coral Species: Orbicella annularis

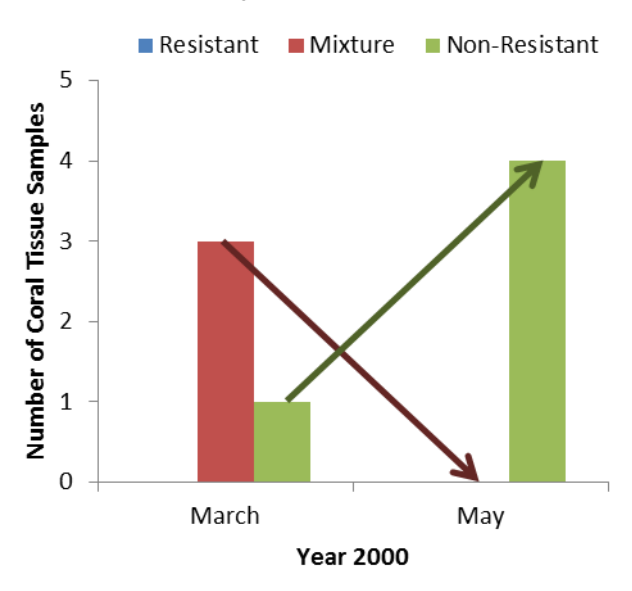


Figure 3.9. Zooxanthellae clade distribution at Admiral Reef for coral species *O. annularis*. The resistant zooxanthellae clade (blue bar) is clade D1, zooxanthellae clade mixture (red bar) is a combination of resistant and non-resistant clades, and non-resistant zooxanthellae clades (green bar) are clades B1 and C3.

Little Grecian Reef

Species: Orbicella faveolata

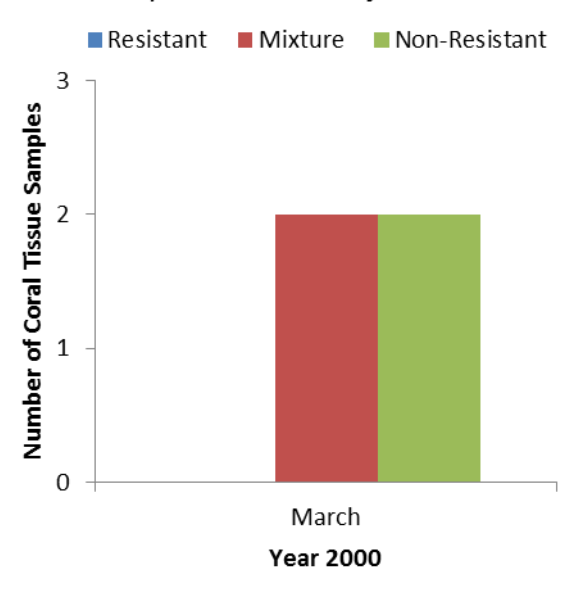


Figure 3.10. Zooxanthellae clade distribution at Little Grecian Reef for coral species *O. faveolata*. The resistant zooxanthellae clade (blue bar) is clade D1, zooxanthellae clade mixture (red bar) is a combination of resistant and non-resistant clades, and non-resistant zooxanthellae clades (green bar) is clade B1.

Acknowledgements

We thank the National Science Foundation for the support of this study (OCE-105783).

References

- Berkelmans, R., De'ath, G., Kininmonth, S. & Skirving, W. J. A comparison of the 1998 and 2002 coral bleaching events on the Great Barrier Reef: spatial correlation, patters, and predictions. *Coral Reefs.* **23**, 74-83 (2004).
- Berkelmans, R. & Van Oppen, M. J. H. The role of zooxanthellae in the thermal tolerance of corals" a "nugget of hope" for coral reefs in an era of climate change. *Proc. R. Soc.* **273**, 2305-2312 (2006).
- Brown, B.E. Coral bleaching: causes and consequences. *Coral Reefs.* **2100**, 129-138 (1997).
- Buddemeier, R. W. & Fautin, D. G. Coral bleaching as an adaptive mechanism. *BioScience*. **43**, 320-326 (1993).
- Burns, L. & Brinkman, D. Organic biomarkers to describe the major carbon inputs and cycling of organic matter in the central Great Barrier Reef region. *Estuar. Coast. Shelf Sci.* **93**, 132-141 (2011).
- Dodds, L. A., Black, K. D., Orr, H. & Roberts, J. M. Lipid biomarkers reveal geographical differences in food supply to the cold-water coral Lophelia pertusa (Scleractinia). *Mar. Scol. Prog. Ser.* **397**, 113-124 (2009).
- Downs, C. A., Mueller, E., Phillips, S., Fauth, J. E. & Woodley, C. M. A molecular biomarker system for assessing the health of coral (Montastraea Faveolata) during heat stress. *Mar. Biotechnol.* **2,** 533-544 (2000).
- Elvidge, C. D., Dietz, J. B., Berkelman, R., Andréfouët, S., Skirving, W., Strong A. E. & Tuttle, B. T. Satellite observation of Keppel Islands (Great Barrier Reef) 2002 coral bleaching using IKONOS data. *Coral Reefs.* **23**, 123-132 (2004).
- Fitt, W. K., McFarland, F. K., Warner, M. E. & Chilcoat, G. C. Seasonal patterns of tissue biomass and densities of symbiotic dinoflagellates in reef corals and relation to coral bleaching. *Limnol. Oceanogr.* **45**, 677-685 (2000).
- Glynn, P. W. & D'Croz, L. Experimental evidence for high temperature stress as the cause of El Niño coincident coral mortality. *Coral Reefs.* **8,** 181-191 (1990).
- Grottoli, A. G., Rodrigues, L. J., & Palardy, J. E. 2006. Heterotrophic plasticity and resilience in bleached corals. *Nat. Lett.* **440**, 10-13 (2006).

- Harland, A. D., Navarro, J. C., Spencer Davies, P. & Fixter, L. M. Lipids of some Caribbean and Red Sea corals: total lipid, wax esters, triglycerides and fatty acids. *Mar. Biol.* **117**, 113-117 (1993).
- Hernández-Pacheco, R., Hernández-Delgado, E. A. & Sabat, A. M. Demographics of bleaching in a major Caribbean reef-building coral: Montastraea annularis. *Ecosphere*. **2,** 1-13 (2011).
- Houlbrèque, F. & Ferrier-Pagès, C. Heterotrophy in tropical scleractinian corals. *Biol. Rev.* **84**, 1-17 (2009).
- Hughes, T. P., *et al.* Climate change, human impacts, and the resillience of coral reefs. *Science* **301**, 929-934 (2003).
- Imbs, A. B. & Yakovleva, I. M. Dynamics of lipid and fatty acid composition of shallow-water corals under thermal stress: an experimental approach. *Coral Reefs.* **31**, 41-53 (2012).
- Jones, A. M., Berkelmans, R., van Oppen, M. J. H., Mieog, J. C. & Sinclair, W. A community change in the algal endosymbionts of a scleractinian coral following a natural bleaching event: field evidence of acclimatization. *Proc. R. Soc. B.* **275**, 1359-1365 (2008).
- Jones, A. & Berkelmans, R. Potential costs of acclimatization to a warmer climate: growth of a reef coral with heat tolerant vs. Sensitive symbiont types. *PLOS.* **5**, (2010).
- Kemp, D. W. *et al.* Catastrophic mortality on inshore coral reefs of the Florida Keys due to severe low-temperature stress. *Glob. Chang. Biol.* **17**, 3468-3477 (2011).
- Kinzie III, R. A., Takayama, M., Santos, S. R. & Coffroth, M. A. The adaptive bleaching hypothesis: experimental tests of critical assumptions. *Biol. Bull.* **200**, 51-58 (2001).
- LaJeunesse, T. C. Inverstigating the biodiversity, ecology, and phylogeny of endosymbiotic dinoflagellates in the genus *Symbiodinium* using the ITS region: in search of a "species" level marker. *J. Phycol.* **37**, 866-880 (2001).
- LaJeunesse, T. C. Diversity and community structire of symbiotic dinoflagellates from Caribbean coral reefs. *Mar. Biol.* **141,** 387-400 (2002).
- Little, A. F., Van Oppen, M. F. & Willis, B. L. Flexibility in algal endosymbioses shapes growth in reef corals. *Science*. **403**, 1492-1495 (2004).
- Mazurek, M. A., Simoneit, B. R. T., Cass, G. R. & Gray, H. A. Quantitative high-resolution gas chromatography and high-resolution gas chromatography-mass spectrometry Nlysis of carbonaceous fine aerosol particles. *Int. J. Environ. Anal. Chem.* **29**, 119-139 (1987).
- Medeiros, P. M. & Simoneit, B. R. T. Analysis of sugars in environmental samples by gas chromatography mass spectrometry. *J. Chromatogr. A.* **1141**, 271-278 (2007).

- Muscatine, L. Glycerol excretion by symbiotic algae from corals and tridacna and its control by the host. *Science*. **157**, 516-519 (1967).
- Porter, J. W., Fitt, W. K., Sperot, H. J., Rogerst, C. S. & White, M. W. Bleaching in reef corals: physiological and stabe isotope responses. *Proc. Natl. Acad. Sci.* **86**, 9342-9346 (1989).
- Rodrigues, L. J. & Grottoli, A. G. Energy reserves and metabolism as indicators of coral recovery from bleaching. *Limnol. Oceanogr.* **52,** 1874-1882 (2007).
- Rodrigues, L. J., Grottoli, A. G., & Pease, T. K. Lipid class composition of bleached and recovering Porites compressa Dana, 1846 and Montipora capitata Dana, 1846 corals from Hawaii. *J. Exp. Mar. Bio. Ecol.* **358**, 136-143 (2008).
- Rowan, R. Thermal adaptation in reef coral symbionts. *Nature*. **430**, 742 (2004).
- Rowan, R., Knowlton, N., Baker, A. & Jara, J. Landscape ecology of algal symbionts creates variation in episodes of coral bleaching. *Lett. to Nat.* **388**, 265-269 (1997).
- Schoepf, V. *et al.*. Coral energy reserves and calcfication in a high-CO2 world at two temperatures. *PloS One* **8**, 1-11 (2013).
- Thornhill, D. J., LaJeunesse, T. C., Kemp, D. W. & Schmidt, G. W. Multi-year, seasonal genotypic surveys of coral-algal symbiosis receal prevalent stability or post-bleaching reversion. *Mar. Biol.* **148**, 711-722 (2006).
- Treignier, C., Tolosa, I., Grover, R., Reynaud, S and Ferrier-Pagès, C. Carbon isotope composition of fatty acids and sterols in the scleractinian coral Tubinaria reniformis: effect of light and feeding. *Limnol. Oceanogr.* **54**, 1933-1940 (2009).
- van Oppen, M. J. H. Mahiny, A. & Done, T. Geographic patterns of zooxanthellae types in three coral species on the Great Barrier Reef sampled after the 2002 bleaching event. *Coral Reefs.* **24**, 482-487 (2005).
- Volkman, J.K., Barrett, S.M., Blackburn, S.I., Mansour, M.P., Sikes, E.I., Gelin, F., 1998. Microalgal biomarkers: A review of recent research developments. *Org. Geochem.* **29**, 1163-1179.
- Wakeham, S. G. *et al.* Organic biomarkers in the twilight zone- time series and settling velocity sediment traps during MedFlux. *Deep. Res. Part II.* **56,** 1363-1368 (2009).

CHAPTER 4

CONCLUSIONS

The advantages of using a multi-biomarker approach are clearly demonstrated in this thesis work. The ability to identify and quantify specific compounds in an environmental sample is an essential tool for understanding a system on the molecular level. No technique is perfect to elucidate the wide range of sizes and polarities of all organic compounds in a sample, but molecular biomarkers provide unique information and are a versatile analytical technique.

Additionally, new biomarkers are continually being determined, thus widening the applicability of the technique to other disciplines such as pharmaceutical and food industries, and forensic science (Medeiros and Simoneit, 2007).

The work in this thesis demonstrates the utility of molecular biomarkers in providing information about organic carbon source, transport, distribution, and transformation. In the second chapter, biomarker and isotope data from the Gulf of Mexico sediments clearly demonstrated that at least part of the subsurface oil plume observed after the spill reached the seafloor, peaking by the end of 2010. Furthermore, it was hypothesized that the diluted biomarker signal seen following this mass oil sedimentation event was due to the resuspension and horizontal movement of the sediments. In the third chapter, biomarker data from coral tissue samples allowed seasonal and long-term signals to be distinguished. This data showed a clear reaction to stress induced by high sea surface temperatures in August as well as the long-term

recovery of the coral tissue samples from the 1997-1998 El Niño, the strongest on record (McPhaden, 2015). The overall response to the seasonal thermal stress was an increase in energy reserve compounds (monosaccharides and sugar alcohols) as if preparing for a bleaching event and *n*-alkanols (more specifically hexadecanol, a biomarker for zooplankton), and a decrease of membrane components (sterols and fatty acids). The resistant zooxanthellae clade was chemically distinct from the others with higher monosaccharide and sugar alcohol concentrations and lower levels of *n*-alkanols- an indication that the corals did not participate in as much heterotrophy (consumption of zooplankton) to overcome the thermal stress due to the larger reserves of energy. The long-term recovery from the 1997-1998 El Niño presented itself as increased levels of monosaccharides and sugar alcohols in March of 2000 similar to what was seen in August, a period of thermal stress.

This thesis has presented an insight into the elucidation of biomarkers, and their applications as molecular tracers for natural and anthropogenic processes. The number of novel compounds as well as the applications of biomarker tracers is expected to keep increasing. The utilities of GC and MS for contemporary interdisciplinary sciences will also continue to expand, especially as the analytical instrument capabilities develop further with increased sensitivities, ease of operation, lower maintenance, better separation technology, improved ionization efficiencies, etc. Because many applications of GC and MS are interdisciplinary, it would be of great utility to incorporate the missing mass spectra with corresponding GC retention data of the numerous natural products, synthetic compounds, geological biomarkers, environmental biomarkers, and their various derivatives (TMS, Ac) documented by organic geochemists and environmental chemists into the commercial MS libraries. This would greatly enhance the quality and reliability of future literature data.

References

McPhaden, M. J. Playing hide and seek with El Niño. Nature Clim. Change. 5, 791–795 (2015).

Medeiros, P. M. & Simoneit, B. R. T. Gas chromatography coupled to mass spectrometry for analyses of organic compounds and biomarkers as tracers for geological, environmental, and forensic research. *J. Sep. Sci.* **30**, 1516-1536 (2007).

APPENDIX A

EXPORT OF TERRIGENOUS DISSOLVED ORGANIC MATTER IN A BROAD ${\bf CONTINENTAL~SHELF}^1$

¹Medeiros, P. M., Babcock-Adams, L., Seidel, M., Castelao, R. M., Hollibaugh, J. T., Di Iorio, D. & Dittmar, T. To be submitted to *Estuar. Coast. Shelf Sci*.

Abstract

Export of terrigenous dissolved organic matter (DOM) from rivers to the ocean is an important component of the carbon cycle. Observations from six research cruises in 2014 were used to characterize the seasonal evolution of the distribution of terrigenous DOM in the broad and shallow continental shelf of the South Atlantic Bight (SAB). While DOM with a strong terrigenous signature was restricted to a band near the coast early in the year, molecular formulae that are plausibly indicators of riverine inputs (t-Peaks) extended all the way to the shelf break in late spring. The offshore transport of the t-Peaks was consistent with advection in a surface layer due to upwelling-favorable winds. On those time scales spanning about one month, t-Peaks were mostly resistant to bio and photo degradation, and their decrease in relative abundance over the shelf was consistent with dilution of the river plume due to entrainment of marine water associated with wind-driven mixing. Since the t-Peaks are photo-degradable on longer time scales, it is possible that photo-mineralization and/or photo-transformations contributed to their removal during summer and fall. Comparisons between optical measurements and ultrahigh resolution mass spectrometry data revealed that the fraction of the DOM pool with a riverine signature in the SAB can be estimated using the spectral slope coefficient of chromophoric DOM in the 275-295 nm range ($S_{275-295}$). This opens up the possibility of mapping the distribution of riverine DOM over the SAB shelf in high spatial resolution, a crucial step for quantifying shelf-slope exchange.

1. Introduction

Rivers represent an important source of dissolved organic carbon (DOC) to the ocean, having a significant impact on the biogeochemistry of ocean margins. The total DOC flux to the ocean is estimated at 250-260 Tg C year⁻¹ (Hedges et al., 1997; Raymond and Spencer, 2015), being sufficient to support the turnover of DOC throughout the marine environment (Williams and Druffel, 1987). The fate of this terrigenous DOC in the ocean has important ramifications for the global carbon cycle, but remains enigmatic (Hedges et al., 1997; Cauwet, 2002; Benner, 2004; Fichot and Benner, 2014). Multiple studies have shown that a large fraction of the material is remineralized in ocean margins (Hedges et al., 1997; Opsahl and Benner, 1997; Bianchi, 2011; Letscher et al., 2011; Fichot and Benner, 2014). This is because terrestrial dissolved organic matter (DOM) can experience substantial alterations over relatively short time scales (e.g., Benner and Opsahl, 2001; Hernes and Benner, 2003; Hansell et al., 2004; Spencer et al., 2009; 2015), often due to a combination of photo-oxidation, microbial degradation, and flocculation (e.g., Sholkovitz, 1978; Hernes and Benner, 2003). Despite that, a portion of the terrigenous DOM has been shown to be transported offshore in many coastal regions (Vodacek et al., 1995; Bates and Hansell, 1999), escaping the continental margin (e.g., Fichot et al., 2014; Medeiros et al., 2015c; Seidel et al., 2015) and being transported to the open ocean (Opsahl and Benner, 1997; Medeiros et al., 2016).

Even though the transfer of organic matter from land to sea is one of the most important pathways for preservation of terrigenous production in modern environments (Hedges, 1992), much remains to be learned about the processes controlling the distribution of terrigenous DOM in coastal environments. Understanding the production, transport and fate of terrigenous DOM in aquatic ecosystems is of direct relevance to studies addressing a variety of issues (Spencer et al.,

2012), from water quality to bacterioplankton community structure and function (Crump et al., 2009; Krupa et al., 2012). Tracing the distribution of terrigenous DOM over continental shelves is challenging, however, because of the highly dynamic nature of those environments. Although a fraction of freshwater DOM is indistinguishable from marine DOM (Repeta et al., 2002), significant differences have been reported between the composition of riverine and marine DOM (e.g., Sleighter and Hatcher, 2008; Medeiros et al., 2015c). Marine DOM is comparatively enriched with molecular formulae with high H/C ratios (characteristic of a shift to more aliphatic structures) compared to DOM from freshwater samples (Sleighter and Hatcher, 2008; Medeiros et al., 2015a). Rivers are known to be important sources of aromatic compounds to the ocean (e.g., Mannino and Harvey, 2004; Stubbins et al., 2010; Ziolkowski and Druffel, 2010). As such, characterizing the DOM composition at the molecular level provides useful information about the distribution of terrigenous material over the shelf.

Off the southeastern United States, in the South Atlantic Bight (SAB), rivers have been recently characterized as having unusually high yields of terrigenous chromophoric DOM (CDOM), indicating the importance of the SAB with respect to biogeochemical cycling of CDOM (Spencer et al., 2013). The distribution of the CDOM optical properties on the SAB inner shelf has been shown to be strongly related to the flux of terrestrial organic matter through river discharge (Kowalczuk et al., 2003; 2009). DOC along the salinity gradient from the terrestrial source toward the open ocean appears to behave mostly conservatively in the northern sector of the SAB (Avery et al., 2004). Optical analyses indicate, however, that radical changes in the CDOM composition occur along the river-to-oceanic salinity gradient (Kowalczuk et al., 2003), possibly associated with photo degradation of aromatic compounds (Gonsior et al., 2009). The combination of alternating cycles of sunlight and microbial activity has also been shown to result

in efficient degradation of DOM and marine humic substances (Miller and Moran, 1997; Moran et al., 2000). Here, we use an extensive data set collected in the SAB during 6 research cruises in 2014 and detailed analyses of DOM composition at the molecular level to investigate the seasonal evolution of the distribution of terrigenous DOM over the shelf. We further assess the different mechanisms controlling that distribution, including variations in hydrological conditions, atmospheric forcing, and the potential importance of degradation processes.

2. Experimental Methods

2.1. Study Area and Samples Collection

Six mapping surveys were carried out in the central South Atlantic Bight (SAB) in 2014 (Figure A1). The surveys, in April, May, July, August, September and November (Figure A.S1), were intended to sample shelf conditions under different seasons and to capture the peak in discharge from the Altamaha River in spring. The surveys were composed of zonal sections, starting at the mouth of the estuaries around Sapelo Island off the coast of Georgia and extending offshore to the 400 m isobath (Figure A1). In total, one hundred samples were collected for DOC, CDOM, stable carbon isotopes and ultrahigh resolution mass spectrometry.

Approximately 70-80 additional samples were collected in each cruise for DOC and CDOM analyses only.

Samples were collected at the surface at each station (**Figure A1**). Bottom samples were also collected at selected stations offshore of the 30 m isobath. Immediately after collection, water samples were filtered (sequentially through 0.7 µm Whatman GF/F filters pre-combusted at 450°C for 5 h and pre-washed 0.2 µm Pall Supor membrane filters) and aliquots were collected for DOC and CDOM analyses. Filtrates were acidified to pH 2 (concentrated HCl) and

DOM was isolated using solid-phase extraction (SPE) cartridges (Agilent Bond Elut PPL) as in Dittmar et al. (2008).

Water from the Altamaha River (salinity S=0) was also collected in May 2013 and immediately incubated in the dark for 70 days following Medeiros et al. (2015b,c). Water samples were first filtered through 0.7 μ m Whatman GF/F filters (pre-combusted at 450°C for 5 h) to remove photosynthetic organisms, collected into combusted 1 L amber glass bottles in triplicate, and kept in the dark. At the end of the experiment, after 70 days, all samples were filtered, acidified, and DOM was extracted using PPL cartridges as described before.

2.2. Chemical Analyses

DOC concentrations from water samples and SPE extracts (i.e., dried and resuspended in ultrapure water) were measured with a Shimadzu TOC-L_{CHP} analyzed with daily potassium hydrogen phthalate (KHP) standard curves and regular analysis of Consensus Reference Materials obtained from the University of Miami (Hansell, 2005). SPE efficiency was 72 \pm 5% of the DOC. CDOM absorbance was measured with an Agilent UV-VIS 8453 Spectrophotometer and converted to absorption coefficients as in D'Sa et al. (1999). The spectral slope coefficient in the 275-295 nm range (S₂₇₅₋₂₉₅) was estimated using a nonlinear exponential fit of the absorption coefficients in that range, and are reported in units of nm⁻¹. Bulk δ ¹³C of extracted DOC (SPE-DOC) were analyzed with a Finnigan MAT 251 isotope ratio mass spectrometer after complete drying. All isotopic compositions were expressed relative to the standard VPDB (Vienna Pee Dee Belemnite), and procedural blanks did not yield detectable amounts of carbon isotope contamination.

The molecular composition of the DOM extracts (15 mg C L⁻¹ in 1:1 methanol/water) was analyzed by ultrahigh-resolution mass spectrometry using a 15T Fourier transform ion cyclotron resonance mass spectrometer (FT-ICR MS; Bruker Daltonics) with electrospray ionization (negative mode) as in Seidel et al. (2014). Molecular formulae were calculated in the mass range between 150 and 850 Da. Additional details of molecular formulae assignment are given in Seidel et al. (2014). Approximately 4,000 molecular formulae were identified in the complex DOM mixture in each sample. As in previous studies (e.g., Flerus et al., 2012; Lechtenfeld et al., 2014), FT-ICR MS data evaluation was based on normalized peak magnitudes.

Patterns of variability in FT-ICR MS-derived DOM composition were distinguished by principal component (PC) analysis (Bro and Smilde, 2014 after normalization by the standard deviation between samples and mean centering). The first two PCs were significantly different (95% confidence level) from results from PC analysis of spatially and temporally uncorrelated random processes (Overland and Preisendorfer, 1982). We focused here on the first PC, which is significantly correlated with δ^{13} C signatures (**Figure A.S2a**). The loading of PC 1 was examined as a van Krevelen diagram, an element-ratio plot displaying molar ratios of H/C and O/C. Major chemical classes typically found in DOM have characteristic molar ratios, clustering within specific regions in van Krevelen space (Kim et al., 2003). Based on extensive comparisons with geochemical tracers (e.g., lignin, dissolved black carbon, δ^{13} C DOC) in multiple regions, the pattern revealed by the loadings of PC 1 (**Figure A.S2b**) has been shown to be related to gradients in terrigenous vs marine signatures in DOM composition (Medeiros et al., 2015a,c). As such, PC 1 provides information about the contribution of terrigenous and marine sources to the DOM pool (as analyzed by FT-ICR MS).

Additional information about terrigenous inputs was obtained by tracking the distribution of the t-Peaks, a set of 184 molecular formulae that have been recently identified as plausible indicators of riverine input (Medeiros et al., 2016). The frequency of occurrence and relative abundance of the t-Peaks in the global ocean were shown to be statistically correlated with known tracers of terrigenous inputs, and they were also observed in all samples from four different major rivers characterized by vastly different landscape and vegetation coverage spanning equatorial, subtropical and Arctic regions (Medeiros et al., 2016). One of the rivers used in the study identifying the t-Peaks was the Altamaha River. Here, we used the t-Peaks to further identify and track the presence of terrigenous DOM over the shelf. We quantified both their frequency of occurrence (i.e., the fraction of the 184 t-Peaks observed in each sample) as well as their contribution to the total magnitude of all peaks in the spectrum (i.e., the sum of the relative intensity of all t-Peaks divided by the sum of the relative intensity of all peaks in the spectrum for each sample). Medeiros et al. (2016) also proposed a new index indicative of riverine inputs (Iterr) based on the ratio of the relative abundances of molecular formulae with relative abundance highly correlated negatively and positively with δ^{13} C SPE-DOC. The ratio increases with the terrigenous signature of the sample, and has been shown to be highly correlated with tracers of terrigenous input. We computed that ratio for all samples in this study.

2.3. Environmental Data

Hydrographic data were collected during the research cruises using a Sea-Bird conductivity-temperature-depth (CTD) instrument. Winds were measured at the NOAA National Data Buoy Center (NDBC) buoy 41008 located at 31.4°N, 80.87°W (see **Figure A1** for location). Neutral wind stress was calculated following Large and Pond (1981), and then low-

pass filtered (half-power point of 40 h) to remove short-period fluctuations (**Figure A2a**). Freshwater discharge in the region is dominated by the Altamaha River. Daily values of discharge (**Figure A2b**) at Doctortown, GA were obtained at the UGSG website. Climatological discharge was computed as the average for each day of the year between 1932 and 2014. DOC concentrations were measured at the Altamaha River from October 2000 to April 2009 as part of the Georgia Coastal Ecosystem Long Term Ecological Research program (GCE-LTER). The (average \pm 1 standard deviation) time interval between sampling during that period was 5.5 \pm 6.6 days. The DOC flux was computed at 15 day intervals by multiplying the average DOC concentration by the average river discharge during that period (**Figure A2c**).

2.4. Plume Mixing Model

The scenario in which buoyant water is transported offshore by upwelling favorable winds was explored in great detail by Fong and Geyer (2001) and Lentz (2004). They showed that, while the plume is advected offshore, it is susceptible to significant mixing. A two-dimensional model developed by Lentz (2004) was used to quantify plume mixing due to winds. The primary model assumption is that competition between wind-driven vertical mixing and geostrophic adjustment associated with buoyancy forcing at the offshore edge of the plume results in continual entrainment. Assuming that wind-driven vertical mixing satisfies a bulk Richardson criterion, the dilution of the plume as it mixes with ambient water can be computed (e.g., Castelao et al., 2008). Model predictions have been shown to compare well with observations (Lentz, 2004).

3. Results and Discussion

3.1. Seasonal Evolution of Terrigenous DOM over the Shelf

The wind stress during 2014 exhibited the typical "weather band" variability, with fluctuations of the order of a few days (**Figure A2a**). Alongshore winds oscillated frequently between upwelling and downwelling favorable early in the year, until approximately mid-April. After that, winds became predominantly upwelling favorable until late September. From October until the end of the year, the frequency of downwelling favorable wind events increased substantially.

The peak in the historical averaged discharge in the Altamaha occurs in mid-March to early April. The seasonal evolution of discharge from the Altamaha River in 2014 was generally consistent with climatological values (**Figure A2b**). A large pulse in discharge was observed in late April, between the first and second research cruises. After that, river discharge was small for most of the summer and fall, increasing slightly toward the end of the year. Although no high resolution DOC flux estimates are available for 2014, climatological values from 2000 to 2009 show a picture that is consistent with the climatology in river discharge (**Figure A2c**). River discharge and DOC flux from 2000 to 2009 were correlated in the Altamaha river (r = 0.91, p < 0.001), suggesting that the DOC flux out of the river in 2014 was likely large until late May, decreasing substantially after that.

Hovmoller diagrams of surface water properties along the transect extending offshore from the Altamaha River mouth (see **Figure A1** for location) are shown in **Figure A3**. Surface salinity exhibited strong seasonal variability (**Figure A3a**), with the freshest water occurring near the coast in spring, when the coastal band with low-salinity water extended to about 40-50 km offshore. From April to mid-May, freshwater was transported offshore, which is consistent

with the wind transition to predominantly upwelling favorable winds (**Figure A2a**). Loss of freshwater from the inner shelf has been shown to be related to northward alongshore wind stress (Blanton and Atkinson, 1983). Salinity over the shelf away from the coastal zone increased after that (**Figure A3a**) following the decrease in river discharge (**Figure A2b**).

We investigated the seasonal evolution of multiple geochemical tracers indicative of riverine inputs to track the distribution of terrigenous DOM over the shelf (**Figure A3b-f**). The different parameters revealed a consistent picture. In mid-April, when river discharge was large and winds oscillated between upwelling and downwelling favorable frequently, terrigenous DOM was observed in a relatively broad band near the coast. In mid-May, however, comparatively high PC 1 values (which are associated with terrigenous DOM; Figure A.S2) were observed throughout the shelf, all the way to the shelfbreak. The frequency of occurrence of the t-Peaks, their contribution to the total magnitude of all peaks in the FT-ICR MS spectrum, and the index indicative of riverine inputs (Iterr) were also enhanced all the way to the shelfbreak. The distribution of δ^{13} C SPE-DOC also revealed an increased terrigenous signature over the mid-shelf in mid-May, although observations were not available near the shelfbreak. During that time, vertical profiles of these quantities indicated that the increase in the terrigenous signature over the mid-shelf was restricted to the upper water column (**Figure A4a,b**), which is consistent with the increase being associated with the offshore transport of low-salinity waters by upwelling favorable winds in a surface Ekman layer. Vertical profiles during the other months in which observations were available were nearly depth-independent. Profiles offshore of the shelfbreak, around the 400 m isobath, were also depth-independent. Unfortunately no profile offshore of the shelfbreak was available for mid-May (**Figure A4c,d**), when the significant

increase in the terrigenous contribution to the total DOM pool over the mid and outer shelf was observed.

The different parameters revealed that the terrigenous signature over the shelf was substantially reduced during summer (**Figure A3**), being mostly limited to inshore of the 15-20 m isobath. It is important to emphasize that, despite the intensive field effort conducted in 2014 with 6 research cruises, no observations were collected between mid-May and mid-July. As such, it is not clear if terrigenous DOM was transported beyond the shelfbreak between those two cruises.

3.2. What Controls the Distribution of t-Peaks over the Shelf?

Since the t-Peaks have recently been proposed as plausible indicators of riverine inputs (Medeiros et al., 2016), it is instructive to investigate what processes controlled their distribution over the shelf. Evidently, due to their frequency of occurrence and contribution to the total magnitude of all peaks in FT-ICR MS spectra being enriched in rivers (Medeiros et al., 2016), t-Peaks were abundant near the coast in early April, when river discharge was high (**Figure A3e,f**). The region where the t-Peaks made an important contribution to the total DOM pool widened from early April to mid-May, presumably due to the influence of upwelling-favorable winds transporting low-salinity waters offshore. At that time, their contribution to the total intensity in the FT-ICR MS spectra decreased with distance from shore. What processes controlled that decrease?

Since the temporal evolution of the distribution of the t-Peaks closely resembles the evolution of surface salinity over the shelf (compare **Figure A3f** with **Figure A3a**), one likely candidate is mixing of riverine and oceanic water. Previous studies have shown that significant

mixing occurs when buoyant water from a river plume is transported offshore by upwellingfavorable winds (Fong and Geyer, 2001; Lentz, 2004). We used the two-dimensional model developed by Lentz (2004) to estimate the expected amount of mixing between plume and ambient waters as the plume was advected offshore in a surface Ekman layer in response to winds. We used the plume characteristics (e.g., salinity anomaly) from the April cruise (April 4th) as initial conditions, and ran the model until May 17th, when *in situ* observations from the May cruise were available. Model results showed that wind-driven mixing would be enough to decrease the salinity anomaly of the plume on mid-May to about 30±8% of the initial salinity anomaly in early April (**Figure A5**). This agreed very well with the actual salinity anomaly measured on May 17th offshore, which was 32% of the anomaly in early April near the coast. This suggested that wind-driven mixing alone was enough to explain the observed dilution in the plume between April and May. We also computed the anomaly in the contribution of the t-Peaks to the total magnitude of all peaks in the FT-ICR MS spectrum. The anomaly was defined as the difference between the contribution of the t-Peaks at a given sample and the contribution of the t-Peaks in the marine end-member (i.e., the average of the samples collected at depth off the shelf). The calculation revealed that the anomaly offshore in the plume in mid-May was 33.5% of the anomaly near the coast in early April (Figure A5), once again agreeing with the expected mixing between plume and ambient water. Collectively, these results suggested that the decrease in the contribution of the t-Peaks to the total magnitude of all peaks as the low-salinity plume was transported offshore could be explained by wind-driven mixing alone, without the need to invoke degradation processes.

Further support for this interpretation was obtained by analyses of temporal changes in the distribution of t-Peaks during a 70-day long dark incubation of Altamaha River water

(**Figure A.S3**). The frequency of occurrence of the t-Peaks remained unaltered at 100% during the course of the incubation. Furthermore, the contribution of the t-Peaks to the total magnitude of all peaks in the spectrum also remained unaltered, suggesting that the t-Peaks were not preferentially degraded, at least on the time scale of the incubation. This is consistent with the interpretation that the distribution of the t-Peaks over the shelf between April and May was mostly controlled by mixing.

Photo-mineralization has been shown to be an important removal mechanism for terrigenous DOM (Obernosterer and Benner, 2004). This is because terrigenous DOM is generally enriched in polycyclic aromatic compounds and in polyphenols (e.g., Mannino and Harvey, 2004; Stubbins et al., 2010; Ziolkowski and Druffel, 2010; Jaffé et al., 2013). Dissolved aromatic compounds can be highly susceptible to photo-degradation (Opsahl and Benner, 1998). Since the aromaticity index (a measure of the aromaticity of the molecules; Koch and Dittmar, 2006) of the t-Peaks is high at 0.53 ± 0.10 (Medeiros et al., 2016), one would expect them to be highly photo-degradable. Unfortunately, no investigation of changes in composition of Altamaha River DOM due to photo-degradation was conducted in parallel to the shelf wide sampling. However, photo incubation experiments have been recently pursued using water collected near the Amazon River mouth (Seidel et al., 2015). Since all 184 t-Peaks were also observed at the Amazon River mouth (Medeiros et al., 2016), this allowed us to investigate the t-Peaks' response to solar irradiation. During the course of the irradiation experiment, which lasted 5 days, the frequency of occurrence of the t-Peaks remained unaltered at 100%. The contribution of the t-Peaks to the total magnitude of all peaks in the spectrum also remained surprisingly unaltered. This suggested that, at least over the scale of a few days, the t-Peaks were mostly resistant to photo-degradation. One important factor to consider is that, in the first few days of the

experiment, the flow-through seawater in the incubation tank contained a high suspended matter load reflecting the *in situ* reduced light conditions in the mixed layer of the Amazon River plume (Seidel et al., 2015). This may have led to reduced exposure to solar irradiation, decreasing photo-degradation.

A much longer photo-irradiation experiment has been previously conducted using water from the Congo River (Stubbins et al., 2010), which initially also contained all 184 t-Peaks (Medeiros et al, 2016). The 57 days continuous solar simulator irradiation used in that study equated to 38 days under 12 hours of daylight at the mouth of the Congo River. The duration of the irradiation experiment was chosen so that over 95% of the initial CDOM light absorbance was removed, ensuring the occurrence of large shifts in DOM quality that could be readily observed by FT-ICR MS (Stubbins et al., 2010). At the end of the experiment, 94% of the t-Peaks were completely consumed (see Supporting Table of Stubbins et al., 2010), revealing that at longer time scales, most of the t-Peaks are indeed photo-degradable.

At first glance, the 38 day-long experiment (Stubbins et al., 2010) could be thought to be comparable to the 42 day-interval between the research cruises in early April and mid-May represented in the mixing model (**Figure A5**). However, the experiment likely represents an extreme case compared to shelf conditions observed in the South Atlantic Bight following the peak in river discharge. This is because Altamaha River water contains high clay and silt concentrations (Bhatti et al., 2009), which likely reduces light penetration in plume waters near the river mouth. Additionally, a given water parcel in the Altamaha River plume will only be near the top of the mixed layer where strong photo-degradation can occur a small fraction of the time. Therefore, a given water parcel would presumably have to remain in the mixed layer much longer than 38 days to experience the same amount of photo-degradation experienced in the

Congo River irradiation experiment. If we assume that the effective photochemical depth in the plume is about 10-20% of the mixed layer depth (for example, an effective light penetration of a few meters in a 15-20 m-thick surface mixed layer; Kieber et al., 1990), then the 5-day long irradiation experiment in the Amazon River (Figure A6) may be more directly relevant to the photo-degradation of the t-Peaks in the South Atlantic Bight from early April to mid-May. If that is true, then the t-Peaks would be not only mostly resistant to biodegradation (Figure A6), but also to photo-degradation on scales of 1 month or so under the observed shelf conditions in the SAB. That is consistent with the interpretation that the observed decrease in the relative abundance of the t-Peaks between early April and mid-May can be explained by wind-driven mixing of plume and oceanic waters (Figure A5) as the lens of low-salinity water was transported offshore (Figure A3). Since the t-Peaks are photo-degradable on longer time scales, it is possible that photo-mineralization and/or photo-transformations contributed to their removal during summer and fall. Other factors that may have contributed to the reduced signature of the t-Peaks during summer include additional dilution and northward (and possibly off shelf) export.

3.3. High Resolution Observations of Terrigenous DOM over the Shelf

The spectral slope coefficient of CDOM in the 275-295 nm range ($S_{275-295}$) has been shown to be a reliable tracer for terrigenous dissolved organic carbon in river-influenced ocean margins (e.g., Fichot and Benner, 2012; 2014). Here, we used the results from the principal component analysis (i.e., the PC 1 values, **Figure A3c** and **Figure A.S2**) to estimate the fraction of the DOM in each sample that was of terrestrial origin (tDOM). Similarly to the previous studies in other regions, $S_{275-295}$ for the 6 research cruises in the South Atlantic Bight was found to be significantly correlated to the riverine signature of the DOM pool (**Figure A6a**). tDOM for

each sample could therefore be derived from $S_{275-295}$ using two different linear fits, depending on the value of $S_{275-295}$ (**Figure A6a**). The correlation coefficient between the measured and estimated tDOM was r = 0.91 (p<0.0001) (**Figure A6b**). We note that using two separate linear fits led to better results than using a single nonlinear fit.

The results presented above indicated that it is possible to quantify the distribution of riverine DOM over the South Atlantic Bight shelf using optical measurements. That is a great advantage, since those are easier and less time-consuming to obtain compared to FT-ICR MS, which allows for observations to be collected in high spatial resolution. That is also crucial for future efforts to quantify shelf-slope exchange of riverine carbon in the South Atlantic Bight, since offshore export of shelf water is thought to occur at least partially in relatively narrow (~10 km wide) filaments (Atkinson et al., 1978) that are easily missed by low resolution observations. The spatial distribution of surface tDOM based on $S_{275-295}$ observations in early April is shown in **Figure A7** as an example, together with the salinity distribution in the surface layer. Consistently with the results presented in the previous section, the distributions of tDOM and salinity were spatially correlated. Tongues of increased tDOM could be observed extending offshore from near the mouth of the Altamaha River and Sapelo Sound, and tDOM decreased offshore. There was also a general tendency for high tDOM and low salinity values to extend farther offshore in the northern part of the sampling area. This was likely because freshwater input to the south of the Altamaha River in the South Atlantic Bight is quite small (Atkinson et al., 1983). As upwelling favorable winds transported the low-salinity waters offshore in a surface Ekman layer, plume waters were also presumably transported alongshelf by the wind-driven mean circulation, which is predominantly northward during spring/summer (Lee et al., 1991). This may help explain why the frequency of occurrence of the t-Peaks and their contribution to the total

intensity of all peaks in the FT-ICR MS spectrum decreased rapidly offshore of the shelfbreak in May 2014 (**Figure A3f**). Since the terrigenous material was likely transported alongshelf at the same time that it was transported offshore (e.g., **Figure A7**), any off shelf export of terrigenous material from the Altamaha River would presumably have occurred to the north of the main transect where FT-ICR MS analysis were concentrated (**Figure A1**). Off shelf export of terrigenous DOM along the Altamaha River transect would presumably only be observed if there were significant inputs to the south of the Altamaha River, which is not the case (Atkinson et al., 1983).

4. Conclusions

We investigated the distribution of terrigenous DOM over a shallow, broad continental shelf at seasonal scales, as well as the underlying mechanisms controlling that distribution, using ultrahigh resolution mass spectrometry and stable carbon isotope analyses. Observations were collected during multiple research cruises in the South Atlantic Bight off the southeastern United States, from early spring to fall. Terrigenous DOM was found to be restricted to a band near the coast early in the year, being rapidly transported offshore all the way to the shelfbreak in a surface layer once winds become predominantly upwelling favorable. As the low salinity plume was transported across the shelf, wind-driven mixing and entrainment of marine water resulted in the progressive dilution of the terrigenous DOM signature. The signature of the terrigenous DOM over the shelf during summer and fall was substantially smaller, likely due to a combination of reduced riverine input and northward (and possibly off-shelf) export. Since the t-Peaks are photo-degradable on long time scales, it is also possible that photo-transformations contributed to their reduced signature at that time. Comparing the spectral slope coefficient of

CDOM in the 275-295 nm range (S275-295) with the overall riverine signature of the DOM based on mass spectrometry data from all seasons revealed a statistically significant correlation. That is important, because optical measurements are less costly and less time consuming to obtain. As such, the availability of high resolution optical measurements spanning large sectors of the South Atlantic Bight would contribute to better constrain shelf-slope exchange of riverine carbon in the region.

Figures

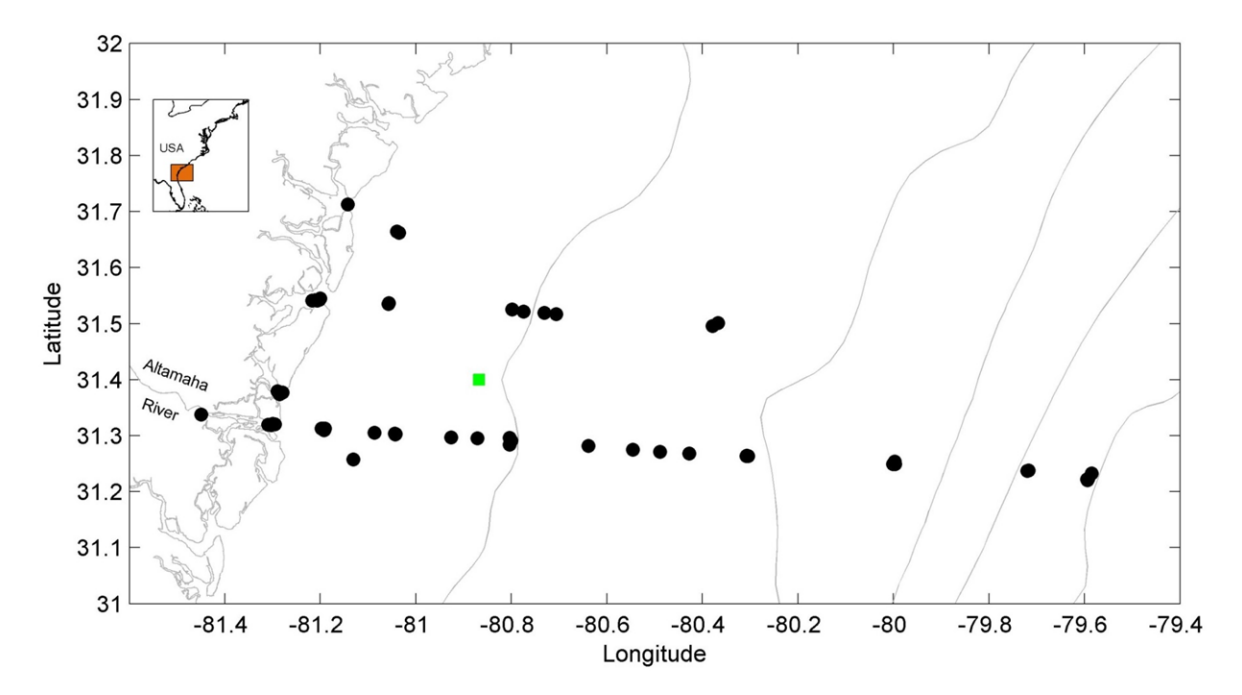


Figure A1. Study area off southeastern United States showing sampling location (black circles). Location of NOAA NDBC buoy 41008 at Gray's Reef is shown by the green square. Topographic contours shown are 20, 40, 60, 200 and 400 m (gray lines).

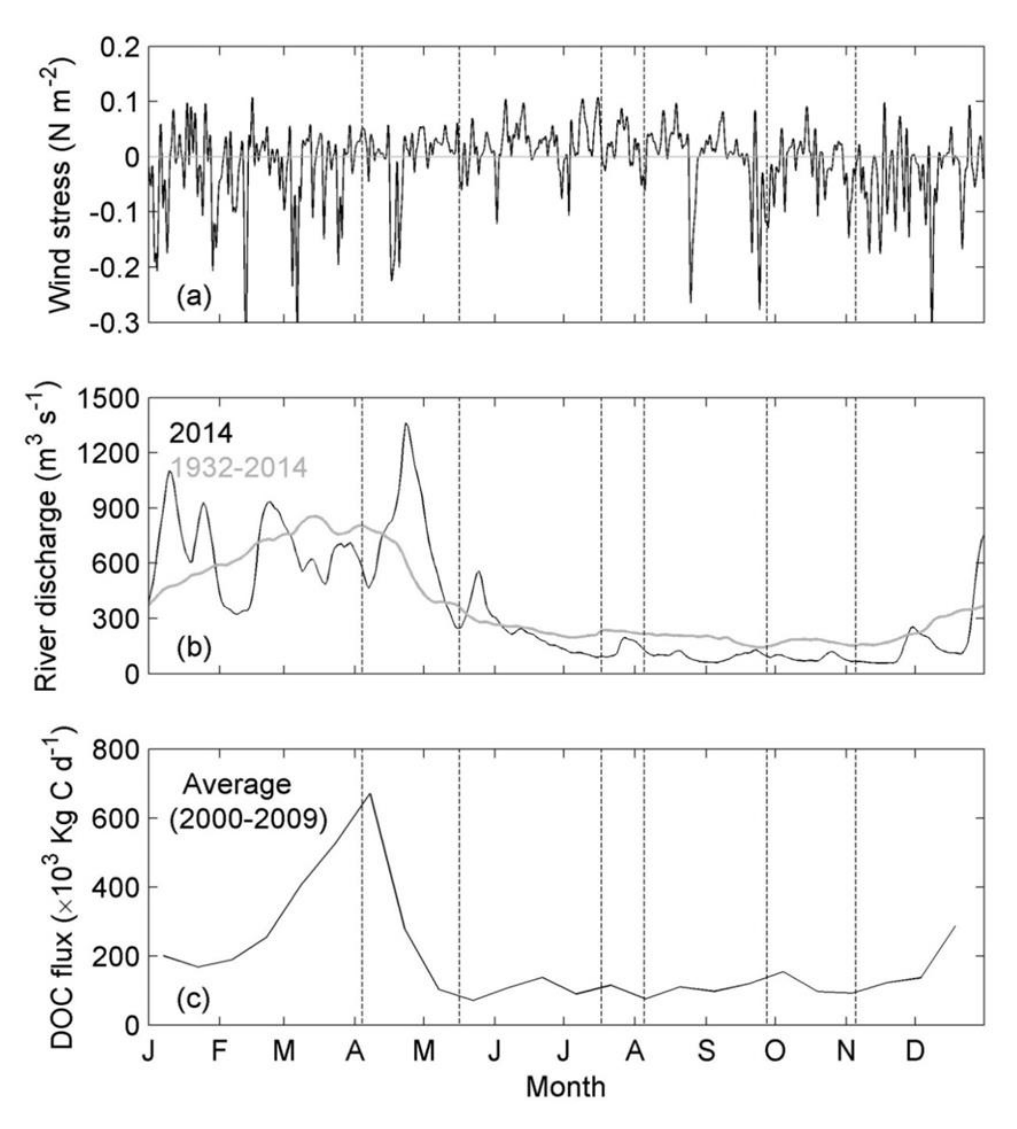


Figure A2. (a) Observed alongshore component of the wind stress from NOAA NDBC buoy 41008 during 2014. (b) Altamaha River discharge measured by USGS at Doctortown, GA is shown in black, along with the long-term average in gray. (c) The seasonal evolution of the DOC flux from the Altamaha River averaged from 2000 to 2009 is also shown.

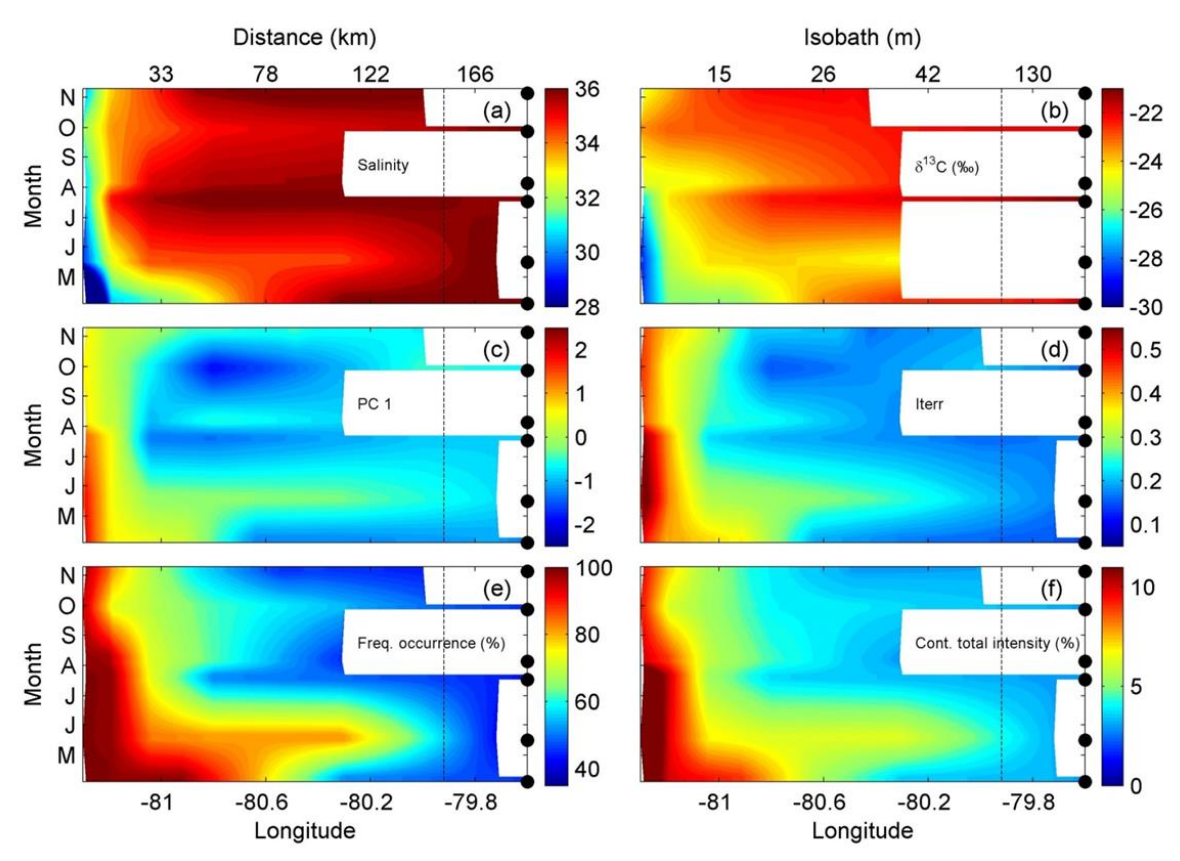


Figure A3. Time evolution of (a) surface salinity, (b) δ^{13} C SPE-DOC (‰), (c) first principal component of FT-ICR MS-derived DOM composition, (d) *Iterr* (an index indicative of riverine input; Medeiros et al., 2016), (e) frequency of occurrence of the t-Peaks (%), and (f) their contribution to the total magnitude of all peaks in the FT-ICR MS spectrum (%) as a function of distance from the coast along main transect extending from the mouth of the Altamaha River to the continental slope (see Figure 1 for location). Dashed vertical line shown approximate location of the shelfbreak. Black circles on the right of each panel shows timing of research cruises.

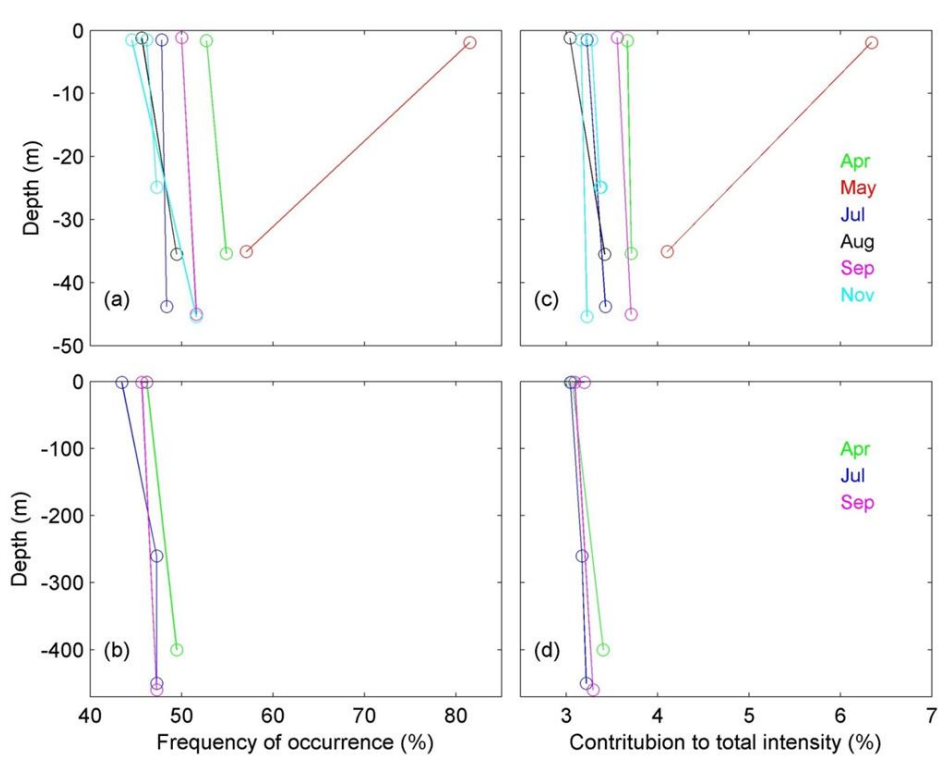


Figure A4. Vertical profiles of (**a,b**) frequency of occurrence of the t-Peaks (%) and (**c,d**) their contribution to total magnitude of all peaks in the FT-ICR MS spectrum (%) in the SAB. Profiles shown on top panel are for mid-shelf around the 35-45 m isobath, while bottom panels show offshelf profiles near the 400 m isobath. Colors represent different months.

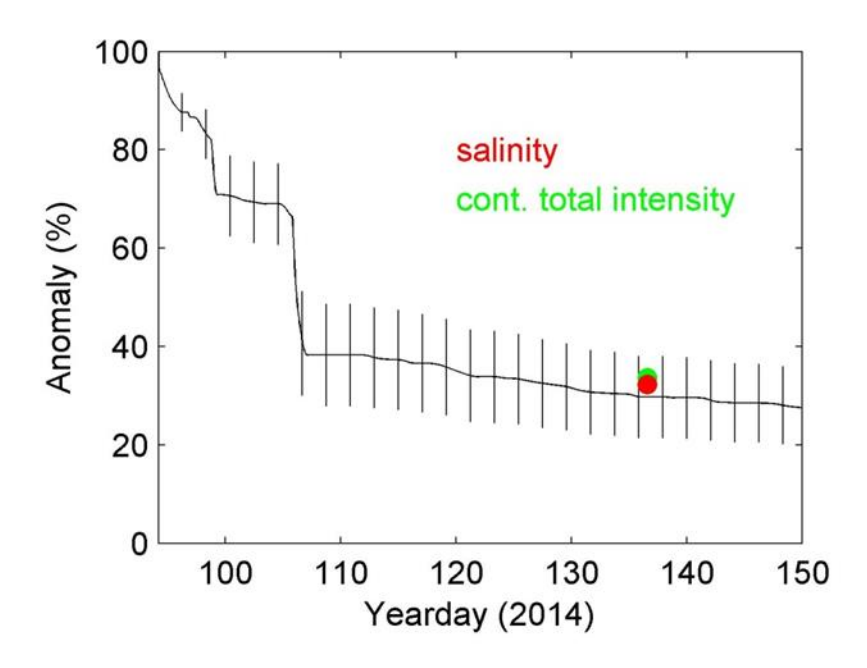


Figure A5. Time series of expected change in salinity anomaly of the plume due to wind forcing based on the Lentz (2004) model. Anomaly at the initial state (i.e., in the model and measured during research cruise in April) is defined to be 100 %. Red circle show measured salinity anomaly during the research cruise in May. Green circle shows anomaly of contribution of the t-Peaks to the total intensity of all peaks in the FT-ICR MS spectrum during the same period (anomaly at the initial state in April was also defined to be 100%).

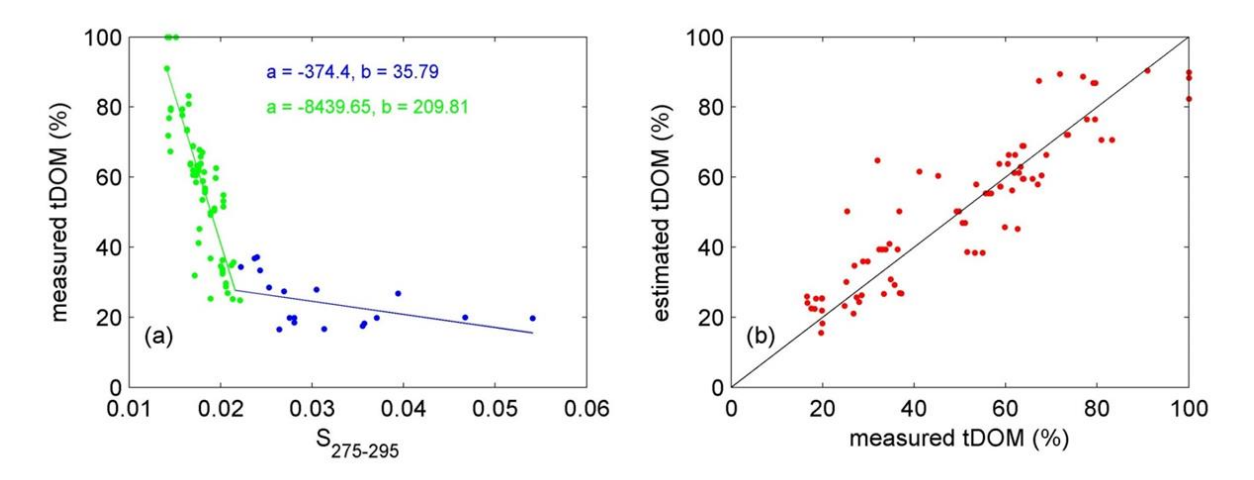


Figure A6. (a) Scatter plot of spectral slope coefficient of CDOM in the 275-295 nm range ($S_{275-295}$) and measured terrigenous DOM (%) based on two end-member mixing model using the first principal component of FT-ICR MS-derived DOM composition for each sample. Black lines are linear fits to observations. (b) Measured vs estimated terrigenous DOM (%). Estimated terrigenous DOM was computed based on $S_{275-295}$ and linear slope coefficients.

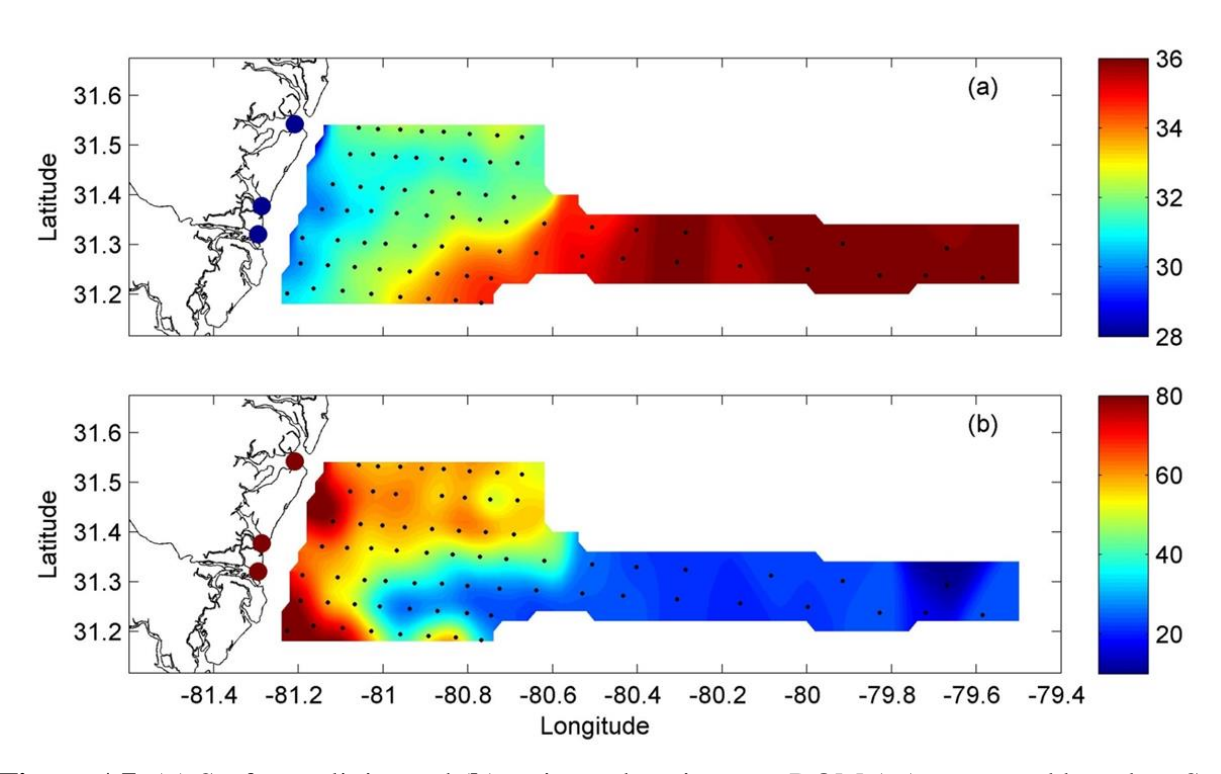


Figure A7. (a) Surface salinity and (b) estimated terrigenous DOM (%) computed based on $S_{275-295}$ and linear slope coefficients during research cruise in April 2014.

Acknowledgements

We gratefully acknowledge the support by the National Science Foundation through the Georgia Coastal Ecosystems Long Term Ecological Research program (GCE-LTER, OCE-1237140) and the Sapelo Island Microbial Carbon Observatory (SIMCO, OCE-1356010), as well as NASA (Ocean Surface Topography Science Team NNX13AD80G and Ocean Vector Winds Science Team NNX14AM70G). We thank the University of Georgia Marine Institute at Sapelo Island for logistical support, and the officers and crew of the R/V *Savannah* for the highly successful operations on board. Y. Wang, Y. Yuan and Q. Liu assisted with data collecting during the research cruises.

References

- Atkinson, L. P., J. O. Blanton, and E. B. Haines (1978), Shelf flushing rates based on the distribution of salinity and freshwater in the Georgia Bight, *Estuar. Coast. Mar. Sci.*, 7, 465-472.
- Atkinson, L. P., T. N. Lee, J. O. Blanton, and W. S. Chandler (1983), Climatology of the southeastern United States continental shelf waters, *J. Geophys. Res.*, 88, 4705-4718.
- Avery Jr., G.B., R. J. Kieber, J. D. Willey, G. C. Shank, and R. F. Whitehead (2004), Impact of hurricanes on the flux of rainwater and Cape Fear River water dissolved organic carbon to Long Bay, southeastern United States, *Global Biogeochem. Cy.*, *18*, GB3015. doi:10.1029/2004GB002229.
- Bates, N., and D. Hansell (1999), A high resolution study of surface layer hydrographic and biogeochemical properties between Chesapeake Bay and Bermuda, *Mar. Chem.*, 67, 1-16.
- Benner, R. (2004), What happens to terrestrial organic matter in the ocean?, *Mar. Chem.*, 92 (1–4), 307–310, doi:10.1016/j.marchem.2004.06.033.
- Benner, R. and S. Opsahl (2001), Molecular indicators of the sources and transformations of dissolved organic matter in the Mississippi River plume. *Org. Geochem.*, *32*, 597-611.
- Bhatti, A. M., D. Rundquist, J. Schalles, L. Ramirez and S. Nasu (2009), A comparison between above-water surface and subsurface spectral reflectances collected over inland waters, *Geocarto Internat.*, 24, 133-141, doi:10.1080/10106040802460707.
- Bianchi, T. S. (2011), The role of terrestrially derived organic carbon in the coastal ocean: A changing paradigm and the priming effect, *Proc. Natl. Acad. Sci. U. S. A.*, *108*(49), 19,473–19,481, doi:10.1073/pnas.1017982108.
- Blanton, J. O. and L. P. Atkinson (1983), Transport and fate of river discharge on the continental shelf of the southeastern United States, *J. Geophys. Res.*, 88, 4730-4738.
- Bro, R. and A. Smilde (2014), Principal component analysis, Anal. Methods, 6, 2812-2831.
- Castelao, R., O. Schofield, S. Glenn, R. Chant, and J. Kohut (2008), Cross-shelf transport of freshwater on the New Jersey shelf, *J. Geophys. Res.*, 113, C07017, doi:10.1029/2007JC004241.
- Cauwet, G. (2002), in *Biogeochemistry of Marine Dissolved Organic Matter*, edited by D. A. Hansell and C. A. Carlson, pp. 579–609, Academic Press, San Diego, Calif.

- Crump, B. C., B. J. Peterson, P. A. Raymond, R. M. W. Amon, A. Rinehart, J. W. McClelland, and R. M. Holmes (2009), Circumpolar synchrony in big river bacterioplankton, *Proc. Natl. Acad. Sci. U. S. A.*, 106, 21,208–21,212, doi:10.1073/pnas.0906149106.
- Dittmar, T., B. Koch, N. Hertkorn, and G. Kattner (2008), A simple and efficient method for the solid-phase extraction of dissolved organic matter (SPE-DOM) from seawater, *Limnol. Oceanogr. Methods*, *6*, 230-235.
- D'Sa, E. J., R. G. Steward, A. Vodacek, N. V. Blough, and D. Phinney (1999), Determining optical absorption of colored dissolved organic matter in seawater with a liquid capillary waveguide, *Limnol. Oceanogr.*, 44, 1142–1148.
- Fichot, C. G. and R. Benner (2012), The spectral slope coefficient of chromophoric dissolved organic matter (S₂₇₅₋₂₉₅) as a tracer of terrigenous dissolved organic carbon in riverinfluenced ocean margins, *Limnol. Oceanogr.*, 57, 1453-1466.
- Fichot, C.G. and R. Benner (2014), The fate of terrigenous dissolved organic carbon in a riverinfluenced ocean margin, *Global Biogeochem. Cy.*, 28, 300–318, doi:10.1002/2013GB004670.
- Fichot, C. G., S. E. Lohrenz, and R. Benner (2014), Pulsed, cross-shelf export of terrigenous dissolved organic carbon to the Gulf of Mexico, *J. Geophys. Res. Oceans*, 119, 1176–1194, doi:10.1002/2013JC009424.
- Flerus, R., O. Lechtenfeld, B. Koch, S.L. McCallister, P. Schmitt-Kopplin, R. Benner, K. Kaiser, and G. Kattner (2012), A molecular perspective on the ageing of marine dissolved organic matter. *Biogeosciences*, *9*, 1935-1955.
- Fong, D. A., and W. R. Geyer (2001), Response of a river plume during an upwelling favorable wind event, *J. Geophys. Res.*, 106(C1), 1067–1084.
- Gonsior, M., B. M. Peake, W. T. Cooper, D. Podgorski, J. D'Andrilli, and W. J. Cooper (2009), Photochemically induced changes in dissolved organic matter identified by ultrahigh resolution Fourier transform ion cyclotron resonance mass spectrometry, *Environ. Sci. Technol.*, 43, 698-703.
- Hansell, D.A., D. Kadko, N.R. Bates (2004), Degradation of terrigenous dissolved organic carbon in the western Arctic Ocean. *Science*, *304*, 858-861.
- Hedges, J. I. (1992), Global biogeochemical cycles: progress and problems, *Mar. Chem.*, *39*, 67–93.
- Hedges, J., R. Keil, and R. Benner (1997), What happens to terrestrial organic matter in the ocean? *Org. Geochem.*, 27, 195-212.

- Hernes, P.J. and R. Benner (2003), Photochemical and microbial degradation of dissolved lignin phenols: Implications for the fate of terrigenous dissolved organic matter in marine environments, *J. Geophys. Res.*, 108(C9), 3291, doi:10.1029/2002JC001421.
- Jaffé, R., Y. Ding, J. Niggemann, A.V. Vähätalo, A. Stubbins, R.G.M. Spencer, J. Campbell, and T. Dittmar (2013), Global charcoal mobilization from soils via dissolution and riverine transport to the oceans, *Science*, *340*, 345–347.
- Kieber, R. J., X. Zhou, and K. Mopper (1990), Formation of carbonyl compounds from UV-induced photodegradation of humic substances in natural waters: Fate of riverine carbon in the sea, *Limnol. Oceanogr.*, 35, 1503-1515.
- Kim, S., R. Kramer, and P. Hatcher (2003), Graphical method for analysis of ultrahigh resolution broadband mass spectra of natural organic matter, the van Krevelen diagram, *Anal. Chem.*, 75, 5336-5344.
- Koch, B. P., and T. Dittmar (2006), From mass to structure: an aromaticity index for high-resolution mass data of natural organic matter, *Rapid Commun. Mass Spectrom.*, 20, 926-932.
- Kowalczuk, P., P. W. Cooper, R. F. Whitehead, M. J. Durako, and W. Sheldon (2003), Characterization of CDOM in organic rich river and surrounding coastal ocean in the South Atlantic Bight. *Aquatic Sciences*, 65, 384–401.
- Kowalczuk, P., W. J. Cooper, M. Durako, H. Young, and A. Kahn (2009), Characterization of dissolved organic matter fluorescence in the South Atlantic bight with use of PARAFAC model: Interannual variability, *Mar. Chem.*, 113, 182-196.
- Krupa, M., R. G. M. Spencer, K. W. Tate, J. Six, C. van Kessel, and B. A. Linquist (2012), Controls on dissolved organic carbon composition and export from rice-dominated systems, *Biogeochemistry*, *108*, 447–466, doi:10.1007/s10533-011-9610-2.
- Lechtenfeld, O.J., G. Kattner, R. Flerus, S.L. McCallister, P. Schmitt-Kopplin, and B.P. Koch (2014), Molecular transformation and degradation of refractory dissolved organic matter in the Atlantic and Southern Ocean. *Geochim. Cosmochim. Acta*, 126, 321-337.
- Lee, T. N., J. A. Yoder, and L. P. Atkinson (1991), Gulf Stream frontal eddy influence on productivity on the southeast U.S. continental shelf, *J. Geophys. Res.*, 96, 22,191–22,205, doi:10.1029/91JC02450.
- Lentz, S. (2004), The response of buoyant coastal plumes to upwelling favorable winds, *J. Phys. Oceanogr.*, 34, 2458–2469.
- Letscher, R., D.A. Hansell, and D. Kadko (2011), Rapid removal of terrigenous dissolved organic carbon over the Eurasian shelves of the Arctic Ocean, *Mar. Chem.*, 123: 78-87.

- Mannino, A. and H.R. Harvey (2004), Black carbon in estuarine and coastal ocean dissolved organic matter, *Limnol. Oceanogr.*, 49, 735-740.
- Medeiros, P.M., M. Seidel, T. Dittmar, W.B. Whitman, and M.A. Moran (2015a), Drought-induced variability in dissolved organic matter composition in a marsh-dominated estuary, *Geophys. Res. Lett.*, 42, 6446-6453.
- Medeiros, P. M., M. Seidel, J. Niggemann, R. G. M. Spencer, P. J. Hernes, P. L. Yager, W. L. Miller, T. Dittmar and D. Hansell (2016), A novel molecular approach for tracing terrigenous dissolved organic matter into the deep ocean, *Global Biogeochem. Cy., submitted.*
- Medeiros, P.M., M. Seidel, L.C. Powers, T. Dittmar, D.A. Hansell, and W.L. Miller (2015b), Dissolved organic matter composition and photochemical transformations in the northern North Pacific Ocean, *Geophys. Res. Lett.*, 42, 863–870, doi:10.1002/2014GL062663.
- Medeiros, P.M., M. Seidel, N.D. Ward, E.J. Carpenter, H.R. Gomes, J. Niggemann, A.V. Krusche, J.E. Richey, P.L. Yager, and T. Dittmar (2015c), Fate of the Amazon River dissolved organic matter in the tropical Atlantic Ocean. *Global Biogeochem. Cy.*, 29, 677–690. doi: 10.1002/2015GB005115.
- Miller, W. L., and M. A. Moran (1997), Interaction of photochemical and microbial processes in the degradation of refractory dissolved organic matter from a coastal marine environment, *Limnol. Oceanogr.*, 42, 1317-1324.
- Moran, M. A., W. M. Sheldon, and R. G. Zepp (2000), Carbon loss and optical property changes during long-term photochemical and biological degradation of estuarine dissolved organic matter, *Limnol. Oceanogr.*, 45, 1254-1264.
- Obernosterer, I., and R. Benner (2004), Competition between biological and photochemical processes in the mineralization of dissolved organic carbon, *Limnol. Oceanogr.*, 49, 117-124.
- Opsahl, S., and R. Benner (1997), Distribution and cycling of terrigenous dissolved organic matter in the ocean. *Nature*, *386*, 480-482.
- Opsahl, S., and R. Benner (1998), Photochemical reactivity of dissolved lignin in river and ocean waters, *Limnol. Oceanogr.*, 43, 1297–1304.
- Overland, J., and R. Preisendorfer (1982), A significance test for principal components applied to a cyclone climatology, *Mon. Weather Rev.*, 110, 1–4.
- Raymond, P. and R. Spencer (2015), Riverine DOM, 509-533, In Biogeochemistry of Marine Dissolved Organic Matter, Edited by Hansell, D. and C. Carlson, 2nd edition, , 693pp.
- Repeta, D., T. Quan, L. Aluwihare, and A. Accardi (2002), Chemical characterization of high molecular weight dissolved organic matter in fresh and marine waters, *Geochim. Cosmochim. Acta*, 66, 955-962.

- Seidel, M., M. Beck, T. Riedel, H. Waska, I. Suryaputra, B. Schnetger, J. Niggemann, M. Simon, and T. Dittmar (2014), Biogeochemistry of dissolved organic matter in an anoxic intertidal creek bank, *Geochim. Cosmochim. Acta*, 140, 418-434.
- Seidel. M., P.L. Yager, N.D. Ward, E.J. Carpenter, H. R. Gomes, A.V. Krusche, J.E. Richey, T. Dittmar, and P.M. Medeiros (2015), Molecular-level changes of dissolved organic matter along the Amazon River-to-ocean continuum, *Mar. Chem.*, doi:10.1016/j.marchem.2015.06.019.
- Sholkovitz, E. R. (1978), The flocculation of dissolved Fe, Mn, Al, Cu, Ni, Co and Cd during estuarine mixing, *Earth Planet. Sci. Lett.*, *41*, 77-86.
- Sleighter, R. and P. Hatcher (2008), molecular characterization of dissolved organic matter (DOM) along a river to ocean transect of the lower Chesapeake Bay by ultrahigh resolution electrospray ionization Fourier transform ion cyclotron resonance mass spectrometry, *Mar. Chem.*, 110, 140-152.
- Spencer, R. G. M., G. R. Aiken, M. M. Dornblaser, K. D. Butler, R. M. Holmes, G. Fiske, P. J. Mann, and A. Stubbins (2013), Chromophoric dissolved organic matter export from U.S. rivers, *Geophys. Res. Lett.*, 40, 1575–1579, doi:10.1002/grl.50357.
- Spencer, R. G. M., K. D. Butler, and G. R. Aiken (2012), Dissolved organic carbon and chromophoric dissolved organic matter properties of rivers in the USA, *J. Geophys. Res.*, 17, G03001, doi:10.1029/2011JG001928.
- Spencer, R.G.M., P.J. Mann, T. Dittmar, T.I. Eglinton, C. McIntyre, R.M. Holmes, N. Zimov, and A. Stubbins (2015), Detecting the signature of permafrost thaw in Arctic rivers, *Geophys. Res. Lett.*, 42, 2830–2835.
- Spencer, R.G.M., A. Stubbins, P.J. Hernes, A. Baker, K. Mopper, A.K. Aufdenkampe, R.Y. Dyda, V.L. Mwamba, A.M. Mangangu, J.N. Wabakanghanzi, and J. Six (2009), Photochemical degradation of dissolved organic matter and dissolved lignin phenols from the Congo River, *J. Geophys. Res.*, 114, G03010, doi: 10.1029/2009JG000968.
- Stubbins, A., R.G.M. Spencer, H. Chen, P.G. Hatcher, K. Mopper, P.J. Hernes, V.L. Mwamba, A.M. Mangangu, J.N. Wabakanghanzi, and J. Six (2010), Illuminated darkness: Molecular signatures of Congo River dissolved organic matter and its photochemical alteration as revealed by ultrahigh precision mass spectrometry, *Limnol. Oceanogr.*, 55, 1467-1477.
- Vodacek, A., F. Hoge, R. Swift, J. Yungel, E. Peltzer, and N. Blough (1995), The use of in situ and airborne fluorescence measurements to determine UV absorption coefficients and DOC concentrations in surface waters, *Limnol. Oceanogr.*, 40, 411-415.
- Williams, P.M., and E.R.M. Druffel (1987), Radiocarbon in dissolved organic matter in the central North Pacific Ocean. *Nature*, 330, 246-248.

Ziolkowski, L.A. and E.R.M. Druffel (2010), Aged black carbon identified in marine dissolved organic carbon, *Geophys. Res. Lett.*, *37*, L16601, doi:10.1029/2010GL043963.

SUPPLEMENTARY INFORMATION

EXPORT OF TERRIGENOUS DISSOVED ORGANIC CARBON IN A BROAD ${\bf CONTINENTAL~SHELF}^1$

¹Medeiros, P. M., Babcock-Adams, L., Seidel, M., Castelao, R. M., Hollibaugh, J. T., Di Iorio,

D. & Dittmar, T. To be submitted to Estuar. Coast. Shelf Sci.

Figures

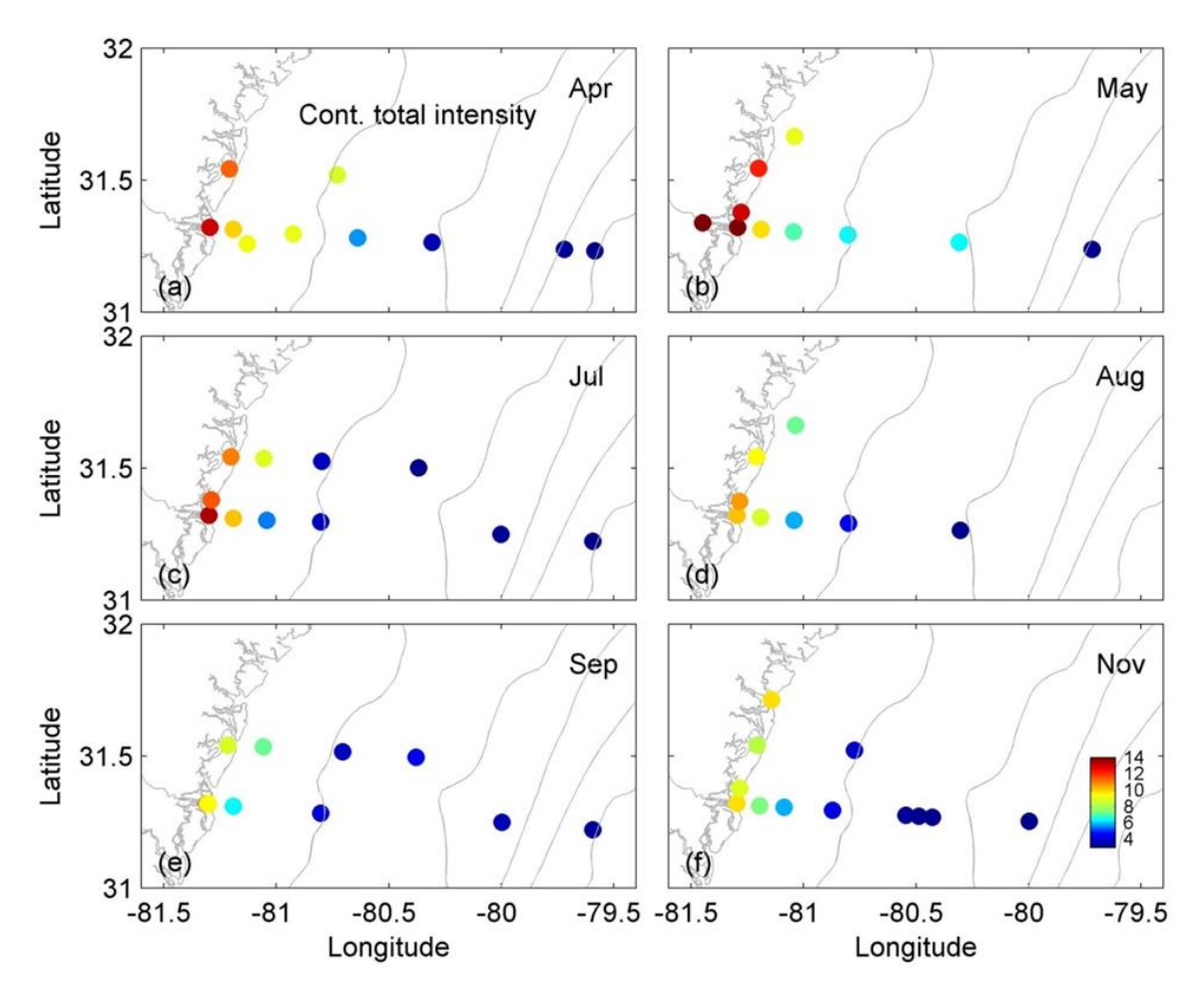


Figure A.S1. Spatial distribution of contribution of the t-Peaks to the total magnitude of all peaks in the FT-ICR MS spectrum (%) for the six research cruises in 2014. Timing of sampling is shown on the top right corner of each panel. Sample up the river in May was collected in 2013.

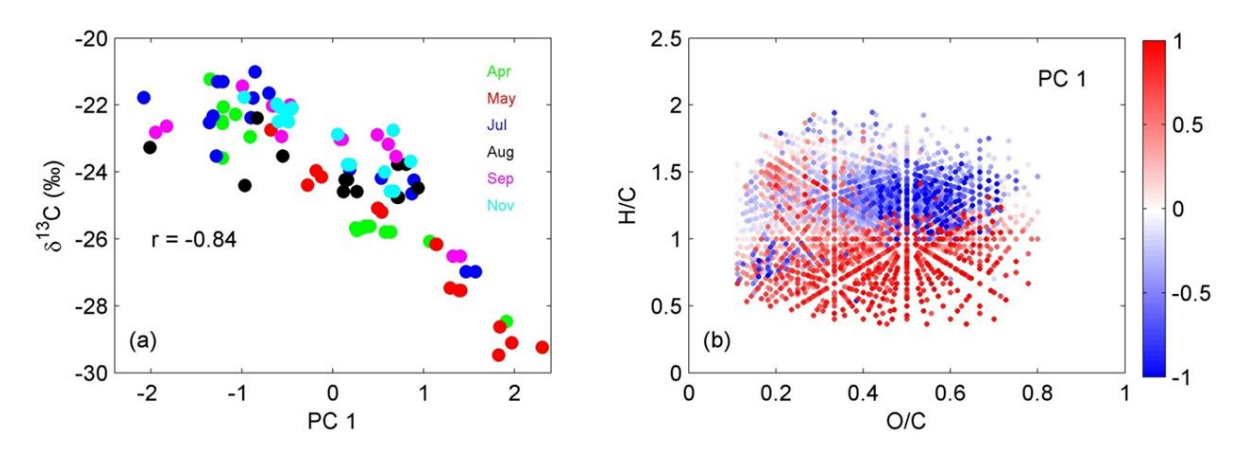


Figure A.S2. (a) Scatter plot of first principal component of FT-ICR MS-derived DOM composition and δ^{13} C SPE-DOC (‰) color coded for each month. Correlation coefficient (r) is also shown. (b) Loadings of PC1 shown in van Krevelen space.

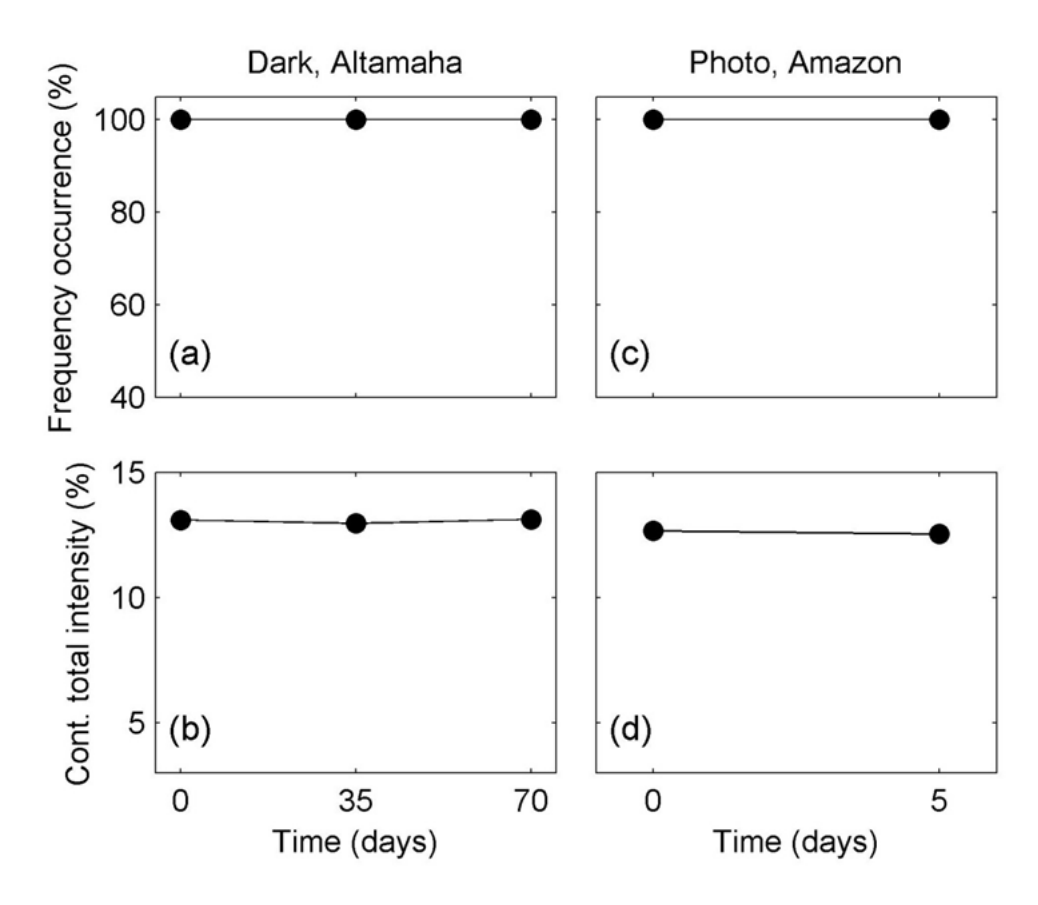


Figure A.S3. Time series of (**a,c**) frequency of occurrence of the t-Peaks (%) and (**b,d**) their contribution to the total magnitude of all peaks in the FT-ICR MS spectrum during (**a,b**) dark microbial incubations using Altamaha River water and (**c,d**) photo-irradiation experiments using Amazon River water.